Fall 12-17-2021

Development of Polymeric CXCR4 Targeting Carriers for siRNA Delivery to Treat Acute Kidney Injury

Weimin Tang
University of Nebraska Medical Center

Development of Polymeric CXCR4 Targeting Carriers for siRNA Delivery to Treat Acute Kidney Injury

by

Weimin Tang

A DISSERTATION

Presented to the Faculty of
the University of Nebraska Graduate College
in Partial Fulfillment of the Requirements
for the Degree of Doctor of Philosophy

Pharmaceutical Sciences
Graduate Program

Under the Supervision of Professor David Oupický

University of Nebraska Medical Center
Omaha, Nebraska

October, 2021

Supervisory Committee:

David Oupický, Ph.D.
Daryl J Murry, Pharm.D.
Rongshi Li, Ph.D.
Erika I Boesen, Ph.D.

Acknowledgments

I would like to express my most profound and sincere thanks to my mentor and advisor, Prof. David Oupický for all his guidance, support, and patience during the five-year journey as his PhD student. His unlimited passion for science, innovation and his impressive talent have inspired me since the first day I joined the lab. His advice on my research as well as my career have been priceless. It is my great honor to be his student, and I couldn't ask for a better PhD mentor.

I would also like to sincerely thank my committee members, Profs. Daryl J. Murry, Rongshi Li, Erika I. Boesen, and Babu Padanilam for their professional guidance and valuable suggestions for my research.

My thanks also go to Dr. Jing Li and Dr. Fei Yu for continues guidance and teaching me cell culture and polymer synthesis techniques. I would like to thank Dr. Hee-Seong Jang for teaching me the ischemia-reperfusion animal model and helping with p53 IHC staining. I thank Dr. Kirk W. Foster for helping me with the kidney injury score and teaching me how to analyze the tissue slides. I also thank Dr. Heather Jensen Smith for helping me with the intravital imaging studies. I thank Dr. Panja Sudipta for helping with the C-CS synthesis and characterization. I thank all my former and current lab mates for their help and support in and out of the lab. I also thank the Department of Pharmaceutical Sciences, University of Nebraska Medical Center for providing me the great opportunities and study experiences. I also thank the financial support from the UNMC fellowship program.

Last but not least, I would like to thank my family for their endless love and unlimited encouragement. And thanks for all my friends for their company and support during those five years.

Abstract:

Development of Polymeric CXCR4 Targeting Carriers for siRNA Delivery to Treat Acute Kidney Injury

Weimin Tang, Ph.D.

University of Nebraska Medical Center, 2021

Supervisor: David Oupický, Ph.D.

Acute kidney injury (AKI) is a major kidney disease that is characterized by a sudden loss of renal function which manifests by a decrease in urine output and an increase in serum creatinine. AKI is a global healthcare burden associated with high morbidity, mortality, and increasing cost. Currently there are no effective pharmacological treatments available. Apoptosis induced by p53 has been demonstrated as an important pathological mechanism for the development of AKI. Meanwhile, CXCR4/SDF-1 axis has been associated with the inflammation during AKI, and CXCR4 is overexpressed on injured tubules. This dissertation hypothesized that polycations with CXCR4 targeting ability could enhance the accumulation of p53 siRNA in injured tubule cells, and simultaneous blockade of CXCR4 would lead to enhanced AKI therapy.

An overview of renal anatomy, pathophysiology and biomarkers of AKI, the application of nanomedicine in AKI is given in Chapter 1.

Chapter 2 reports that PCX can effectively deliver siRNA into the injured renal tubule cells due to the CXCR4 binding effect, and PCX/sip53 showed great anti-apoptosis effect in cisplatin challenged HK-2 cells. Moreover, the in vivo bio-distribution study showed

that PCX can enhance the accumulation of siRNA in the injured kidneys, especially the tubules. Renal p53 and CXCR4 expressions were confirmed in two widely used AKI mice models. Finally, the enhanced renal accumulation of PCX/sip53 showed great therapeutic potential in the cisplatin induced AKI (CIS-AKI) mice model.

Chapter 3 reports that modified chitosan (CS) with α-cyclam-p-toluic acid (CPTA) can introduce CXCR4 binding ability. After formulating with siRNA, CPTA modified CS (C-CS) showed improved siRNA protection ability. In vitro studies showed enhanced cellular uptake of C-CS/siRNA and gene knockdown effect. Moreover, in vivo biodistribution showed C-CS/siRNA can effectively accumulate in the injured kidney and retain there for at least 24 hours due to its CXCR4 binding ability. Finally, the treatment with C-CS/sip53 showed great therapeutic potential in ischemia-reperfusion induced AKI (IRI-AKI) mice model.

Chapter 4 reports the synthesis and characterizations of polymeric plerixafor (PP) derivatives. All the polymers showed excellent CXCR4 binding ability in vitro. The hydrophilic moieties modified PP (PP-OH) showed less protein binding, which may benefit for in vivo applications. Finally, the biodistribution study was conducted and PP-OH showed the highest accumulation in injured kidneys, which may provide advanced ideals for the development of CXCR4 binding carriers for drug delivery to injured kidneys.

In chapter 5, conclusions and future directions are given.

Table of Contents

List of Figures

List of Schemes

List of Tables

List of Abbreviations

AKI – Acute Kidney Injury

ATP – Adenosine Triphosphate

BAX – BCL2-associated X Protein

BUN – Blood Urea Nitrogen

CIS-AKI – Cisplatin Induced AKI

CKD – Chronic Kidney Disease

CoQ – Coenzyme Q

CPTA – α-Cyclam-p-toluic acid

CXCR4 – C-X-C Chemokine Receptor 4

DAMPs – Damage-Associated Molecular Patterns

DLS – Dynamic Light Scattering

DONs – DNA Origami Nanostructures

EPCs – Endothelial Progenitor Cells

ESRD – End-stage Renal Disease

ETC – Electron Transport Chain

fCNTs – Ammonium-Functionalized Signal-Walled Carbon Nanotubes

GBM – Glomerular Basement Membrane

GFM – Glomerular Filtration Membrane

GFR – Glomerular Filtration Rate

HA – Hyaluronic Acid

HSCs – Hematopoietic Stem Cells

ICAM-1 – Intracellular Adhesion Molecule-1

IRI-AKI – Ischemia Reperfusion Induced AKI

KDIGO – Kidney Disease Improving Global Outcomes

KIM-1 – Kidney Injury Molecule 1

LMICs – Low-to-middle Income Countries

LMWC – Low Molecular Weight Chitosan

L-sTd – Small-Sized L-DNA Tetrahedron

MNP – Mesoscale Nanoparticles

MOMP – Permeability of Outer Mitochondrial Membrane

mRNA – Messenger RNA

NGAL – Neutrophil Gelatinase–Associated Lipocalin

NK Cells – Nature Killer Cells

PIDD – p53-induced Protein with a Death Domain

PTCs – Proximal Tubule Cells

PUMA – p53 Upregulated Modulator of Apoptosis

RET – Reverse Electron Transport

RNAi – RNA Interference

ROS – Reactive Oxygen Species

Scr – Serum Creatinine

SDF-1 – Stromal Cell-Derived Factor

siRNA – Small Interfering RNA

sTds – Small-Sized DNA Tetrahedrons

TEM – Transmission Electron Microscopy

Chapter 1. Introduction

1. Renal Anatomy

The kidneys are bean-shaped structures located in the retroperitoneal space on the posterior abdominal wall on each side of the spine. Because of the position of the liver, the right kidney is often located slightly more inferior and lower than the left kidney. During renal filtration, the blood enters the kidney through the renal arteries and exits through the renal veins. Furthermore, through the ureters, the urine is transported to the bladder after renal filtration. The kidneys could be divided into three regions: the renal cortex, medullar, and pelvis (Scheme. 1A). The basic structure and functional units of kidneys are called nephrons, and they locate in the cortex and medullar of the kidneys. The adult human kidneys contain 1-2.5 million nephrons, those basic kidney unites are fundamentally necessary for maintain the balance between fluid homeostasis, osmoregulation, and waste filtration [1]. Nephrons are composed of the renal corpuscle, distal tubule, proximal tubule, loop of Henle, collecting ducts, and peritubular capillaries which surround the tubules in the tubulointerstitium (Scheme. 1B) [2]. According to the position of glomeruli and the length of the loop of Henle, nephrons have been divided into two types. The cortical nephrons with shorter loops of Henle with glomeruli locate in the outer cortex, and the juxtamedullary nephrons, which have long loops of Henle with glomeruli near the corticomedullary border. The ratio of cortical to juxtamedullary nephrons is around 85:15 and 75:25 in humans and mice, respectively [3]. As shown in Scheme 1C, the blood is transported into the renal corpuscle through the afferent arteriole,

then further transported to the glomeruli. The relatively high blood pressure in the glomerular cavity induces the blood fluids filtered into the Bowman's space, then further flow to the proximal tubules for further reabsorption and secretion. The proximal tubules are covered with microvilli which play an important role in keeping the balance between urinary reabsorption and secretion of the filtered blood fluids. The unfiltered residual blood is then outflowed through the efferent arteriole to the peritubular capillaries and renal vein and finally join to the main bloodstream [4].

The renal filtration of the blood fluids happens in the glomerulus (Scheme. 1D), and the glomerular filtration membrane (GFM) [5-10], which is supported by mesangial cells, plays a pivotal role in renal filtration. The GFM consists of four different layers: endothelial glycocalyx, endothelial cells, glomerular basement membrane (GBM), and the podocytes (Scheme. 1E). Each layer has its unique size cut-off or charge properties. The layer of endothelial glycocalyx is composed of glycosaminoglycans like heparin sulfate, hyaluronic acid, and chondroitin sulfate, and it plays an essential role in preventing protein leakage during renal filtration due to its negatively charged property [9]. A monolayer of endothelial cells forms the endothelial cell layer, which has 70-90 nm fenestrations. The GBM with a pore size in the range of 2-8 nm, and mainly consist with laminin, proteoglycans and type IV collagen. The laminin and proteoglycans (mainly heparin sulfate) form the network and the collagen forms the backbone of GBM. The layer of podocyte faces the Bowman's space and locate on another side of GBM, it has a pore size in the range of 4-11 nm and covered with a glycocalyx with a thickness around 200 nm [4]. Based on this specific four-layer structure of GFM, the permeability for renal

filtration not only depends on size [11] but also charge [12]. Under normal conditions, the size and charge selectivity of GFM ensures that only small solutes and water could be filtrated from plasma to the urine [13]. High molecular-weight components such as red blood cells and albumin are retained in the blood during renal filtration. The impairment of this barrier results proteinuria which is a hallmark of glomerular diseases [14].

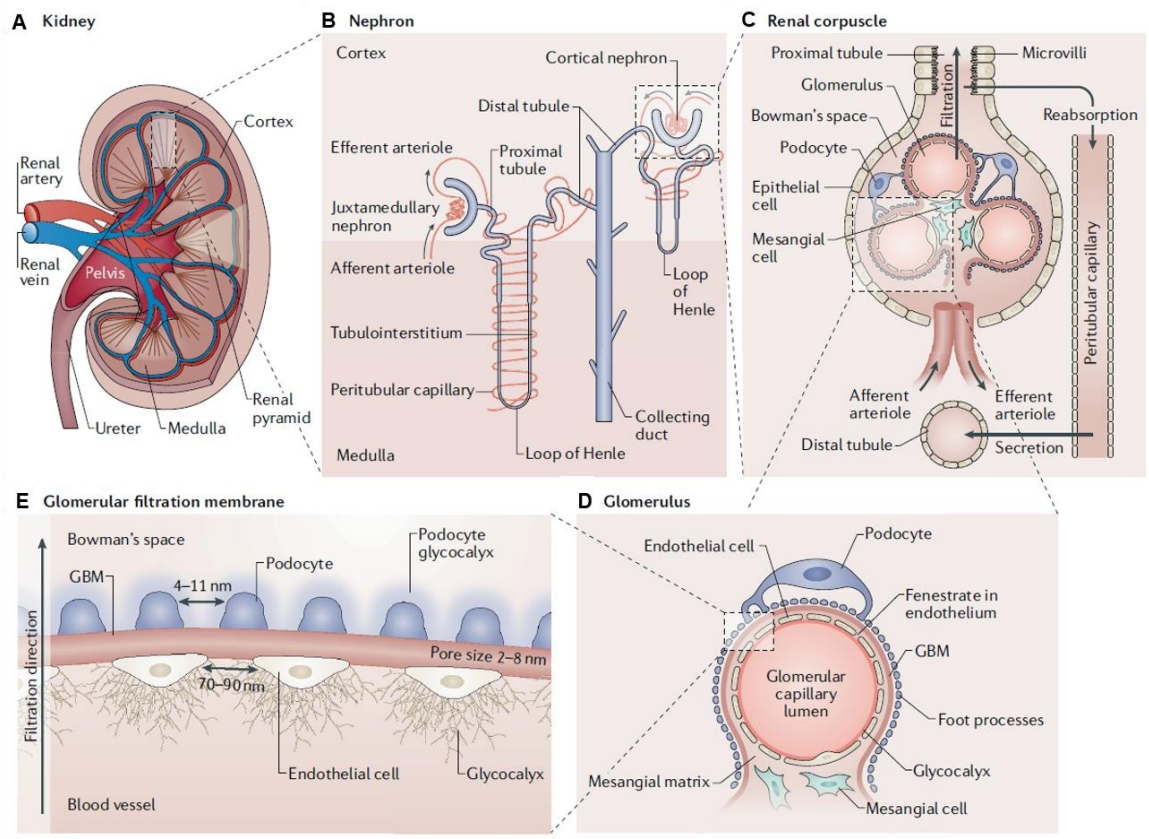

Scheme 1. Renal anatomy. (A) The bean shaped structure of kidney and is divided into three regions: renal cortex, medulla and pelvis. (B) Detailed structure of nephron which consist of the renal corpuscle, distal tubule, proximal tubule, loop of Henle, collecting duct and peritubular capillary. (C) The cross section of renal corpuscle. (D) Detailed structure of glomerulus, it composed of mesangial cells, glomerular capillary lumen, and GFM. (E) Detailed structure of GFM which consist with glycocalyx, endothelial cells, GBM, podocyte, and podocyte glycocalyx. (Adapted from [4]).

2. Acute Kidney Injury

Acute kidney injury (AKI) is characterized by a sudden decrease in renal function which is associated with complex pathophysiological mechanisms [15, 16]. Despite the progresses in understanding the underlying pathophysiology, AKI continues to be a public health concern in the global and impacting ~13.3 million patients every year and without any pharmacological treatments available [17, 18]. In 266 studies (included a total of 4,502,158 patients) that used KDIGO (Kidney Disease: Improving Global Outcomes) definition of AKI, this disease affected 21% of hospital admissions of LMICs (low-to-middle income countries), which broadly agree the worldwide incidence of AKI (Scheme 2) [19]. AKI is mainly caused by decreased blood flow, direct damage to kidneys, blockage of the urinary tract clinically, and frequently diagnosis with an incident around 5.0% to 7.5% in hospitalized patients and 50% to 60% in critical ill patients [15, 20-24]. Moreover, AKI usually associate with high morbidity, mortality, and increased cost, about 1.7 million death every year [18]. With the improvements in patients care and the availability of low nephrotoxic drugs, the mortality rates in critically ill patients with AKI have declined, however the mortality rates are still significantly high, especially in AKI patients who require dialysis [25-27]. Patients who survive from AKI are at increased risk of developing chronic kidney disease (CKD) which is defined by continued kidney disease for a period of more than 90 days [28], and end-stage renal disease (ESRD) which can lead to poor life quality and high long-term costs for patients who recovered from AKI [29-31]. Given those many reasons, treatments are needed to decrease AKI associated high morbidity, mortality and cost.

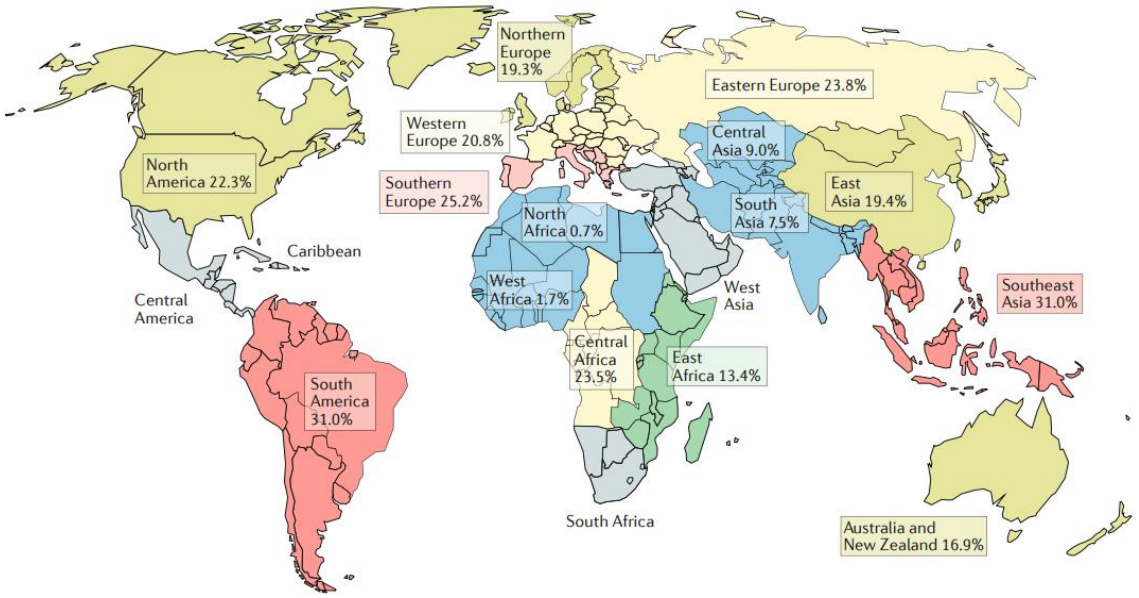

Scheme 2. Published estimates of the incidence of AKI as defined using KDIGO criteria vary widely across the world. The percentages shown in the scheme indicate the ratio of the hospitalized population with AKI. (Adapted from [19])

2.1. Pathophysiology of AKI

Filtration and excretion of nitrogenous waste produces from blood is one of the most important functions of kidney, and the elevated level of blood urea nitrogen (BUN) and serum creatinine (Scr) served as an indicator for decreased renal function which resulted from kidney injury. AKI is defined by rapid decrease glomerular filtration rate (GFR) which result in retention of BUN and Scr, thus the diagnosis of AKI is based on the measurement of these blood substances in patients over time and the rapid decrease of GFR usually occurs over the course of hours to days for AKI patients [32, 33]. The underlying pathophysiology of AKI has been well studied by scientists in the last few decades. Animal models of AKI which represent nephrotoxicity and ischemia-reperfusion injury provided important insights for us to understand the behind mechanism of AKI [17]. Based on the AKI animal models, scientists have disclosed fundamental information on disease mechanisms of AKI.

2.1.1. Animal models for AKI study

Ischemia reperfusion induced AKI (IRI-AKI) and cisplatin induced AKI (CIS-AKI) are the most two widely used animal models for AKI study. Ischemia is a leading cause of AKI clinically, which could result from several conditions, such as renal vascular occlusion or obstruction, cardiac surgery, and kidney transplantation. Even the in vitro studies of isolated renal cells are valuable to study the pathophysiology of ischemic AKI, it is imitated to mimic the complexity of human body. Thus, the in vivo animal models are needed to better understand the pathophysiology of AKI. Various animal models of

ischemic AKI have been developed and tested in the decades and currently there are two kinds of renal ischemia-reperfusion (IR) models are mainly used: the bilateral renal ischemia reperfusion [34-44] and unilateral renal ischemia reperfusion model [45-51]. Based on whether the contralateral kidney is removed, unilateral renal ischemia reperfusion model can be further divided into two subtypes: with contralateral nephrectomy or without contralateral nephrectomy. Because of the more relevance to human pathologic conditions where both kidneys are normally affected by blood supply, the bilateral ischemia reperfusion AKI model is the most used one in many studies [34, 52-56]. The initial ischemia reperfusion AKI models were developed with large size animals, then rat and mice became the most popular models since 1960 and 1990 respectively. The small size animal model requires less drug consumption for experimental testing when compared with large size animals [57].

Except ischemia reperfusion induced kidney injury, chemical agents induced AKI is a frequent entity in clinical medicine. The kidneys are the major target organ for toxic effect drugs [58]. Even it is difficult to estimate nephrotoxic AKI due to the variation of patient populations and the standards for AKI, nephrotoxicity has been reported that associate with about 8-60% of hospitalized AKI cases [59]. Cisplatin, a platinum-based chemotherapeutic drug that have been widely used in the treatment of a variety of solid tumors [60], is frequently limited by various significant side effects, especially its nephrotoxicity. Almost one-third of patients develop nephrotoxicity after a single dose of cisplatin at the dose of 50-100 mg/m^2 [61, 62]. To prevent the AKI and improve the survival rate in cancer patients who receiving cisplatin-based chemotherapy, it is necessary to

understand the pathogenesis of cisplatin induced renal injury. The decreased renal plasma flow and GFR, and the increased renal vascular resistance make the cisplatin nephrotoxicity an idea model for nephrotoxic AKI study [63].

2.1.2. Inflammation and immune cells infiltration in AKI

Inflammation is complex process that is needed to eliminate harmful pathogens and mediate tissue repair after injury. Nevertheless, excess and unresolved inflammation could promote autoimmune disorder, fibrosis, and tissue damage [64, 65]. The release of cytokines and recruitment of neutrophiles and macrophages at the site of injury are recognized as hallmarks of the early inflammation response. Moreover, recent data showed that T cells also participate in early inflammatory responses in AKI [66]. The Immune mechanisms involved in the pathogenesis of AKI have been studied most extensively in IRI-AKI and CIS-AKI animal models. This part is focused on the introduction of the involvement of immune cells in AKI (Scheme 3).

The infiltration of neutrophils has been detected in mouse kidneys subjected to ischemia reperfusion injury [67, 68] and biopsy samples from patients with early AKI [69, 70]. As one of the important effector cells in the innate immune system, neutrophils transmigrate into kidney by using adhesion molecules like intracellular adhesion molecule-1 (ICAM-1) and P-selectin after kidney insult. The released cytokine, proteases, and reactive oxygen species (ROS) from infiltrated neutrophils finally promote kidney injury [71]. Recent studies have shown that inhibiting vascular adhesion protein-1 and leukotriene B4-leukotriene B4 receptor axis could block neutrophils infiltration in injured

kidneys, and finally attenuate IRI-AKI and CIS-AKI respectively [72, 73]. Therefore, neutrophils are expected to have an important role in the development of AKI.

Macrophages are also suspected to have an important role for kidney injury. Even the number of resident macrophages in normal kidneys are few, the amount markedly increases soon after IRI, especially in the outer medulla [74]. The activated macrophages has the potential activity of phagocytic and release several cytokines, like IL-1, IL-6, IL-8, IL-12, and TNF, which facilitate the inflammatory cascade and contribute to the establishment of kidney injury [75]. The depletion of monocytes and macrophages systemically, attenuated early kidney injury in an IRI-AKI mice model [76]. Macrophages also play a role in renal repair. By switching from a proinflammatory M1 phenotype to an anti-inflammatory M2 phenotype, the renal repair process promoted [77]. The M2 phenotype switching of macrophages might be due to the phagocytic uptake of neutrophils by macrophages and the change of intrarenal microenvironment [78, 79]. The role of macrophages in cisplatin induced AKI (CIS-AKI) model is not well studied. The renal infiltration of macrophages preceded loss of renal function; however, the inhibition of macrophages infiltration was not enough to prevent CIS-AKI [80, 81].

Except neutrophiles and macrophages, renal dendritic cells and lymphocytes are also play very important role in the development and repairment of AKI. The dendritic cells are act as messengers between innate and adaptive immune systems as they present antigens to T cells. The renal resident dendritic cells mostly consist of TNF-secreting cells at the early phase of IRI-AKI. Moreover, the process of endothelium binding and

migration of dendritic cells might be facilitated during the initial renal inflammatory response after IR [82]. However, the dendritic cells show renal protective effect in the CIS-AKI mice model. The depletion of dendritic cells before and during cisplatin treatment, associated with more severe renal injury and greater mortality [83], which was different to IRI-AKI [84]. Further studies will be needed to extensively understand the role renal dendritic cells in the development of AKI.

The lymphocytes are main cells of the adaptive immune system, and they consist of nature killer (NK) cells, T cells, and B cells [85]. NK cells kill infected cells directly and secrete cytokines that facilitate the inflammatory process and active macrophages as well as neutrophils [86, 87], thus NK cells are expected to play a role in the initiation of AKI. The depletion of NK cells could attenuate renal injury after IRI [88], however, to fully understand the role of NK cells in AKI, more studies are required. The T cells show dynamic changes in amount and phenotype depend on the phase of IRI-AKI (Scheme 2). The $CD4^+$ T cells plays a role in inducing damage of renal tissue in the early phase of injury. The CD4-knockout mice showed less susceptible to IRI-AKI, and after the transfer of $CD4^+$ T cells, the CD4-knockout mice showed severe renal injury in the early injury phase of IRI-AKI [89]. Also, the $CD4^+$ T cells are important mediators in renal injury for CIS-AKI [90, 91]. As for the regulatory T cells, they play a role in renal regeneration and protection. Depletion of regulatory T cells exacerbated renal tubular damage, increased cytokine production, and reduced tubular proliferation, and adoptive transfer of regulatory T cells associated with improved repair and reduced generation of pro-inflammatory cytokines

in IRI-AKI [92]. The renal protective role of regulatory T cells also has been found in CIS-AKI [93, 94].

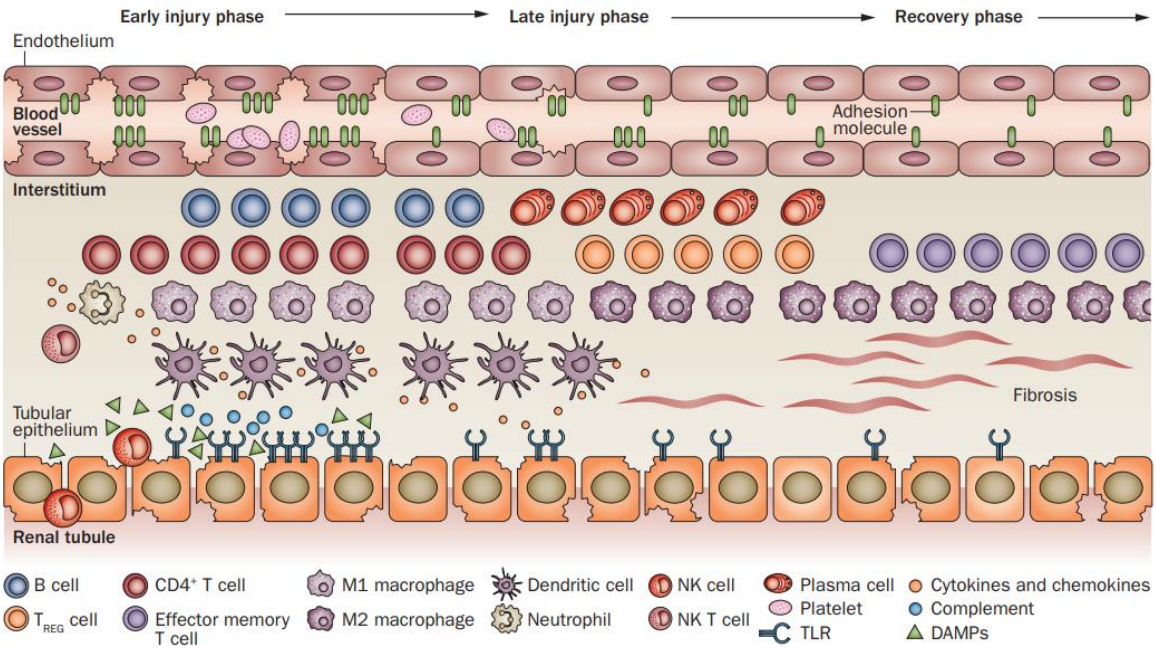

Scheme 3. Important immune cells in each phase of renal IRI. Neutrophils and NK T cells infiltrate into kidney at the early phase of injury and initiation of the inflammatory cascade. At the early and late injury phases, the amount of renal dendritic cells increases and are activated to mediate inflammation. Macrophages have multiple roles in the pathogenesis of renal IRI. At the injury phase, M1 macrophages induce inflammation and tissue injury; At the late injury and recovery phase, M2 macrophages exert anti-inflammatory functions and facilitate renal tubular regeneration during the recovery stage. T cells also show dynamic changes in number and phenotype depending on the phase of renal IRI. B cells are activated and differentiate in the injury phase, and limit tubular regeneration in the recovery phase (Adapted from [75]).

2.1.3. Role of oxidative stress in AKI

Oxidative stress plays a pivotal role in the pathophysiology of AKI. It well studied that the early burst of reactive oxygen species (ROS), which mainly come from mitochondria, are the dominant injurious effector upon reperfusion [95, 96]. Even there are other superoxide sources like the xanthine oxidase pathway and NADPH oxidases also play an important role in IRI-AKI, the activation of those pathways is occurred after the mitochondrial burst of superoxide formation [95, 97, 98]. After IR, the ROS which generated by mitochondria have been shown to act directly as a damage-associated molecular patterns (DAMPs), and the activation of innate and adaptive immune response by DAMPs further induce tissue damage [99]. A specific metabolic pathway of superoxide generation has been identified by Chouchani et al. recently (Scheme 4). They reported that the superoxide was generated through reverse electron transport at complex I of the electron transport chain. And this process was shown to be driven by the pool of the citric acid cycle metabolite, succinate, that accumulates during ischemia [100]. Mitochondria play an important role in the process of necrosis and apoptosis which underlie tubular injury and cell death following IRI [96]. The apoptosis pathway which associates with mitochondrial is characterized by the increasing of the permeability of outer mitochondrial membrane (MOMP) with the release of proapoptotic factors like cytochrome c. The released proapoptotic factors triggers the formation of the apoptosome which consist with cytochrome c, apaf-1 and caspase-9. The downstream caspase-activation pathways then are activated by the apoptosomes and finally result in apoptosis [101].

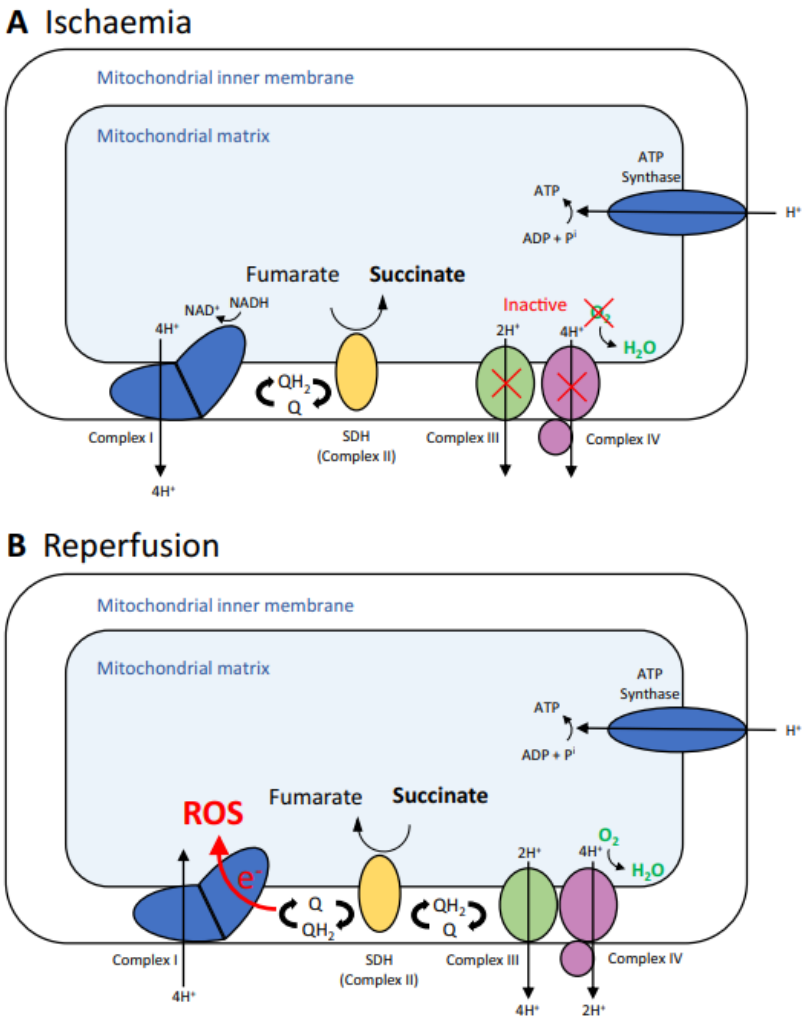

Scheme 4. Mitochondrial generation of reactive oxygen species (ROS) during IRI. Under normoxic conditions, the electron transport chain (ETC) transfers electrons from NADH and FADH2 to oxygen via a series of redox reactions. In this process, H+ is pumped out of the mitochondria generating a proton motive force. It is this proton motive that drives the production of energy, in the form of adenosine triphosphate (ATP), by ATP synthase. (A) During ischaemia, without oxygen to accept electrons, the ETC rapidly ceases and the electron donors and carrier pools such as NADH and coenzyme Q (CoQ) become maximally reduced. Mitochondria briefly compensate for this by the oxidation of

fumarate to succinate thereby replenishing the reduced carrier pools but generating a pool of succinate in the process. (B) On reperfusion, the succinate that accumulates during ischaemia is rapidly oxidised maintaining a reduced CoQ pool and an environment that favours reverse electron transport (RET) and the generation of ROS (Adapted from [99]).

2.1.4. Role of p53 in AKI

p53, a well-known tumor suppressor protein, has been reported has a much broader role in the development of a variety of human diseases [102]. p53 is a key component of the cell response to cells stress which including oncogene expression, DNA damage, hypoxia, ROS, and nutrient deprivation. In response to those cell stresses, p53 is rapidly induced and undergoes reversal post-translational modifications (PTMs) allowing for its stabilization and activation [102-104]. The pivotal role of p53 in the pathogenesis of AKI has been well studied in the past years (Table 1). p53 participates in the development of AKI and renal repairment is mainly through the regulation of apoptosis, cells cycle arrest, and autophagy (Scheme 5) [105]. p53 regulates different types of cell death such as apoptosis, necrosis, and ferroptosis [106-108], and renal tubular cell death which caused by p53 is the major contributor to the pathogenesis of AKI [109]. The mechanism of p53 induced apoptosis has been demonstrated in both CIS-AKI and IRI-AKI models. In cisplatin induced AKI, the pro-apoptotic protein p53 upregulated modulator of apoptosis (PUMA), executioner caspase-6 and -7, and p53-induced protein with a death domain (PIDD) are the primary mediators of p53 induced tubule cells apoptosis [105, 110, 111]. Following ischemia reperfusion, the PUMA, BCL2-associated X protein (BAX) and SIVA1 apoptosis inducing factor (SIVA1) are responsible for tubule cells apoptosis [112, 113]. Meanwhile, the translocation of p53 to mitochondrial during AKI has been reported [114] and the directly binding between p53 and BCL-2 family could directly induce cell apoptosis by activating the caspase cascade [115].

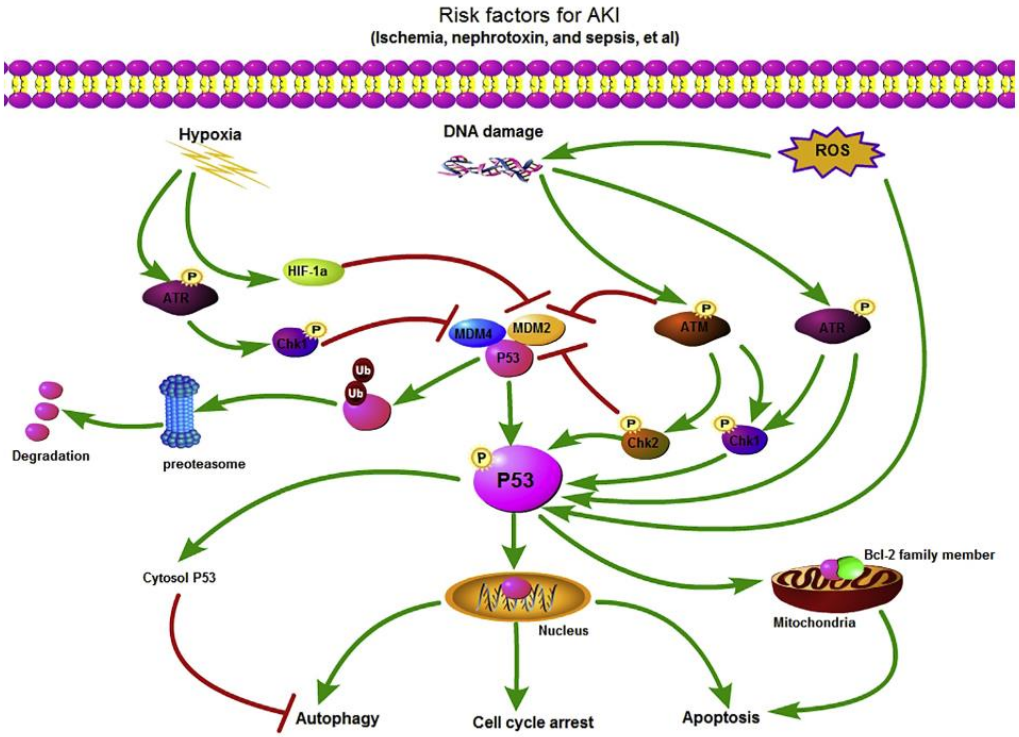

Scheme 5. Regulation of p53 in AKI development and progress to CKD. After renal insults, hypoxia, DNA damage, and/or ROS production in kidney cells subsequently activate p53 through phosphorylation. Upon activation, nuclear p53 transactive a wide range of genes involved in apoptosis, cell cycle arrest, and autophagy. Cytoplasmic p53 functions in a transcription-independent manner by its direct interactions with cytoplasmic proteins, such as apoptotic effectors (Adapted from [105]).

Table 1 (Adapted from [105])

Summary of animal studies on the effect of p53 inhibition in kidney injury and repair.

AKI model	Approach for p53 inhibition	Time of p53 deletion or inhibition	Effects on AKI and renalfibrosis	References
IRI in rat	p53 siRNA	Single dose at 4 h post IR	Attenuate AKI	[116]
IRI in mice	Targeted p53 deletion in RPTECs	Germline deletion by Pepck-cre	Attenuate AKI, reduce renalfibrosis	[117]
IRI in mice	Targeted p53 deletion in RPTECs	Germline deletion by Pepck-cre	Attenuate AKI	[113]
IRI in mice	Global p53 deletion	Germline deletion	Aggravate AKI and renalfibrosis	[118]
IRI in mice	Pifithrin-α	At the time of renal surgery andthen daily for 7 days	Aggravate AKI and renalfibrosis	[118]
IRI in mice	Chimeric mice lacking p53 in leukocytes	At the time of surgery and then dailyfor 7 days	Aggravate AKI and renalfibrosis	[118]
IRI in rats	Pifithrin-α	At day 14 after r surgery	Aggravate renalfibrosis	[119]
UIRI in mice	Pifithrin-α	At 4 h before cisplatin and then dailyfor 2 days	Aggravate renalfibrosis	[120]
IRI in rat	p53 siRNA	Germline deletion by Pepck-cre	Attenuate AKI	[116]
Cisplatin-AKI in mice	Targeted p53 deletion in RPTECs	A single dose at the same time of	Attenuate AKI	[113]
Cisplatin-AKI in mice	Pifithrin-α	cisplatin treatment	Attenuate AKI	[121]
Cisplatin-AKI in mice	Global p53 deletion	Germline deletion	Attenuate AKI	[121]
AA-AKI in mice	Global p53 deletion	Germline deletion	Attenuate AKI	[122]
AA-AKI in mice	Pifithrin-α	At the time of AA injection and thendaily for 3 days	Attenuate AKI	[122]
Glycerol-AKI in rats	Pifithrin-α	Before glycerol injection	Protection against AKI	[123]
VAN-AKI in mice	Global p53 deletion	Germline deletion	Protection against AKI	[124]

2.1.5. Role of CXCR4 in AKI

Inflammation is another significant pathophysiology component of AKI. Cytokines and chemokines were involved in response to nephrotoxicity or renal ischemia-reperfusion induced kidney injury. The renal expression of CXC chemokine receptor 4 (CXCR4) and its ligand stromal cell-derived factor (SDF-1) are greatly increased after AKI [125]. It has been demonstrated that SDF-1 plays as a chemotactic for a number of leukocytes, such as neutrophils, monocytes, and lymphocytes [126-128], those leukocytes are believed as the key mediators of kidney injury [129, 130]. It has been reported that CXCR4 express on hematopoietic stem cells (HSCs) which locate in the bone marrow. The interaction between CXCR4 and SDF-1 results in the retention of HSCs within the bone marrow [131, 132]. CXCR4 also expressed on endothelial progenitor cells (EPCs) [133]. Both HSCs and EPCs showed the renal protection effect in preclinical rodent models of AKI [134-138]. Using CXCR4 antagonist like AMD3100, could disrupt CXCR4/SDF-1 interactions, and mobilize HSCs from bone marrow into the systemic circulation [139], which may improve the treatment of AKI. A study from Zuk et al. showed that single injection of AMD3100 improved renal function as indicated by the improved renal histology, reduced vascular leak and cell death, and the reduction of proinflammatory cytokines and chemokines [140]. Either by local anti-inflammatory effects or by systemic stem cells mobilization, inhibition of CXCR4 shows great potential for AKI therapy. Moreover, the overexpressed CXCR4 on renal tubule cells in injured kidneys [125] may could be used as a target for the delivery of therapeutic agent for AKI treatment.

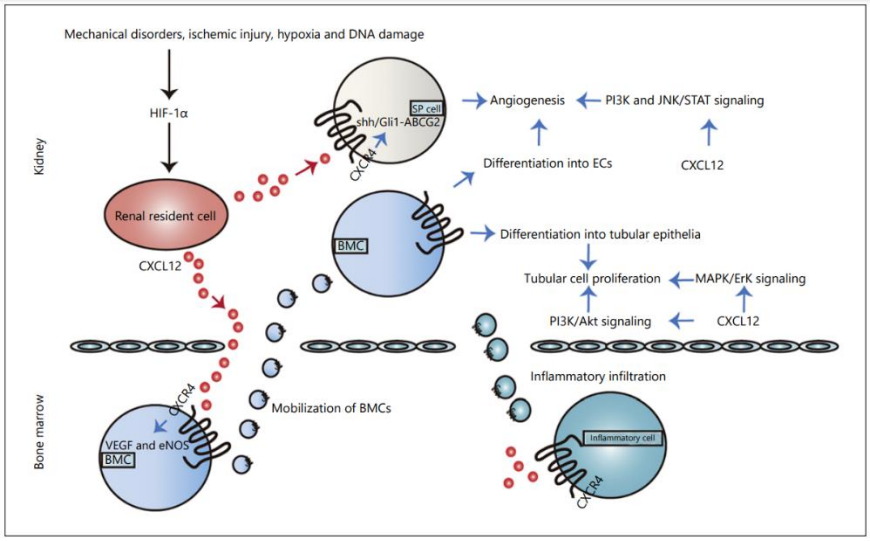

Scheme 6. Correlation between CXCL12 and AKI. Various pathological stimuli induce HIF-1α, which enhances the CXCL12/CXCR4 axis, ultimately improving AKI regeneration. On the one hand, the CXCL12/CXCR4 axis promotes angiogenesis by VEGF and eNOSmediated BMCs differentiation into ECs, SP cells-initiated recovery via Shh/Gli 1-ABCG2 pathway. In addition, diverse signaling pathways are also involved, such as PI3K and JNK/STAT signaling pathways. Additionally, the CXCL12/CXCR4 axis also increases tubular cell proliferation due to BMCs differentiation into the tubular epithelia and diverse pathways activation, such as PI3K/Akt and MAPK/Erk signaling pathways. Furthermore, CXCL12-induced inflammatory infiltration including neutrophils infiltration, T-cell depletion, and macrophage initiation is also involved in AKI. AKI, acute kidney injury; EC, endothelial cell; BMC, bone marrow-derived cell; eNOS, endothelial nitric oxide synthase; SP, side population; TEC, tubular epithelia cell (Adapted from [141], the final, published version of this article is available at http://www.karger.com/?doi=000514913).

2.2. Diagnosis, biomarkers, and management of AKI

Unlike another acute organ injures, AKI does not come with any immediate symptoms like chest pain, blindness, and dyspnea; thus, the diagnosis of AKI requires specific technical assessment. GFR has been used as an overall index of renal function for decades, and usually the GFR is measured by using serum markers, such as creatinine. However, the direct measurement of GFR is difficult, existing evidence indicate that worse outcome of AKI is associated with small increase of serum creatinine (Scr) [142, 143]. Meanwhile, urine output is another sensitive maker of renal function and tubular injury [144], but the relationship between GFR, tubular injury and urine output is complex [145]. According to the guideline of 2012 Kidney Disease Improving Global Outcome (KDIGO) for the diagnostic criteria of AKI and acute kidney disease (AKD), the adequate fluid resuscitation is no longer required to be performed before using the criteria, also the urinary obstruction is excluded [146]. Moreover, patients with chronic kidney disease (CKD) are pre-disposed to develop AKI, since CKD is an independent risk factor for AKI [147-151]. Nevertheless, the diagnosis of AKI from patients with CKD is difficult, due to the impaired renal function of those patients [152]. Patients with abnormal urine output and serum creatinine levels (62.1%) have a higher incidence of AKI than patients with abnormal serum creatinine levels alone (17.7%) [153, 154]. However, there are several limitations by using creatinine and urine as biomarkers for AKI, as (i) the serum creatinine levels increase only if the kidney lost 50% of the functional nephrons, and it has low sensitivity in healthy kidneys; (ii) the urine output has a low specificity because it can be influence by several factors, like hypovolemia and the use of diuretics [145]. After more

than a decade of intensive research, several novel biomarkers has been identified, including IL-18, kidney injury molecule 1 (KIM-1), neutrophil gelatinase–associated lipocalin (NGAL), and so on [155]. Those novel biomarkers were not listed in the 2012 KDIGO guidelines [146]. Although those biomarkers have a good predictive value, the clinical use is unclear and limitations are existing, such as the poor predictive performance if the timing of renal injury is unknown [156-158]. Different biomarkers relate to multifarious pathophysiological processes of AKI, and it might be helpful for detecting AKI earlier [159]. Those markers might be critical for developing targeted therapy for AKI patients and for clinical trials designing.

As one of those novel biomarkers of AKI, NGAL is a widely expressed 25-kD protein of the lipocalin family, and released by the kidney and immune cells [160]. The levels of urine NGAL are very low in healthy individuals. However, after ischemic or nephrotoxic kidney injury, the NGAL levels in plasma and urine are increase dramatically, indicating a role of NGAL for the kidneys that is comparable to that of troponin for the heart [161]. In children who undergoing congenital heart surgery, NGAL has been shown to have high sensitivity and specificity for predicting AKI [162]. However, when patients have different comorbidities, NGAL have been shown limited predictive performance, it might because immune cell derived NGAL is not necessary for AKI predicting [163, 164]. NGAL has a good prediction value for AKI only when patients with a previously normal kidney function, hence it can be used in patients who has normal renal function and a well described kidney insult or in patients with precedent CKD [161, 165, 166].

Another one of the well-studied novel biomarkers called KIM-1, which is a 38.7-kD transmembrane protein [167]. The expression of KIM-1 is low in the healthy kidneys, however, after ischemia-reperfusion injury, the expression of KIM-1 is upregulated. After 48 hours of injury, the over expressed KIM-1 can be localized to the proliferating dedifferentiated epithelial cells of the proximal tubule [167]. Moreover, the role of KIM-1 is more than a marker for kidney injury, it might have a functional role in the molecular and cellular biology of AKI. In cultured primary kidney cells, the expression of KIM-1 could promote the phagocytosis of apoptotic cells and necrotic debris, thus it has been proposed that KIM-1 might play a role in kidney recovery and regeneration after AKI [168]. KIM-1 alone may not be able to diagnosis AKI with high accuracy because the increased urinary KIM-1 may indicate either injury or the repair response of renal injury, and the combination of KIM-1 with other biomarkers may provide a highly useful way for AKI diagnosis. A study in 2014 has shown the combination of KIM-1 and IL-18 had the best ability to predict severe AKI with an correlation coefficient = 0.93 [169].

3. The application of nanomedicine in AKI

With the extensive effort in the mechanistic research of AKI, several chemical and biological agents have been proved to have therapeutic benefit in the preclinical AKI models [170, 171]. However, the poor bioavailability limits most potential drugs application in AKI, for example some drugs are highly hydrophobic, and some of them are easily degradable in vivo before reach to the target. Moreover, most small molecules and some biological drugs are cleared from kidney very quick and cannot achieve desired therapeutic effect in the injured kidneys. Thus, high doses are usually required and may cause undesired side effects [172]. Nanomedicine might be a game changer for AKI treatment due to one of the most common uses of nanomedicine is in the delivery and controlled release of therapeutic molecules. Nanomedicine holds the greatest for the change of drug pharmacokinetics [173]. The engineered nanomaterials have been used to incorporate small molecule drugs as well as macromolecule drugs such as nucleic acids, proteins, and peptides. One of the advantages of encapsulating drugs in nanoparticles is the suspension of insoluble drugs [174]. Nanoparticles with specific tissue or cells targeting ability would allow for reduction of off-targeting side effects. The targeting ability often achieved by using molecular recognition entities, such as small molecules, peptides, antibodies, and nucleic acids which may chemically or physically attached to or coat nanoparticles [175, 176]. This part focuses on recently developed novel nanoparticles for AKI treatment and discuss the engineered nanocarriers with kidney targeting ability that can deliver therapeutic reagents to kidneys for enhanced AKI therapy. Finally, discuss the future directions of nanomedicine in the application of AKI therapy.

3.1. Passive targeting and active targeting

Based on the physiochemical properties, the targeted delivery can be divided to categories: passive targeting and active targeting. Both targeted delivery methods have significant effects on enhanced therapeutic efficacy and reduced side effects by specifically delivering the therapeutic agents to the targets [177]. For passive targeting, the distribution of formulation in the sites of interest mainly depends on their size, charge, and molecular weight. This is due to at the site of interest like tumor and inflammation, the endothelium of blood vessels (a typical biological barrier for nanomedicine) changes with higher permeability than in the normal condition, which gives nanoparticles with specific size to pass through and reach to the site of interest [178, 179]. For renal delivery, due to the specific biological structures of kidney (as mentioned in the section of renal anatomy), in addition to vascular endothelium, the biological barriers also include the GFM which also plays a pivotal role in renal passive targeting. Generally, formulations sized less than 10 nm or with molecular weight lower than 70 kDa are easily filtrated through GFM to access tubules [180, 181]. Nanoparticles with size from 10 nm to 130 nm are mostly accumulated in glomeruli after diffusing through the glomerular vasculature [182, 183]. As for particles with larger size (200-400 nm), they can access the proximal tubule by secretion [184]. The charge of nanoparticles is another important factor for passive targeted delivery, due to the negatively charge of GFM, particles with positive charge generally show higher renal accumulation [179, 181, 185, 186]. However, a high level of surface positive charge may associate with nonspecific protein binding [187]. Hence, it is necessary to balance the surface change of particles for enhanced drug delivery.

Active targeting is achieved by introducing the delivery systems with specific ligands which receptors are overexpressed by the target cells [177]. Through active targeting, the specific interaction between ligands and receptors would enhance the endocytosis of nanoparticles and ultimately increase the efficiency of drugs when compare with free drug or passive targeted delivery. In the development of AKI, there are several receptors over expressed in the injured renal cells, such as CXCR4 [125], CD44 [188-191], KIM-1 [192], megalin [180, 193-195], and so on. The ligands for those receptors could be utilized in the design of targeted delivery system for the treatment of AKI. During the circulation, passive targeting can help the formulation to cross the biological barriers before it reaches to the targets for subsequent active targeting. Thus, the combination of passive and active targeting gives the best targeting ability for therapeutic drug delivery, and this strategy has been widely used in the design of kidney targeted delivery for AKI therapy.

3.2. Targeted drug delivery systems for AKI therapy

As mentioned earlier, renal tubular injury is one of the main pathological mechanisms that cause AKI. Thus, renal tubule cells are the main targeting site for the design of drug delivery carriers. The biological structure of kidney decides that the drug delivery systems can reach tubule cells by two ways: from the apical or the basolateral side [196]. For the main way, apical side, formulations need to pass the glomerular filtration barriers, like GFM, podocytes, and endothelial cells, then reach the tubule lumen. Under injury conditions, the size restrictions for drug delivery systems will be relaxed due to the enlarged pore in GFM and the loss of podocytes and endothelial cells [197]. As

for the basolateral side, formulations get uptake by proximal tubular cells mainly by penetrating through the endothelial cell of the peritubular capillary [184]. This part is focus on the introduction of several novel advanced renal targeting delivery systems for AKI therapy.

3.2.1 Targeted delivery for antioxidant therapy

Renal cleared materials hold a great potential for renal targeted drug delivery as they can easily pass the glomerular filtration barriers and reach to tubule cell through the apical side. Moreover, some of the ultrasmall particles are composed elements with a readily variable valence state which have the antioxidant ability, such as molybdenum [198], copper [199], and cerium [200]. As mentioned earlier, oxidative stresses play pivotal role in the pathophysiology of AKI. Thus, formulations with ROS scavenging ability are beneficial for applying in the treatment or prevention of AKI. A study from Ni et al. showed a novel multi-antioxidant in the form of POM nanoclusters for antioxidative therapy of AKI in living animals. Those hydrodynamic size of those particles were 10 nm and the particles showed a high level and a long period (>24 h) of accumulation in the injured kidneys. The POM nanoclusters exhibited broad antioxidative activities against multiple toxic ROS from both in vitro and in vivo studies. Based on the renal targeting and ROS scavenging abilities, POM nanoclusters could effectively attenuate AKI and restore renal functions in AKI mice [201]. A type of ultrasmall iridium nanoparticles which were coated with polyvinylpyrrolidone (Ir NPs-PVP) has been reported by Zhang et al. Iridium based nanoparticles showed multienzyme activities including peroxidase,

superoxide dismutase, and catalase, which help maintain cellular redox balance. This kind NPs-PVP showed rapid accumulation in both healthy and injured kidneys, and longer retention was observed in the injured kidneys. Moreover, the NPs-PVP had the ability to alleviate rhabdomyolysis- or cisplatin-induced AKI [202]. In addition of spherical nanoparticles, some other formulation with different shapes also showed favorable renal accumulation and ROS scavenging ability, such as DNA origami and black phosphorus nanosheets (BPNSs) which is a novel material can be oxidized into phosphorus oxides and has the potential to decrease cellular ROS level [203-205]. Hou et al. showed the BPNSs can significantly accumulated in the injured kidneys which because the flake-like structure. And due to the ROS scavenging ability of BPNSs, it ultimately relieved AKI [203]. The ROS sensitivity of DNA bases has been reported, and can be oxidized after interacting with ROS, thus it can be used ROS scavenger. A study from Jang et al. showed the delivery of DNA origami nanostructures (DONs) can clear ROS in the injured kidney (especially the renal tubules) and finally attenuated AKI [204].

Except ultrasmall particles, some other macromolecular materials are also easily cleared from kidney, such as lysozyme, immunoglobulin, and insulin which are endogenous low molecular weight proteins [206]. Also, polymers like low molecular weight chitosan (LMWC) have been reported as a kidney-targeted material due to the interaction with megalin [180]. Directly conjugation of therapeutic drugs to LMWC might improve their renal accumulation due to the targeting ability of the carriers. Liu et al. modified chitosan with L-serine and they found this polymer can rapidly accumulate in kidneys and has a long retention time in injured kidneys, especially in renal tubules,

which may because the specific interaction between KIM-1 and serine. Based on the favorable renal targeting ability of serine modified chitosan, they then continued conjugate a mitochondrial-targeted antioxidative peptide (SS-31) to form a chitosan-based prodrug for AKI treatment. In their study, this prodrug successfully attenuated IRI-AKI through the antioxidant effect of SS-31 [192]. Another SS-31 based nanoparticle developed by the same group also showed excellent therapeutic effect for AKI. In this study, they encapsulated SS-31 with chitosan and hyaluronic acid (HA) through electronic attraction. CD44 is over expressed on renal tubule cells after kidney injury, and due to the specific interaction between HA and CD44, the nanoparticles showed high accumulation in the injured kidneys. Moreover, the treatment successfully relive kidney injury due to the antioxidant effect of SS-31 [189].

3.2.2 Targeted delivery of p53 siRNA for anti-apoptosis therapy

As mentioned before, p53 induced apoptosis has been reported that play a pivotal role in the pathogenesis of AKI. Acute inhibition of p53 can greatly inhibit cell apoptosis and holds a great potential for AKI therapy. Bruce et al. treated p53 siRNA to IRI-AKI and CIS-AKI rats through hydrodynamic injection for AKI attenuation. The results showed the successfully p53 downregulation and it associated with improved renal function [116]. RNA interference (RNAi) has been acknowledged as a promising novel therapeutic strategy through gene regulation. The mechanism of RNAi involves the specific targeting of messenger RNA (mRNA) with complementary small interfering RNA (siRNA) resulting mRNA degradation. Thus, siRNA-based therapeutics can mute genes that

regulate disease and injury temperately and holds great therapeutic potentials. However, due to the poor serum stability and off-target effects, its necessary to develop siRNA carriers that can overcome these obstacles in vivo for siRNA delivery. One of the representative renal siRNA delivery systems is ammonium-functionalized signal-walled carbon nanotubes (fCNTs), this kind materials have a very favorable renal glomerular filtration characteristic, and part of the filtrated fCNTs are reabsorbed by the renal proximal tubular cells [207]. A study from Simone et al. showed that the fictionized fCNT could selectively deliver siRNA to the renal proximal tubule cells with high efficiency in animal models with AKI. Compare to free siRNA, the enhanced delivery with fCNT allowed effective downregulation of several target genes, including Trp53, Mep1b, Ctr1, and EGFP. In the cisplatin included AKI mice model, the treatment with a combination of fCNT/siTrp53 and fCNT/siMep1b significantly improved the progression-free survival when compared with to controls via the reduction of meprin-1β and p53 expression. Moreover, the fCNT/siRNA didn't show toxicological consequences and the rapid pharmacokinetic profiles was observed in primates, suggests that this technology is amenable for use in patients for the prevention of AKI to safely overcome the nephrotoxicity during medical intervention [208]. A recent study from Thai et al. reported that the potential of small-sized DNA tetrahedrons (sTds) for renal siRNA delivery. They prepared four sTds with different sugar backbones, and the biodistribution study showed that the small-sized L-DNA tetrahedron (L-sTd) is the one has most preferential localized into the kidney. After loading p53 siRNA on L-sTd, the formulation can successfully

deliver p53 siRNA to kidney and uptake by the kidney cells. The downregulation of p53 was finally attenuate renal injury [209].

Chapter 2. Selective siRNA delivery to injured kidneys for combined p53 and CXCR4 inhibition in the treatment of acute kidney injury

1. Introduction

Acute kidney injury (AKI) is characterized by a sudden loss of renal function and is associated with high morbidity and mortality [210-212]. Each year, AKI affects over 13 million people worldwide and leads to about 2 million deaths [213]. AKI may be caused by various insults including nephrotoxins, ischemia-reperfusion, and sepsis. Importantly, AKI has the potential to develop into chronic kidney disease [214] and ultimately result in kidney failure [29]. Despite considerable advances in basic research and the growing understanding of the underlying pathophysiology, AKI remains a significant unmet medical need without effective pharmacological treatments [17]. Clinically, the management of AKI mostly relies on renal dialysis or transplantation, which come with a considerable cost and unacceptable mortality [28, 215, 216]. Thus, the development of effective therapies for AKI is necessary and urgently needed.

Inflammation is a complex biological response that is essential for the elimination of microbial pathogens and repairing of injured tissue, as well as a major pathophysiological component of AKI [217]. Inflammatory mediators, such as cytokines and chemokines, are released from activated or injured renal cells, which attract leukocytes to the injury sites, leading to a pro-inflammatory microenvironment [218-220]. C-X-C chemokine receptor 4 (CXCR4) plays a vital role in the inflammatory process [221-224]. After binding with its ligand, stromal cell-derived factor-1 (SDF-1, also known as CXCL12), divergent

intracellular signaling transduction pathways are activated and lead to a variety of responses such as chemotaxis, cell proliferation, recirculation, and hematopoiesis of leukocytes [225, 226]. Growing evidence shows that CXCR4 and SDF-1 are involved in the pathology of AKI [223]. The CXCR4 axis is implicated in regulating trafficking and invasion of inflammatory cells into the injured kidneys. Sustained high expression of CXCR4 in tubules and leukocytes exacerbates the pathology of AKI and contributes to the formation of renal fibrosis. CXCR4 inhibition appears to have beneficial therapeutic effect in experimental AKI animal models, either by local anti-inflammatory effects or by a systemic stem cell-mobilization dependent mechanism [227, 228]. For example, the treatment with a CXCR4 antagonist AMD3100 (Plerixafor) before and after bilateral renal ischemia ameliorated kidney injury [228] as well as attenuated renal fibrosis [227]. Based on that evidence, the inhibition of the CXCR4/SDF-1 axis shows exciting potential as a promising therapeutic method for the treatment of AKI.

One of the most well-known tumor suppressor proteins, p53, has received increasing attention as a therapeutic target in AKI [229]. There are several main factors associated with the activation of p53 during AKI, including DNA damage, hypoxia, and generation of reactive oxygen species (ROS) [229, 230]. The role of p53 in regulating different types of cell death has been reported, including apoptosis, necrosis, and ferroptosis [231-233]. Linkermann et al. have demonstrated that p53-dependent cell death is the major contributor to the pathogenesis of AKI [234, 235]. In cisplatin (CIS) injury model, p53 was phosphorylated and upregulated early during CIS treatment. Inhibition of p53 by pifithrin-α or dominant negative mutant p53 significantly attenuated CIS-induced

apoptosis [236, 237]. Additional recent studies have demonstrated the beneficial effect of p53 inhibition in AKI models [238-242]. The involvement of p53 in renal ischemia-reperfusion injury (IRI) was first described by Kelly et al., who showed that p53 expression was upregulated 24 h post IRI, and the chemical inhibition of p53 by pifithrin-α resulted in the protection of renal functions in a rat model [243]. Targeting of p53 by using short interfering RNA (siRNA), is a viable tactic to prevent or treat AKI as it protects proximal tubule cells (PTCs) and renal function [238]. Also, siRNA-mediated inhibition of p53 target TIGAR, prevents IRI by restoring glycolysis in the ischemic kidney and protects the kidneys from functional and histological damage [244]. These results offer compelling support for the critical role of p53 in the pathogenesis of AKI, and its role as a therapeutic target in AKI.

Although free siRNA displays natural renal tropism, there are several pharmaceutical challenges to the use of free siRNA in the treatment of AKI. The strong negative charge and macromolecular character of siRNA results in a poor ability to cross cell membranes and locate to its site of action in the cytoplasm. This, in turn, required a "hydrodynamic" dosing of large amount of free siRNA (12 mg/kg body weight) to achieve the desired gene silencing effect [238]. Furthermore, as a potent activator of the innate immune system, the large doses of free synthetic siRNA increased the likelihood of adverse immunostimulatory effects [245]. siRNA delivery vehicles could overcome those challenges by protecting siRNA during systemic circulation and improve intracellular delivery, thus minimizing the required siRNA doses [245-247]. Several approaches have been reported to improve the renal siRNA delivery using synthetic and natural polymers.

We reported that negatively charged or neutral polymers with low or intermediate molecular weight selectively accumulate in the AKI kidneys [248]. Low molecular weight chitosan has been one of the most widely used polymeric carriers for renal delivery of siRNA and drugs. A chitosan-based siRNA delivery system and N-acetylated chitosan could specifically target to kidneys [249, 250]. Yang et al. prevented kidney damage by using chitosan/siRNA nanoparticles [251]. Besides chitosan, other polymeric nanoparticles also hold strong potential for drug/siRNA delivery to the kidney. Poly(lactic-co-glycolic acid) (PLGA) nanoparticles with a diameter ~100 nm could selectively accumulate in injured mouse kidneys. The Oltioraz-loaded PLGA nanoparticle effectively reduced tubule necrosis in the ischemic AKI mouse model [252]. Interestingly, the PEG modified PLGA mesoscale nanoparticles (MNP) were selectively localized in renal proximal tubules after intravenous injection while avoiding the typical hepatic distribution. Treatment with MNP loaded with toll-like receptor 9 (TLR9) antagonist effectively attenuated renal injury [253-255]. Alidori et al. demonstrated that ammonium-functionalized single-wall carbon nanotubes could deliver Trp53- and Mep1b-targeted siRNA to PTCs and decreased renal injury in a CIS-induced AKI mouse model [256]. Successfully delivery of p53-targeted siRNA to tubule cells was reported using small-sized mirror DNA tetrahedrons (sTds), and the treatment attenuated AKI [257].

In the present study, we hypothesized that combining CXCR4 targeting and inhibition with downregulation of p53 expression in the injured kidney could not only improve selectivity of the delivery but also significantly alleviate AKI because of the established role of CXCR4 and p53 in AKI pathology (Scheme. 7). We have used

previously reported polymeric CXCR4 inhibitors (PCX) that showed effective siRNA delivery ability and strong CXCR4 inhibition [258] to evaluate their properties in vitro, renal accumulation in AKI mouse models, and therapeutic potential of their polyplexes with p53 siRNA (sip53).

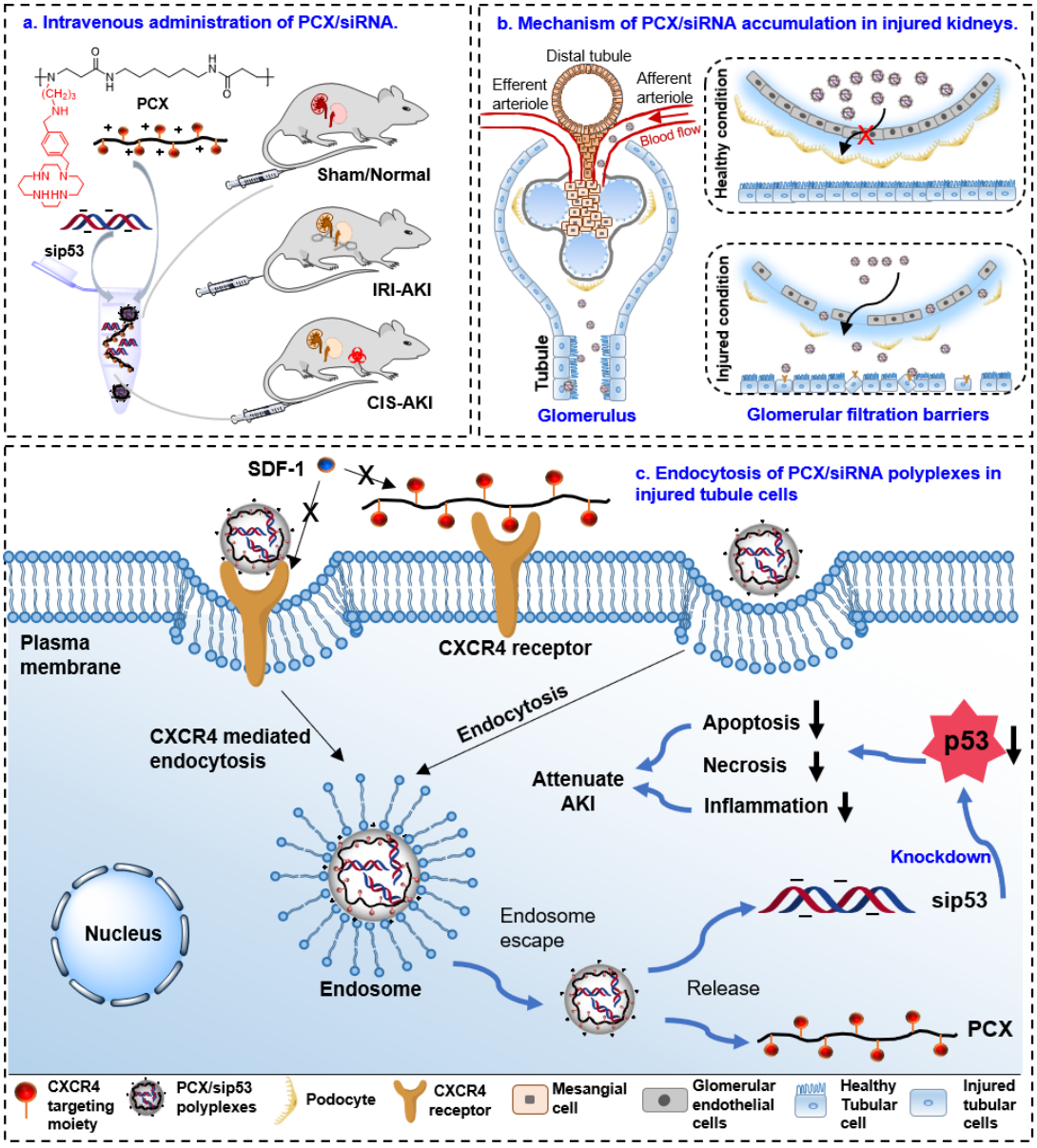

Scheme 7. Selective accumulation and proposed mechanism of action of PCX/sip53 polyplexes in the treatment of AKI.

2. Results

2.1. Formulation and characterization of PCX/siRNA polyplexes

We have previously developed several types of PCX that act as inhibitors of CXCR4 and demonstrated their advantageous activity as part of combination treatments of multiple cancers [259-265]. The PCX can be synthesized as either branched or linear polycations. In this study, we have used the linear PCX that was synthesized by Michael addition copolymerization of phenylene-cyclam derivative with hexamethylenebisacrylamide (Figure 1). The composition and molecular weight of PCX were characterized by ^{1}H NMR (Figure 2) and gel permeation chromatography. The PCX used in the present study had a weight-average molecular weight of 5.9 kDa and dispersity (Đ) of 1.2. The Đ was lower than expected for this type of polymerization due to dialysis purification step, which removed the lower molecular weight fractions and narrowed the molecular weight distribution.

Electrostatic complex formation of PCX with siRNA was first evaluated by gel retardation assay. Polyplexes were prepared by adding PCX solution to siRNA solution at increasing PCX/siRNA (w/w) ratios (Figure 3A). PCX fully complexed the siRNA at w/w ratios ≥ 2. Partial condensation was observed at lower w/w ratios (0.5-1) as indicated by the smear siRNA band in the gel. The hydrodynamic size and zeta-potential of PCX/siRNA polyplexes prepared at w/w ratios of 2, 5, and 10 were measured by dynamic light scattering (DLS) (Figure 3C). The polyplexes prepared at w/w of 2 showed a relatively large size (~300 nm) and were deemed unsuitable for renal delivery. The size

significantly decreased when we increased the w/w to 5 (~127 nm) and 10 (~107 nm). The polydispersity index of the particle size distribution was less than 0.2 for all the tested w/w ratios. As expected, due to the excess PCX adsorbed on the surface of the polyplex nanoparticles, increasing the w/w ratio resulted in an increase of the zeta-potential. The shape and morphology of PCX/siRNA polyplexes were analyzed by transmission electron microscopy (TEM). All the polyplexes had a spherical shape, and higher w/w ratios resulted in smaller sizes, which was in full agreement with the DLS results (Figure 3D).

An ideal siRNA delivery system not only requires stable interactions between siRNA and the carrier during systemic circulation, but also the ability to pass through biological barriers before reaching its cytoplasmic target. One obstacle for nanoparticles to reach the tubule cells is the glomerular filtration barrier (GFB) which consists of glomerular endothelial cells, the glomerular basement membrane (GBM), and the podocyte filtration slits. In those three layers that form GFB, GBM is a 300-nm tissue membrane which consists of abundant heparan sulfate and plays a role in the disassembly of polycation-based nanoparticles [266]. Most of siRNA polyplexes usually have a short blood circulation times due to rapid renal clearance and phagocytic uptake. The renal clearance of polyplexes is most likely due to their binding and disassembly by the heparan sulfate in GBM [266-268]. The concentration of heparin in human plasma is 1 - 2.4 μg/mL [269], which may also contribute to dissociation of polyplexes during the systemic circulation. The sensitivity of the PCX/siRNA polyplexes to heparin-medicated polyelectrolyte exchange was thus analyzed by a displacement assay. Briefly, PCX/siRNA polyplexes (w/w 5) were incubated with different concentrations of heparin for 30 min. As shown in

Figure 3, the polyplexes completely released siRNA at ≥ 80 μg/ml of heparin, which indicated PCX protection against the influence of plasma heparin.

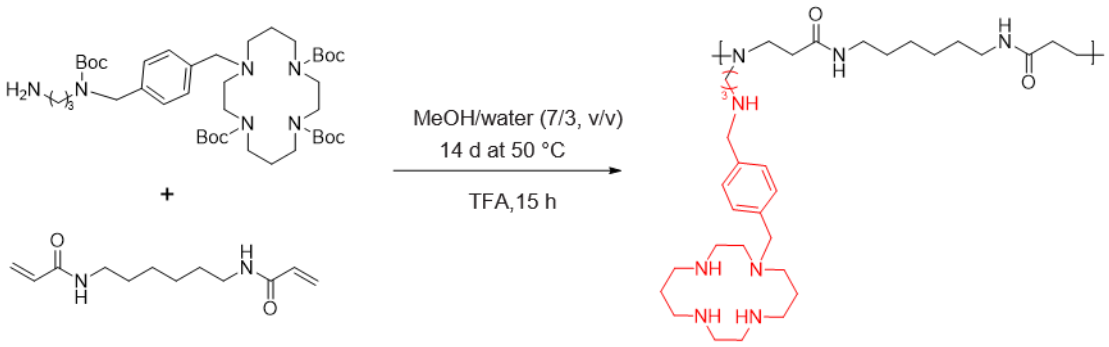

Figure 1. Synthesis of PCX.

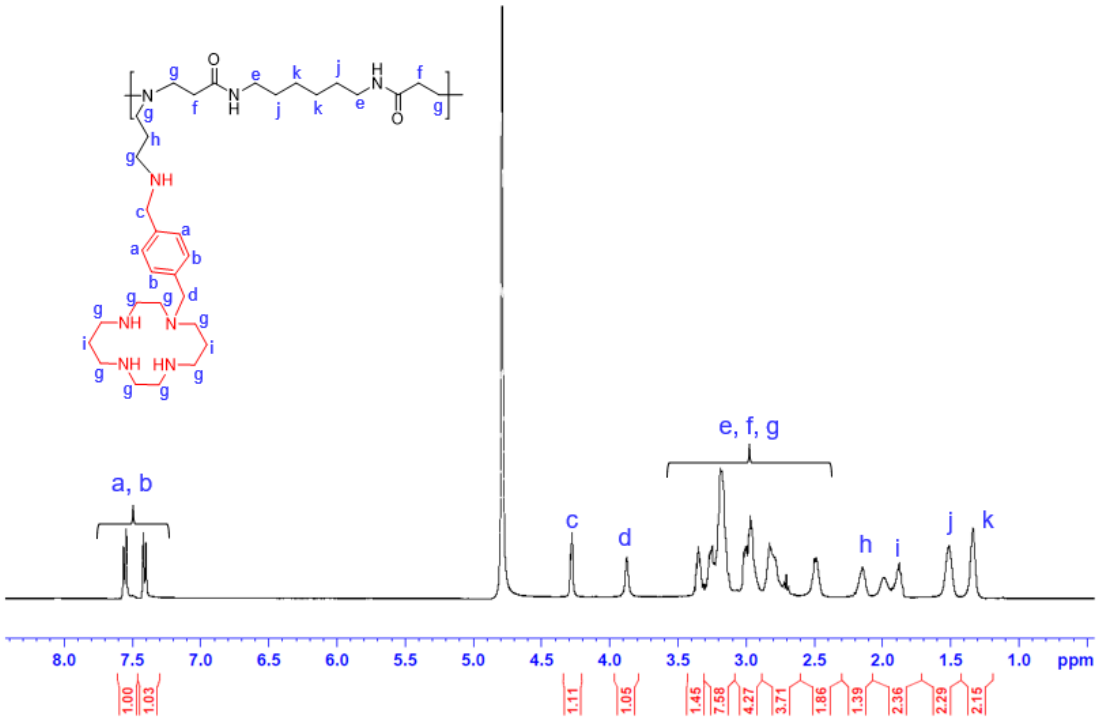

Figure 2. ^{1}H-NMR spectrum of PCX.

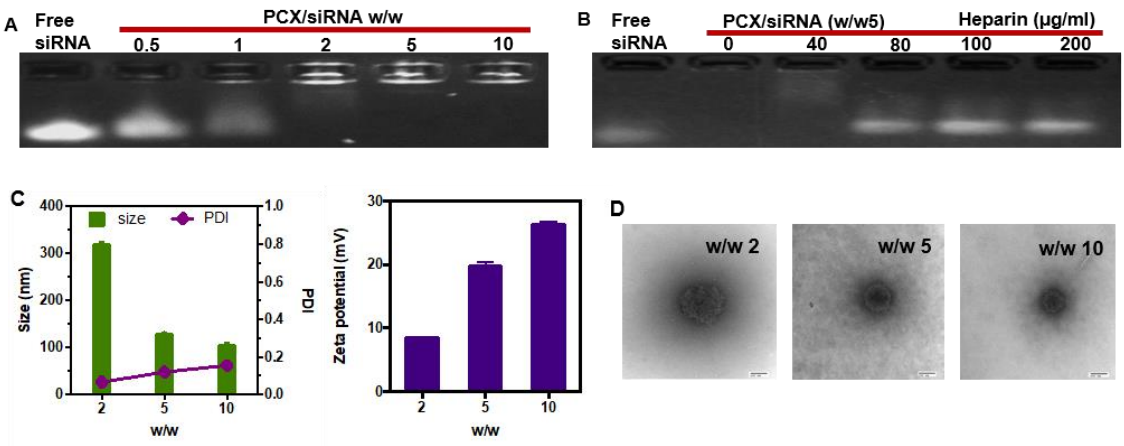

Figure 3. Physicochemical characterization of PCX/siRNA polyplexes. (A) siRNA condensation by PCX in 10 mM HEPES buffer (pH 7.4) using agarose gel electrophoresis. (B) Heparin induced siRNA release from the polyplexes. The polyplexes were prepared at w/w 5 and incubated with increasing concentration of heparin for 1 h at room temperature. (C) Hydrodynamic size and zeta potential of PCX/siRNA polyplexes at different w/w. (D) Representative TEM images of PCX/siRNA polyplexes at w/w 2, 5 and 10. Scale bar, 100 nm. (Please note this study was performed by Dr. Yi Chen and data were adapted from [270])

2.2. In vitro cytotoxicity and cellular uptake of PCX/siRNA polyplexes in tubule cells

We confirmed the CXCR4 antagonism of PCX by using a receptor redistribution assay described in our previous studies (Figure 4). As expected, PCX displayed CXCR4 antagonism with a complete inhibition seen at 2 μg/mL. Toxicity associated with the use of polycations remains a major concern for their application as siRNA delivery vectors. We have measured cytotoxicity of PCX and PCX/siRNA polyplexes in human tubule cell line HK-2. PCX was incubated with the cells for 24 h and the IC50 value was calculated from cell viability data as 9 μg/mL (Figure 5). The cytotoxicity of the PCX/siRNA polyplexes prepared at w/w 5 was measured at 50-200 nM siRNA concentration range. As shown in Figure 5B, the PCX/siRNA polyplexes were safe up to 100 nM siRNA, with cell viabilities exceeding 90%. Elevated cytotoxicity was observed at 150 and 200 nM siRNA.

We next examined the efficacy of the siRNA delivery to HK-2 cells in vitro. Fluorescently labeled PCX (PCX-Cy3) and siRNA (siRNA-Cy5.5) were used in this study to visualize the cellular uptake. Confocal microscopy showed both PCX-Cy3 (red) and siRNA-Cy5.5 (green) were effectively internalized by the cells (Figure 6). Flow cytometry analysis showed that 89% of the HK-2 cells internalized both PCX and siRNA (Figure 6). Both experiments suggested that PCX could deliver siRNA into HK-2 cells effectively. We next studied the transfection activity of the polyplexes in HK-2 cells. PCX/siRNA polyplexes were prepared with 50 nM of p53 siRNA, and incubated with HK-2 cells for 48 hours. At the end of incubation, cells were harvested and the mRNA level of p53 was evaluated by RT-PCR. As shown in Figure 7, the PCX/sip53 polyplexes downregulated

the expression of p53 mRNA (30%), as compared with PBS and scrambled siRNA (siScr) control which showed no effect. Those results confirmed that PCX/siP53 nanoparticles could effectively deliver functional sip53 into HK-2 cells and downregulate the mRNA level of p53.

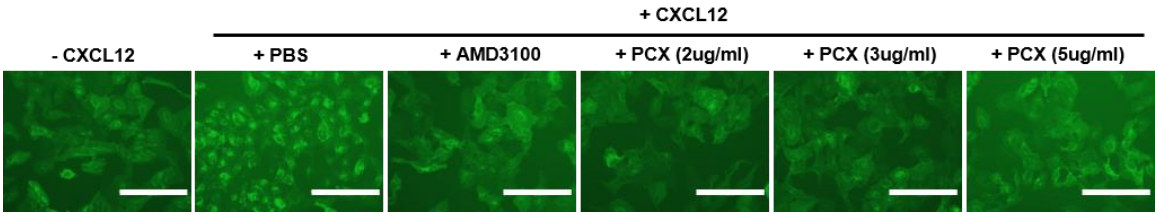

Figure 4. CXCR4 antagonism of PCX vs. AMD3100. CXCR4 redistribution assay in U2OS cells expression GFP-tagged CXCR4 (green). Scale bar = 200 μm.

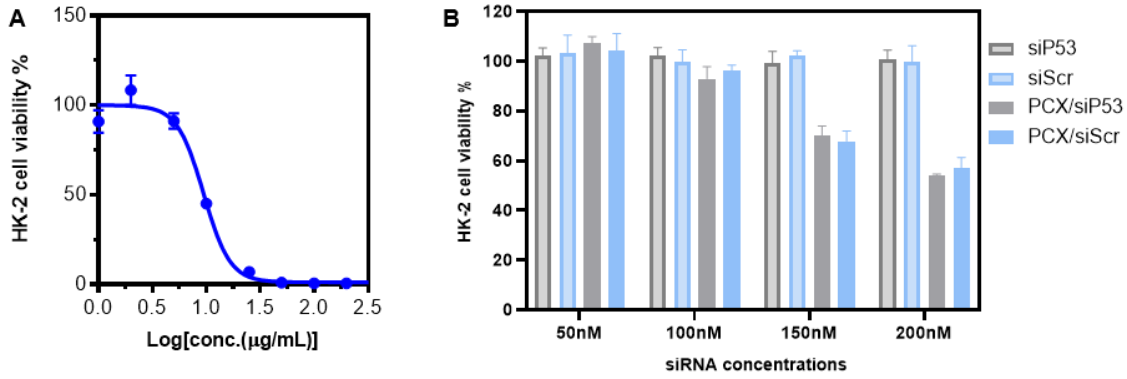

Figure 5. Cytotoxicity of PCX and PCX/siRNA polyplexes in HK-2 cells. (A) Cytotoxicity of PCX in HK-2 cells. (B) Cytotoxicity of PCX/siRNA polyplexes in HK-2 cells at different siRNA concentrations (w/w 5).

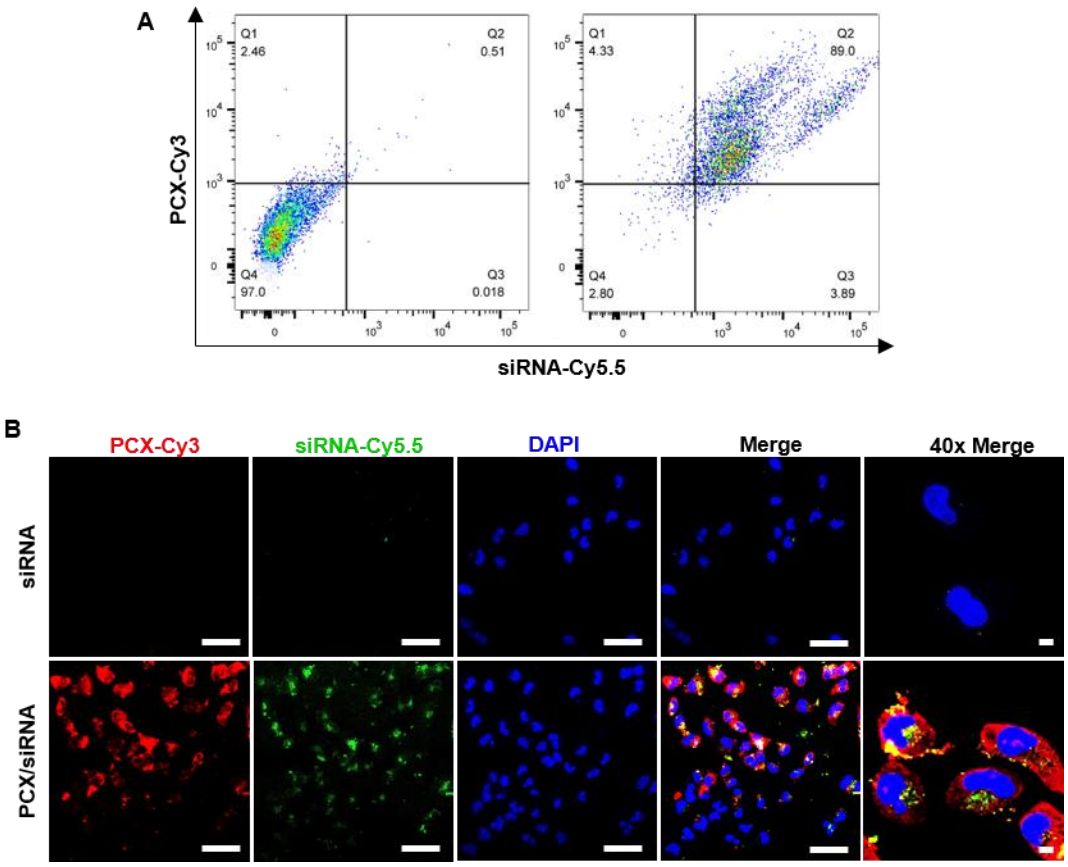

Figure 6. Cellular uptake and in vitro transfection effect of PCX/siP53 in HK-2 cells. (A) Flow cytometry analysis of HK-2 cells treated with PCX-Cy3/siRNA-Cy5.5 for 4 h. (B) Confocal microscopy observation of cellular uptake of PCX-Cy3/siRNA-Cy5.5 polyplexes in HK-2 cells after 4 h of incubation. SiRNA = 50 nM. Scale bar, 20 μm.

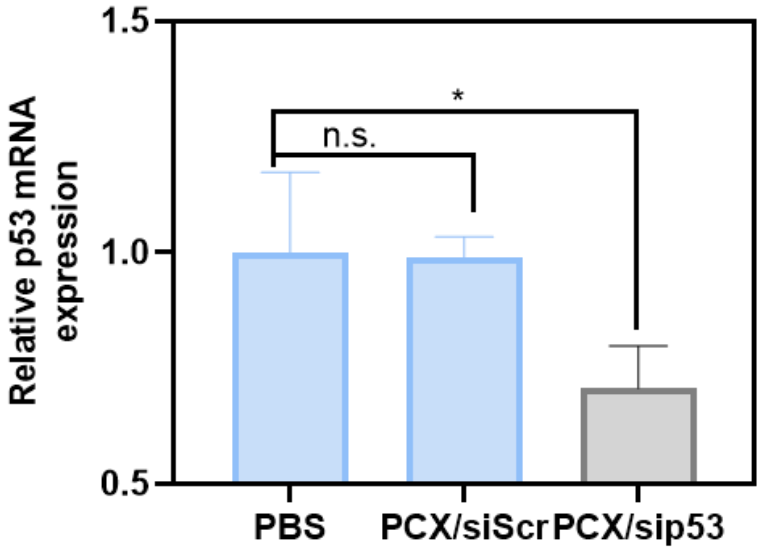

Figure 7. Transfection effect of PCX/siP53 in HK-2 cells. Cells were treated with PCX/siP53 at 25nM of siP53 (w/w 5). n = 3, *p < 0.05, n.s.=no significance difference, as compared with PBS group.

2.3. Upregulation of p53 and CXCR4 in CIS injury model in vitro

We first established the in vitro CIS-induced cell injury model in HK-2 cells. To find optimal conditions for cell injury, the cytotoxicity of CIS in HK-2 cells was evaluated and 5 μM concentration selected as suitable due to its about 50% decrease in cell viability (Figure 8). The effect of CIS on the expression of p53 and CXCR4 was measured by qRT-PCR (Figure 9A and B). The expression of both p53 and CXCR4 mRNA increased significantly with increasing CIS dose. Increased surface CXCR4 receptor expression after CIS injury was also confirmed by flow cytometry (Figure 9). The surface CXCR4 staining increased with increasing CIS incubation time from 19% positive cells at 12 h, to 32% at 24 h, and 75% at 48 h.

After confirming that CIS causes upregulation of both of our therapeutic targets in tubule cells, we next assessed the potential involvement of the CXCR4 receptors in the tubular cell uptake of the PCX/siRNA polyplexes using fluorescently labeled PCX (PCX-Cy3). Cell uptake of the polyplexes in CIS-treated cells was higher than in the untreated cells at all tested time points (Figure 9C). The increased cell uptake may be associated with the overexpression of the CXCR4 receptors in the injured tubule cells. This assumption was confirmed by competitive binding experiment in Figure 9D, where anti- CXCR4 antibody treatment decreased the cell uptake of the polyplexes by 24% and 29% at 2 and 4 h post-incubation, respectively.

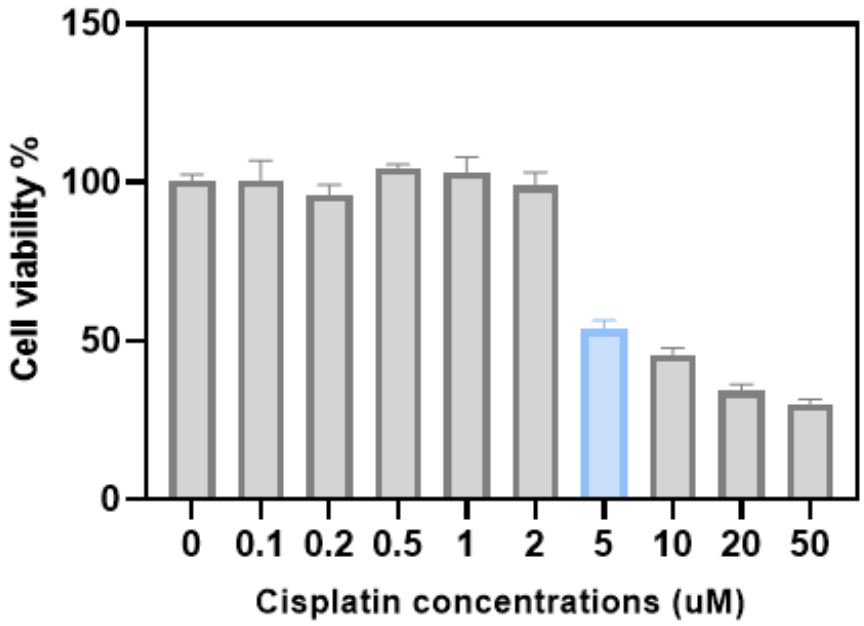

Figure 8. Selection of concentration of cisplatin used for injured cell modeling. A concentration of 5 μM was chosen as optimal cisplatin concentration for modeling injured cells used for the analysis of anti-apoptosis effect of PCX/siP53 owing to the moderate cell viability presented. Cisplatin was used to incubated with cells for 24 h at different concentration, then the cell viability was determined by CellTiter-Blue assay, and three experiments were repeated for each group.

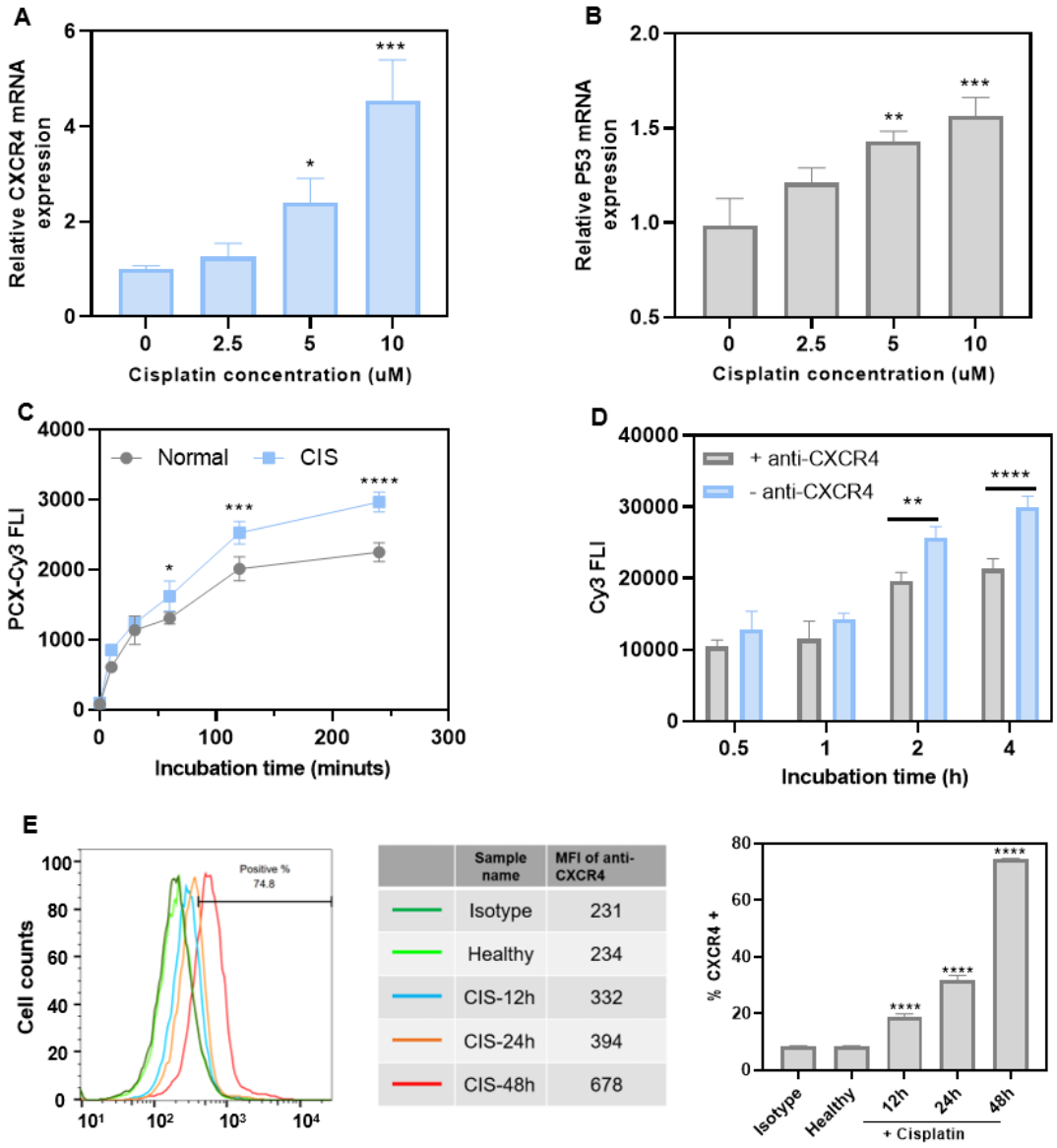

Figure. 9. Effect of cisplatin-induced in vitro cell injury on CXCR4 and p53 expression and PCX/siRNA uptake in HK-2 cells. Characterization of CXCR4 (A) and p53 (B) mRNA expression in healthy and cisplatin-treated HK-2 cells (n = 3 , * $p < 0.05$, ** $p < 0.01$, *** $p < 0.001$ vs. 0 uM group). (C) Flow cytometry analysis of cell uptake of PCX-Cy3/siRNA polyplexes in healthy and cisplatin treated HK-2 cells (n = 3 , * $p < 0.05$, *** $p < 0.001$, **** $p < 0.0001$ vs. cisplatin group). (D) Competitive binding assay with anti-CXCR4 antibody

and its effect on cell uptake of PCX-Cy3/siRNA polyplexes (n = 3 , ** $p < 0.01$, **** $p < 0.0001$ vs. CXCR4 antibody treated group). (E) Cell surface CXCR4 expression. HK-2 cells were incubated with 5 μM cisplatin for 12 h, 24 h, and 48 h, then anti-CXCR4-APC were used to stain the cells (n = 3, **** $p < 0.0001$, vs. healthy group). (Continued Figure 9)

2.4. Attenuation of the CIS injury by PCX/sip53 polyplexes in vitro

We next determined whether treatment with the PCX/sip53 polyplexes protects HK-2 cells from CIS injury. The cells were treated with the PCX/sip53 polyplexes and control PCX/siScr polyplexes at siRNA concentration of 80 nM. Injury was then induced by incubation with 5 μM CIS for 20 h. As shown in Figure 10B, the PCX/sip53 treated group significantly increased HK-2 cell viability when compared with the siScr and untreated (PBS) control groups. Effect of the treatment on apoptosis was also evaluated to further study the protection mechanism of the PCX/sip53 polyplexes. Figure 10A shows that PCX/sip53 had less apoptotic nuclei and more live cells when compared with the untreated and PCX/siScr controls. The apoptotic cells were further quantified using Annexin V-FITC/PI kit (BD Biosciences). The percent of apoptotic cells in PCX/sip53 treated group showed no significant difference with healthy control cells and even PCX/siScr showed decreased percent of apoptotic cells when compared with the untreated CIS group (Figure 10B and C). Similar effect of p53 knockdown was shown in a previous study [271]. Our results extend the finding by demonstrating the role of both p53 and CXCR4 inhibition in protecting tubule cells against injury by CIS.

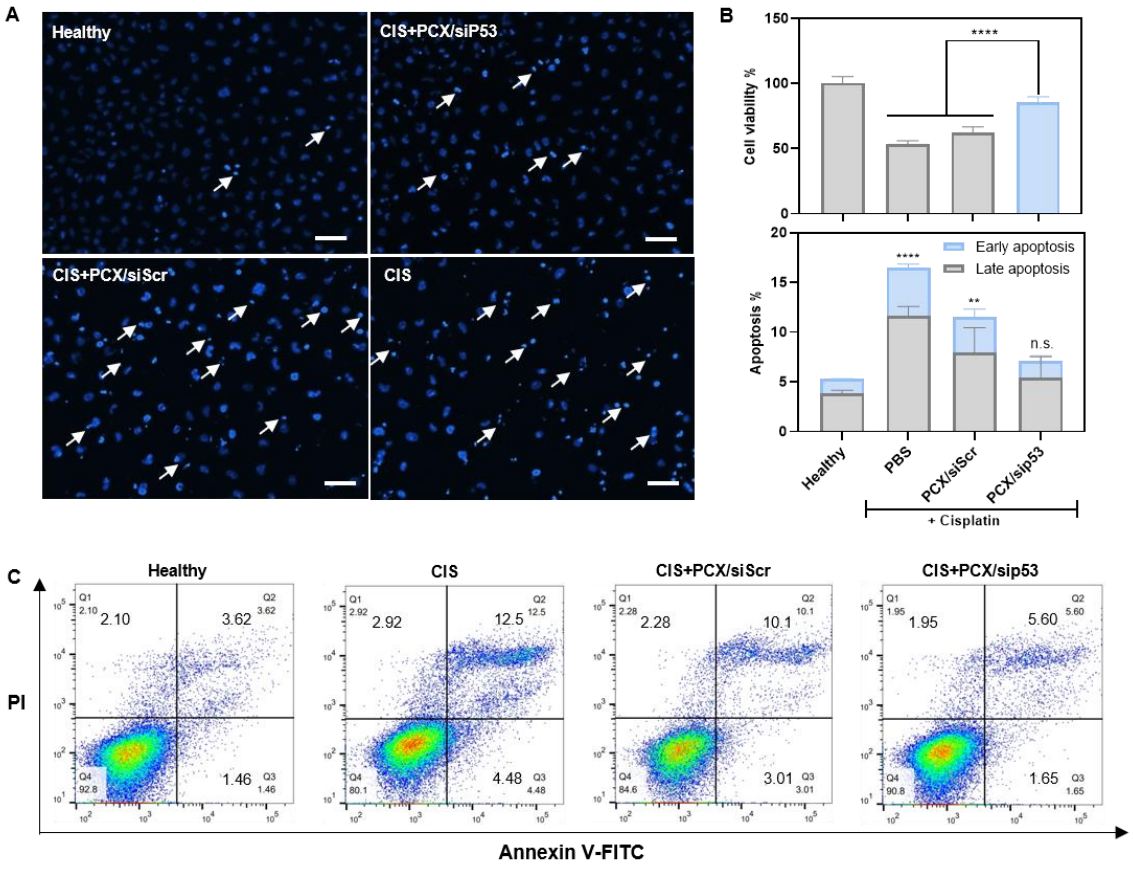

Figure 10. Protective antiapoptotic effect of PCX/siP53 polyplexes in tubule cells in vitro. HK-2 cells were pretreated with PCX/siP53, PCX/siScr and PBS for 24 h and then treated with cisplatin for another 20 h. (A) DAPI staining for cell apoptosis determination (apoptotic cells indicated by arrows, scale bar = 50 μm). (B) Cell viability and percentage of apoptotic cells. For cell viability, n = 6, **** $p < 0.0001$ vs. PCX/sip53 group. For apoptosis, n = 3, **** $p < 0.0001$, ** $p = 0.0075$, n.s.=no significant difference, vs. healthy group. (C) Flow cytometry analysis of apoptosis using Annexin V-FITC staining.

2.5. Biodistribution of PCX/siRNA polyplexes in CIS- and IRI-AKI models

Sufficient accumulation of therapeutic agents in their target tissues is the prerequisite for successful treatment. It is necessary to determine the distribution profiles of PCX/siRNA in vivo before investigating its therapeutic potential. We investigated how the PCX/siRNA polyplexes accumulate in injured kidneys using two widely accepted AKI models. First, intraperitoneal CIS injection was used to establish the CIS-AKI model. The fluorescently labeled polyplexes were injected intravenously three days after the CIS injection and biodistribution assessed after 4 h and 24 h [270]. Free unformulated siRNA-Cy5.5 was used as a control. Free siRNA showed similar levels of renal accumulation in healthy and CIS-AKI mice. In contrast, when the siRNA was given in the form of PCX/siRNA polyplexes, significantly higher accumulation (up to 1.64 fold) in the injured kidneys was observed both at 4 h and 24 h post-injection. Similarly, renal distribution of fluorescently labeled PCX (PCX-Cy3) was determined. We found that both free PCX-Cy3 and PCX-Cy3/siRNA polyplexes accumulated preferentially (up to 5.8 fold) in the injured kidneys than in healthy kidneys. To identify the location of both PCX and siRNA in the kidneys, we applied confocal microscopy to frozen kidney sections. The fluorescence signal from both PCX and siRNA was mostly localized in the tubule area (white arrows point to glomeruli), and with higher fluorescence intensity observed in the injured kidney sections. Importantly, both the siRNA and the PCX were found in the same tubule areas of the injured kidneys as suggested from the yellow color in the merged images. The co-localization of the two fluorescence signals indicates that PCX successfully improved

delivery of siRNA to tubules of the injured kidneys. Overall, these results indicate preferential renal tubule targeting ability of PCX/siRNA in CIS-AKI model [270].

To validate general applicability of the CXCR4-directed polyplexes for improved selectivity of siRNA delivery to injured kidneys, we have used another widely used AKI model based on bilateral IRI (Figure 11). The polyplexes were given by intravenous injection and kidneys and major organs harvested for ex vivo IVIS imaging as above. Similar to the CIS-AKI model, we found significantly enhanced distribution of the polyplexes to the injured kidney when compared with the sham surgery group (Figure 11A). After quantifying the fluorescence intensity, we found that the polyplex accumulation was ~ 2.1 and 3.0 times higher in the injured kidneys than in healthy ones at 4 h and 24 h after injection respectively. Similar to the CIS-AKI model, the frozen kidney sections showed that the polyplexes were mainly accumulated in the tubule area in the injured kidney, and the co-localization of siRNA and PCX was confirmed after merging the fluorescent signals of siRNA with PCX (yellow) (Figure 11B).

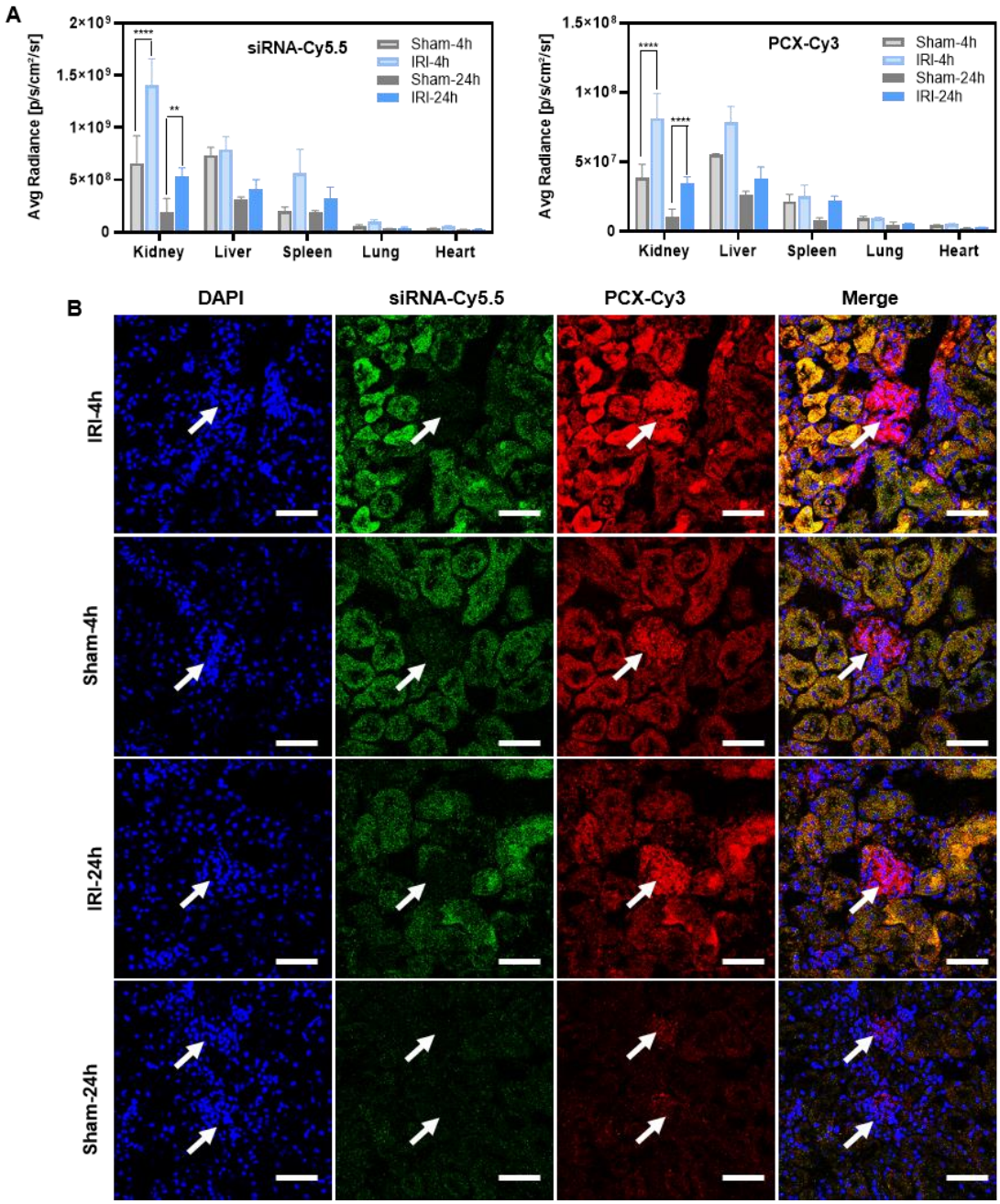

Figure 11. Effect of injury on renal accumulation of PCX/siRNA polyplexes in IRI-AKI. (A) Organ distribution at 4 or 24 h after intravenous injection of PCX-Cy3/siRNA-Cy5.5 polyplexes in healthy and IRI-AKI mice and ex vivo fluorescence imaging and signal quantification (n = 3 (sham), n = 4 (IRI-AKI), **** $p < 0.0001$, ** $p < 0.01$ vs. healthy group.

(B) Representative confocal images of healthy and CIS-AKI kidney sections after intravenous injection of PCX-Cy3/siRNA-Cy5.5 polyplexes (nuclei – blue, siRNA – red, PCX – green, PCX/siRNA colocalization – yellow; arrows indicate glomeruli, scale bars, 50 μm). (Continued Figure 11)

2.6. AKI treatment by PCX/sip53 polyplexes

Before proceeding to testing therapeutic efficacy of the PCX/sip53 polyplexes, we validated the expression of our two targets in mouse models of AKI. We investigated the effect of renal injury on the expression of the two targets in commonly used mouse models of AKI, namely the CIS-AKI model and bilateral IRI-AKI model. Immunohistochemistry staining confirmed increased renal expression of both CXCR4 and p53 in injured kidneys in both AKI models. When compared with healthy mice, both AKI models showed increased renal expression of CXCR4 in cortex tubule cells, with positive cytoplasmic and plasma membrane staining (Figure 12A and C). The AKI kidneys also showed increased expression of p53, which was located in both cortex and medulla and found in the nucleus and the cytoplasm (Figure 12B, D and E).

Having confirmed preferential renal accumulation of the PCX/siRNA polyplexes in AKI mouse models, the ability of PCX/sip53 to alleviate AKI was investigated using the CIS-AKI model. Mice were divided into four treatment groups: PCX/sip53, PCX/siScr, commercial CXCR4 antagonist AMD3100, and PBS. This experimental design allowed us to examine the role of both p53 and CXCR4 in the treatment outcomes. As shown in Figure 13A, eight weeks male C57BL/6J mice were treated by tail vein injection on four consecutive days. On the second day, the animals received a single nephrotoxic dose of CIS (15 mg/kg) to induce AKI. After 4 days of CIS injection, blood was collected for kidney function analysis, mice were sacrificed, and kidneys harvested for periodic acid-Schiff (PAS) staining and in vivo p53 knockdown evaluation. Serum creatinine (SCr) and blood

urea nitrogen (BUN) are important biomarkers of kidney function [272, 273]. The levels of SCr and BUN in the PCX/sip53 polyplex treatment group significantly decreased when compared with the untreated (PBS) control group (Figure 13B and C). Treatment with the CXCR4-inhibiting AMD3100 and PCX/siScr also showed beneficial effects signified by a statistically significant decrease in SCr levels but not in BUN levels. The p53 gene silencing effect of the PCX/sip53 polyplexes was determined from qRT-PCR analysis of the p53 mRNA levels (Figure 13D). Treatment with PCX/sip53 polyplexes showed nearly 50% silencing of the p53 mRNA expression when compared with the untreated group. The treatment with AMD3100 and PCX/siScr showed no significant effect on the p53 expression.

Histological analysis of the kidney sections was used to further examine the therapeutic effect of the PCX/sip53 polyplexes (Figure 13F). Untreated (PBS) CIS-AKI group showed significant extent of necrosis, tubule injury indicated by severe dilation, large areas of cast formation, presence of cytoplasmic protein droplets, loss of brush border, and dead epithelial cells. Although the AMD3100 and PCX/siScr groups showed similar injury profiles to the untreated group, thre was a significant decrease in the cast formation and amount of protein droplets, suggesting beneficial effects of CXCR4 inhibition alone. As expected, the combined CXCR4 and p53 inhibition by the PCX/sip53 polyplexes showed the least tubule injury as indicated by negligible cast formation and decrease in epithelial cell death. The tubule morphology in the treatment group was restored as evidenced by more intact brush borders and few dilated tubules. Finally, the histological damage score in each treatment group was determined in a blind manner by

a renal pathologist (Figure 13) to quantify the therapeutic effect. Overall, these findings show that the combined CXCR4 inhibition and p53 knockdown could restore renal function in the CIS-AKI model.

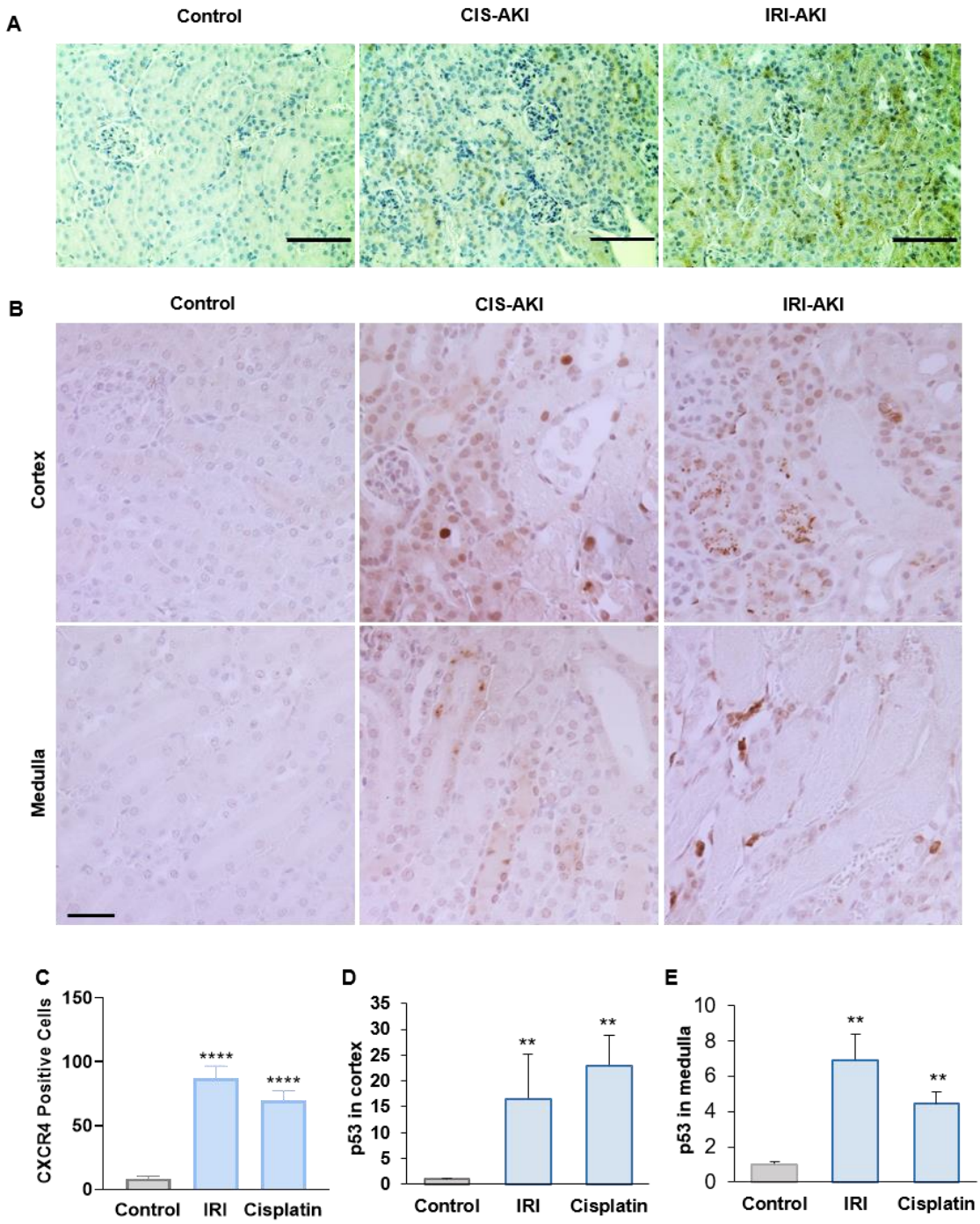

Figure 12. Immunohistochemical staining of CXCR4 (A) and p53 (B) renal expression in CIS-AKI and IRI-AKI mouse models, and the quantification of CXCR4 positive cells (C) and p53 positive cells (D, E), scale bar = 50 μm.

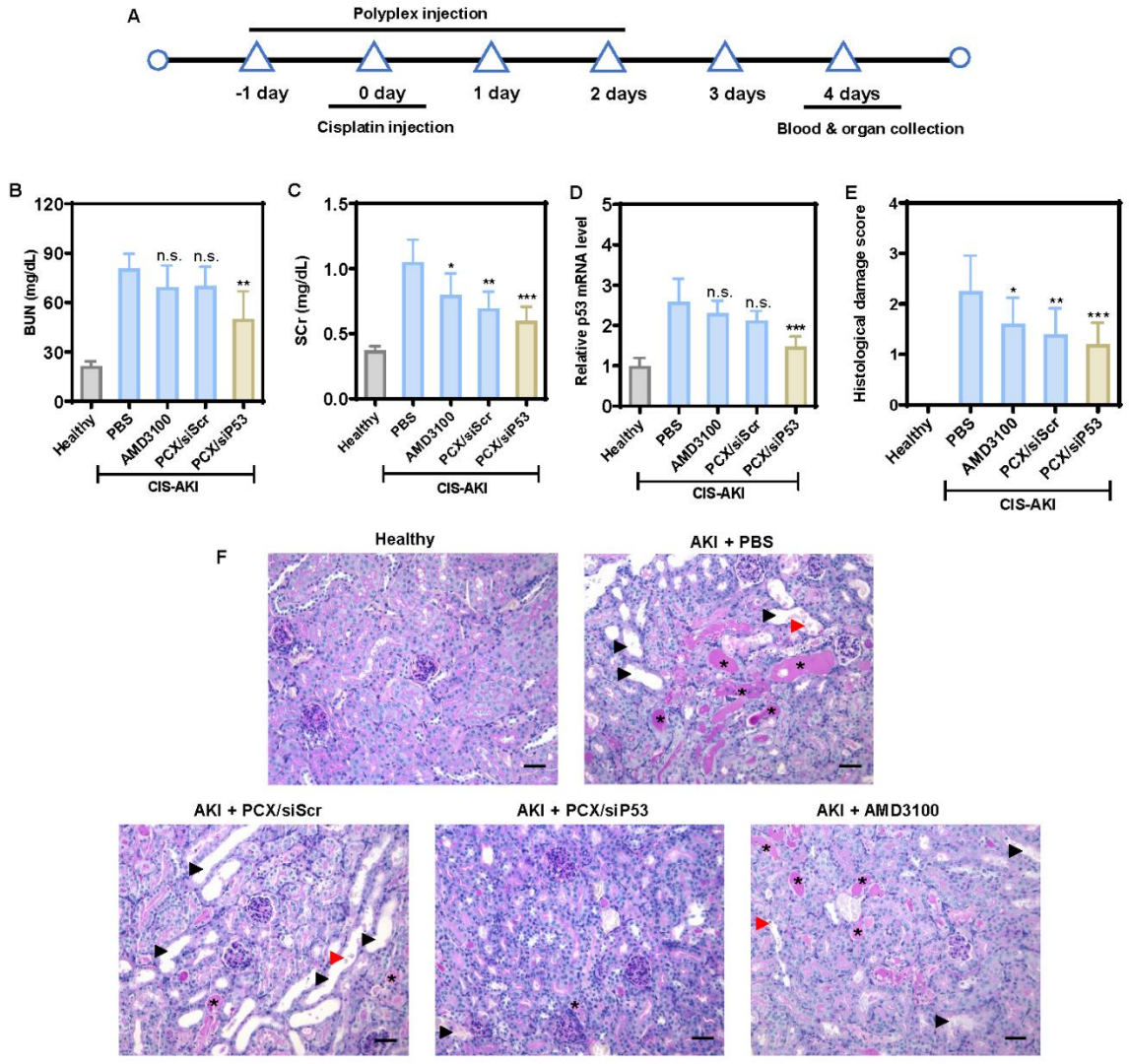

Figure 13. Treatment efficacy of PCX/sip53 polyplexes in CIS-AKI in vivo. (A) Experimental design and treatment plan. Treatment effect on (B) BUN, (C) serum creatinine (SCr), (D) renal p53 mRNA expression, and (E) histological kidney damage score. (F) PAS staining of kidney tissues. Renal injury is shown by cast formation (asterisks), dilatation of tubules (black arrowheads), and sloughing of injured cells (red arrowheads). Data expressed as mean ± SD. n = 4 and 5, * $p < 0.05$, ** $p < 0.01$, *** $p < 0.001$, n.s. no significant difference vs. PBS group, scale bar = 50 μm.

3. DISCUSSION

No effective pharmacological options exist for the treatment or prevention of AKI, contributing to the high mortality and morbidity of the disease [274]. To improve renal therapeutic delivery in AKI, nanomedicine approaches are being increasingly explored for both conventional small molecule drugs and new biologics-based therapeutics such as siRNA. Despite the great potential, use of siRNA is limited by degradation, ineffective delivery, and off-targets effects. In mice, hydrodynamic injection of large doses of free siRNA is a feasible option but one that cannot be translated to humans due to safety risks [116]. To overcome the drawbacks, siRNA can be encapsulated within polyplexes as in this study. We found that polyplexes greatly enhance intracellular uptake of siRNA in HK-2 cells. The internalization in cells injured by CIS treatment was even more efficient, suggesting potential for preferential accumulation in injured kidneys due to overexpression of CXCR4 receptor.

In vivo biodistribution studies showed that the PCX/siRNA polyplexes have the ability to preferentially accumulate in the tubules of the injured kidneys, both in CIS-AKI and IRI-AKI models. The favorable renal tubule targeting ability of PCX/siRNA polyplexes in injured kidneys may be contributed by several factors, including CXCR4-mediated effects and pathophysiological changes that allow transport of nanosized polyplexes to the tubules. The structure and permeability of GFB in injured kidneys change significantly. Reduction in charge and size selectivity were observed after ischemia reperfusion, which indicated an increased formation of large pores in GFB that

allowed for nanoparticles to pass through (Scheme. 7) [275, 276]. There is also the possibility that the anionic charge of GFB may dissociate some of the polyplexes and the free siRNA and PCX may reassemble after the filtration. Once the intact or reassembled polyplexes reach the tubule area, there is increased likelihood of their interaction with the tubule cells that overexpress CXCR4 in response to the injury. Renal tubules are involved in the pathogenesis of multiple renal diseases apart from AKI. Thus, the renal tubule targeting ability of PCX/siRNA polyplexes in injured kidneys positions PCX as a potential carrier for functional siRNA delivery in AKI and other renal diseases. However, some limitations of the proposed mechanism of renal accumulation of PCX/siRNA should be noted. Early in AKI, circulating immune cells, including neutrophils and macrophages, rapidly infiltrate into the injured kidneys in response to the inflammatory cytokines and chemokines [75, 277]. Given that both neutrophils and macrophages express CXCR4, there is a possibility that the polyplex renal transport may be at least partially aided by the immune cells [278, 279]. The participation of the immune cells in the polyplex renal accumulation and the potential role of PCX on the immune microenvironment in the injured kidneys is an important aspect but one that is beyond the scope of the present study.

Based on the biodistribution study, we studied the therapeutic potential of the polyplexes in the CIS-AKI mice model. Chemokines and chemokine receptors like CXCR4 form a vital part of the inflammation process through chemotactic signals for leukocyte activation and migration [125, 140]. Several experimental studies have provided supportive evidence for the pivotal role of p53 in the pathogenesis of AKI [105, 113, 114,

117, 280]. Above, we showed simultaneous activation of both p53 and CXCR4 in the tubule cells after challenge with CIS (Figure 4). Our study showed that PCX based siRNA delivery system could significantly improve the therapeutic effect of p53 siRNA with a less amount of siRNA (0.6 mg/kg), which is indicated by renal function recovery, efficient gene knockdown, and histological damage reduction. There are several reasons related to this improved therapeutic effect. First, p53 siRNA was protected during systemic circulation by the PCX. Second, specific interaction between CXCR4 and PCX enhanced the uptake of PCX/sip53 in the injured renal tubule cells. And third, efficient release of p53 siRNA in injured renal tubule cells facilitated effective therapeutic response (Scheme. 7).

In summary, we developed and tested siRNA polyplexes for selective delivery to injured kidneys with the goal of developing a novel treatment of AKI. We have successfully used CXCR4-directed delivery with PCX to enhance the renal accumulation and deliver therapeutic siRNA to silence the expression of p53. This is the first report that shows the potential of combined CXCR4 inhibition with p53 gene silencing as a therapeutic modality in AKI.

4. MATERIALS AND METHODS

4.1. Materials

N,N′-hexamethylenebisacrylamide (HMBA) was obtained from Polysciences, Inc. Cyclam (1,4,8,11-tetraazacyclotetradecane) was ordered from Alfa Aesar. Dulbecco's modified Eagle medium (DMEM), Dulbecco's phosphate buffered saline (PBS), and FBS were from Thermo Scientific. Cell culture plates and flasks were ordered from BD Biosciences. Human SDF-1α was purchased from Shenandoah Biotechnology, Inc. Keratinocyte Serum Free Medium (K-SFM) and its supplements were ordered from Gibco. RPMI-1640 medium was purchased from Gibco. Pre-designed p53 siRNA was ordered from Sigma Aldrich. Cy5.5 labeled siRNA (siRNA-Cy5.5) were from Dharmacon. Real-time PCR (RT-PCR) primers were ordered from Invitrogen. CXCR4 antibody was ordered from Boster Biological Technology. p53 antibody was ordered from Santa Cruz Biotechnology, Inc. All other reagents were from Fisher Scientific and used as received unless otherwise noted.

4.2. Formulation and characterization of PCX/siRNA polyplexes

Electrophoresis in a 2% agarose gel containing 0.5 ug/mL of ethidium bromide was used to determine the siRNA condensation ability of PCX. Polylexes were prepared by mixing predetermined equal volume of PCX and siRNA solution in 20uM HEPES buffer to achieve the desired w/w ratio. After being vigorously vortexed for 10 s and incubated in room temperature for 30 min, 20 ul of polyplexes prepared at different PCX-to-siRNA weight ratios (0, 0.5, 1, 2, 5, 10) were loaded (containing 0.5 μg of siRNA) and run for 15

min at 110 V in 0.5 × Tris/Borate/EDTA buffer. A KODAK Gel Logic 100 imaging system were used to visualize the gel under UV illumination. In a heparin displacement assay, the polyplexes were prepared at a w/w ratio of 5 and incubated with increasing concentrations of heparin for 30 min at room temperature. Then 20 ul of each samples were analyzed by agarose gel electrophoresis. Dynamic light scattering (DLS) using a ZEN3600 Zetasizer Nano-ZS was used to determine the hydrodynamic size and zeta potential of the polyplexes.

4.3. Cell culture

Human renal tubular cells (HK-2) were grown in Keratinocyte Serum Free Medium (K-SFM) suspended with 0.05 mg/ml of bovine pituitary extract (BPE) and 5 ng/ml of human recombinant epidermal growth factor (EGF). Mouse cortical tubule cells (MCT) were grown in RPMI-1640 supplemented with 10% FBS, penicillin (100 U/mL), streptomycin (100 μg/mL). Human epithelial osteosarcoma U2OS cells stably expressing functional EGFP-CXCR4 fusion protein were purchased from Fisher Scientific and were cultured in DMEM supplemented with 2 × 10−3 M L-glutamine, penicillin (100 U/mL), streptomycin (100 μg/mL), G418 (0.5 mg/mL), and 10% FBS. All cells were maintained in an incubator at 37 °C and 5% CO2.

4.4. Quantitative Real-Time Polymerase Chain Reaction (qRT-PCR)

HK-2 cells were seed in 6-well plates (2 × 105 cells/well). After 24 hours, the cells were treated with different treatments (different concentrations of CIS for 24 h, PCX/sip53 at the concentration of 25nM sip53 for 48 h). Total RNA from cells or kidney tissues was

extracted using the TRIzol reagent (Invitrogen, USA). The QuantiTect reverse transcription kit (Qiagen) was used to reverse-transcribe total RNA (0.5μg) to cDNA. The relative level of mRNA was quantified by RT-PCR with QuantiFast SYBR Green PCR kit (Qiagen) on a Rotor-Gene Q (Qiagen). The following siRNAs were used: human p53 siRNA (sense: 5′-GAGGUUGGCUCUGACUGUA-3′; anti-sense: 5′-UACAGUCAGAGCCAACCUC-3′), mice p53 siRNA (sense: 5′-CCACUACAAGUACAUGUGU-3′; anti-sense: 5′-ACACAUGUACUUGUAGUGG-3′), scramble siRNA (Sense: 5′-AUGAACGUGAAUUGCUCAAUU-3′; anti-sense: 5′-UUGAGCAAUUCACGUUCAUUU-3′).The following primers were used: human p53 (forward 5′-ACCTATGGAAACTACTTCCTG-3′; reverse, 5′-ACCATTGTTCAATATCGTCC-3′), mice p53 (forward 5′-TAGGTAGCGACTACAGTTAG-3′; reverse, 5′-GGATATCTTCTGGAGGAAGTAG-3′), human CXCR4 (forward 5′-AACTTCAGTTTGTTGGCTG-3′; reverse, 5′-GTGTATATACTGATCCCCTCC-3′), mice CXCR4 (forward 5′-AGGTAGCAGTGAAACCTC-3′; reverse, 5′-ATACTCACACTGATCGGTTC-3′), human GAPDH (forward 5′-ACAGTTGCCATGTAGACC-3′; reverse, 5′-TTGAGCACAGGGTACTTTA-3′), and mice GAPDH (forward 5′-CAATGACCCCTTCATTGACC-3′; reverse, 5′-GATCTCGCTCCTGGAAGATG-3′). The Ct values were used to calculate the relative levels of mRNA.

4.5. CXCR4 Antagonism Assay

The CXCR4 antagonism efficacy of PCX was determined by CXCR4 redistribution assay. U2OS cells with the EGFP-CXCR4 fusion protein were seeded in black 96-well microplates for 24 hours. Then, assay buffer was used to wash the cells for 3 times before treatment, then cells were treated with tested compounds for 30 min. SDF1 was added for another 1 h incubation. Cells were fixed and visualized under EVOS xl microscopy by using the GFP channel.

4.6. Analysis of CXCR4 Expression on Cell Surface

After the treatment of CIS, allophycocyanin (APC) labeled CXCR4 antibody (BD Biosciences, CA) was used to incubate with cells for 1 h at 4 °C. The isotype-matched antibody was used to assess the background fluorescence. Cells were subjected to analysis using a FACS Calibur (BD Bioscience, Bedford, MA) and the results were analyzed by FlowJo software (Tree Star Inc., OR).

4.7. Animal models

C57BL/6J male mice were ordered from Jackson Laboratories. Animal experiment protocols have been approved by the University of Nebraska Medical Center Institutional Animal Care and Use Committee. The cisplatin-induced AKI model (CIS-AKI) was established after 3 days of intraperitoneal injection of 15 mg/kg of cisplatin to mice. The ischemia-reperfusion induced AKI model (IRI-AKI) was established as previously reported [57]. Briefly, mice were anesthetized by intraperitoneal administration of ketamine (15 mg/kg) and xylazine (5 mg/kg). Renal ischemia was induced by clamping of

the bilateral renal pedicles. During the ischemic period, mice body temperature was maintained by placing the mice on a 37 °C heating table. After 30 min of clamping, both clamps were released for reperfusion.

4.8. Biodistribution of polyplexes

Eight-week old male C57BL/6J mice were injected intravenously with 200 ul of fluorescently labeled siRNA-Cy5.5, PCX-Cy3, and PCX-Cy3/siRNA-Cy5.5 polyplexes (3 mg/kg PCX-Cy3, 0.6 mg/kg siRNA-Cy5.5). Mice were sacrificed at 4 and 24 h post injection, and imaged using a Xenogen IVIS 200. Kidneys and major organs were harvested for ex vivo fluorescence imaging. The fluorescence signals from each organs were analyzed by using the instrument software. To observe the locations of PCX and siRNA in the kidneys, an OCT compound was used to embed the kidney tissues. The final frozen tissue blocks were cut into 10 μm sections, stained with DAPI, and observed using a confocal microscopy.

4.9. Statistical Analysis

Results are presented as mean ± standard deviation. The differences among multiple groups analyzed by ANOVA and followed by Tukey's multiple comparison test. The statistical significance between the two groups were analyzed by using student's t test. A minimal level of significance was considered as $P < 0.05$. GraphPad Prism 8 was used to perform all statistical analyses.

Chapter 3. Modified chitosan for effective renal delivery of siRNA to treat acute kidney injury

1. Introduction

Acute kidney injury (AKI) is a complex syndrome characterized by an abrupt reduction in kidney function that manifests by an increase in serum creatinine and a decrease in urine output [281]. AKI has become a significant clinical problem and health care burden with rapidly increasing healthcare costs. Currently there is no effective pharmacological treatment available for AKI [282, 283]. Renal ischemia-reperfusion injury (IRI) associated with major surgery is a leading cause of AKI, with patients having 50-80 % chance of developing AKI [284, 285]. The pathogenesis of IRI-AKI is complicated and involved multiple mechanisms, including tubule cells apoptosis/necrosis, oxidative stress, and vasculature damage [286-290]. A well-known tumor suppressor p53 has been shown to have a pivotal role in the pathogenesis of AKI and renal repair after AKI [229]. Upregulation of p53 in tubule cells is a key component of cell response to cellular stress like DNA damage, hypoxia, and reactive oxygen species (ROS) [291]. Upregulation of p53 in renal medulla tubules is observed within 24 h of IRI. The administration of guanosine or pifithrin-alpha could prevent tubule apoptosis and restore renal function [243]. Intravenous injection of synthetic siRNA targeted to p53 (sip53) protected proximal tubule cells (PTCs) and restored the renal function [238]. Furthermore, specific deletion of the p53 gene from renal PTCs protected kidneys against IRI [239, 240]. Treatment with

mesenchymal stem cells-derived exosome (MSC-exos) ameliorated kidney injury due to the repression effect of miR-125b-5p to p53 [292].

Inflammation is another important pathophysiological component of IRI-AKI. As a response to renal IRI and nephrotoxicity, elevated cytokines and chemokines create a pro-inflammatory microenvironment [217]. Renal expression of a chemokine receptor CXCR4 and its ligand stromal cell-derived factor (SDF-1) are greatly increased in AKI [223]. CXCR4/SDF-1 axis is involved in recirculation and hematopoiesis of leucocytes, which are the key cellular mediators of renal injury [293-295]. CXCR4 is also expressed on hematopoietic stem cells (HSCs) and endothelial progenitor cells (EPCs). The renal protective effect of both cells has been shown in preclinical rodent AKI models [296-298]. Disrupting of CXCR4/SDF-1 interactions by a CXCR4 antagonist mobilizes HSCs from the bone marrow to peripheral circulation [299], which results in the attenuation of renal immune response followed by improvement in the course of AKI [227, 228]. Hence, the inhibition of CXCR4/SDF-1 interaction is a potential strategy to treat AKI, either by the local anti-inflammatory effect or by the systematic stem cell mobilization mechanism.

Previous reports showed that sip53 is a potential therapy for AKI. However, the poor stability, large size and strong negative charge make naked siRNA hard to cross the cell membrane and to traffic to its site of action in cytoplasm. Hence, a large dose (12 mg/kg) was required to achieve the desired therapeutic potency [238], which may potentially activate the innate immune system [245]. Thus, there is a need for the development of injured kidney-specific targeted delivery system to improve the siRNA intracellular

delivery, to overcome the off-target and stability challenges, and to minimizing the required siRNA doses. Several approaches for kidney targeted siRNA delivery have been reported to improve the renal distribution and specific cell delivery [256, 257]. Regardless of other delivery systems, the polycationic carriers showed strong potential for AKI treatment. Chitosan is one of the promising carriers for renal drug and gene delivery. Chitosan/siRNA nanoparticles showed good therapeutic potential in unilateral ureteral obstruction AKI [251]. The megalin-mediated specific uptake of chitosan/siRNA in mouse proximal tubule cells allowed successful gene silencing [300]. A recently developed chitosan-based delivery system showed specific renal targeting and exhibited a great therapeutic potential in IRI-AKI [301]. Motivated by the favorable properties of chitosan for renal delivery, we have chosen chitosan as a parent polymer for our study. Modification of chitosan with CXCR4 antagonists/targeting moieties can further strengthen our delivery system in two specific ways. It can increase the cellular uptake to injured tubule cells by the combined effect of CXCR4 receptos, and it can attenuate AKI by inhibiting the CXCR4 [258, 302, 303].

We designed and synthesized a cyclam modified chitosan (C-CS) as a new class of cationic polymer for targeted delivery of sip53 to the tubule cells of injured kidneys (Scheme. 8). Biocompatibility of C-CS and C-CS/siRNA polyplexes were measured in human renal tubule cells HK-2. The biodistribution in AKI was examined by using IVIS imaging system. Pharmacokinetics of C-CS/siRNA was evaluated in sham and IRI-AKI mice. The therapeutic potential of C-CS/sip53 was evaluated in the IRI-AKI mouse model.

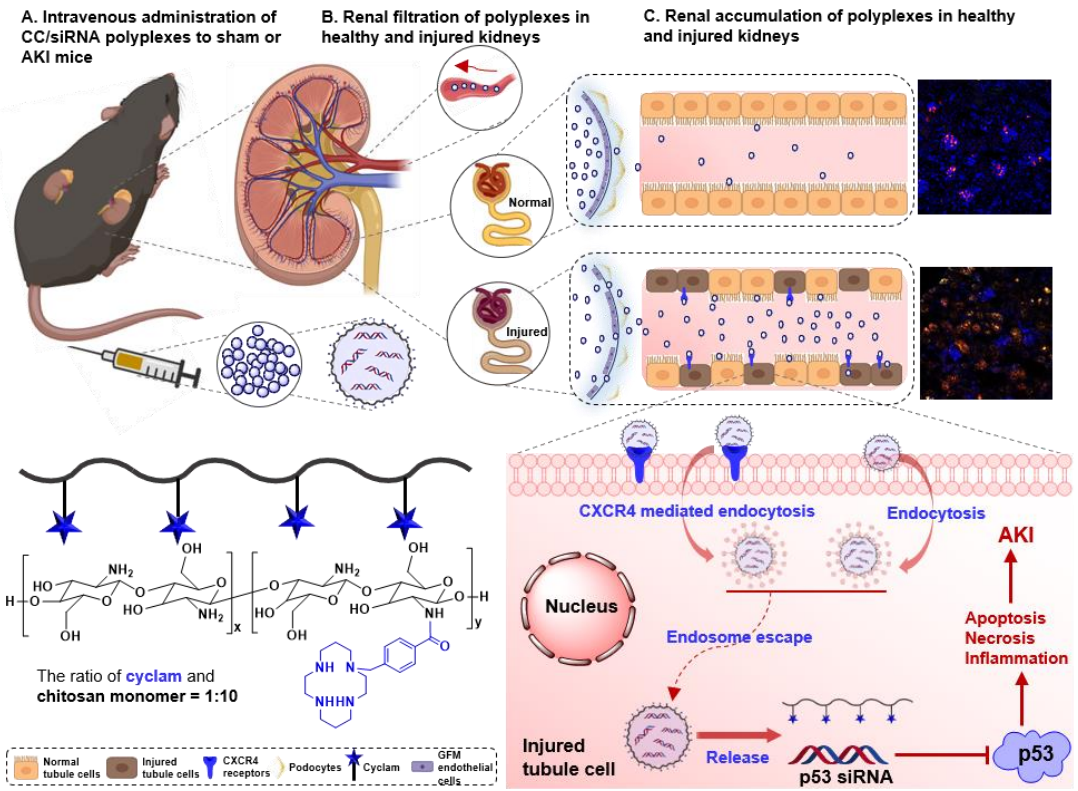

Scheme. 8. Chemical structure of cyclam-modified chitosan (C-CS) and the schematic illustration showing the distribution and therapeutic potential of C-CS/siRNA in IRI-AKI mice. After intravenously administration, C-CS/siRNA polyplexes goes through renal filtration from renal artery. In healthy kidneys, few C-CS/siRNA could be transported to tubule areas due to the intact structure of GFB. However, the impaired structure of GFB in injured kidneys enhances the permeability of C-CS/siRNA from glomeruli to tubules. Specifically expressed CXCR4 receptors on injured tubule cells would enhance the internalization of C-CS/siRNA. The upregulation of p53 in kidney tubule cells is associate with AKI, therefor, the released p53 siRNA from C-CS/siRNA polyplexes after endocytosis, could downregulate p53 expression and attenuate AKI condition.

2. Results and discussion

2.1. Synthesis of α-cyclam-p-toluic acid conjugated chitosan (C-CS)

CS is a copolymer of N-acetyl glucosamine (GlcNAc) and D-glucosamine (Glc) with a well-known renal targeting ability [196]. Aqueous solubility of CS has been a challenge for its delivery application. The solubility can be improved by increasing the degree of GlcNAc deacetylation [304]. Increasing the fraction of Glc units in CS can increase not only the solubility but also its gene condensation ability. Hence, here we have completely deacetylated the commercially available CS by NaOH under reflux condition [305]. Percent of deacetylation was calculated from the NMR spectrum (Figure 14) as 99%.

To further strengthen the renal targeting propensity, we have conjugated the deacetylated CS with a CXCR4-targeting moiety α-cyclam-p-toluic acid (CPTA) (Figure 19A) [306, 307]. CPTA was synthesized by bromo-alkylation of α-bromo-p-toluic acid with cyclam in the presence of LiOH. ^{1}H NMR spectrum of CPTA showed signals at 8.05 (-C**H**-; d) and 7.55 (-C**H**-; e) which were assigned to the aromatic protons of the toluic acid (Figure 15). The spectrum also showed benzylic proton signals at 4.26 (-C**H**$_2$-N; c) along with the methylene proton signals of the cyclam moiety at 3.44-3.11 (-C**H**$_2$-NH-, and-C**H**$_2$-N-; b), and 2.08 ppm (-C**H**$_2$-CH$_2$-NH; a). Synthesis of CPTA was further supported by the appearance of mass spectrum peak at m/z 335.24 corresponds to the exact mass of CPTA-H+ (Figure 16).

CPTA was conjugated to CS by coupling with the amine group of deacetylated CS followed by dialysis to remove the low molecular weight unreacted impurity and finally

yield the desired CS derivative (C-CS) (Figure 19A). The ^{1}H NMR spectrum of C-CS showed aromatic proton signals at 7.80 (-C**H**-; b) and 7.38 (-C**H**-; a) along with the appearance of CS protons between 4.00 to 3.32 ppm (Figure 17). The signals between 3.28 to 2.67 ppm were assigned to the methylene protons of the cyclam moiety. Coexistence of NMR signals corresponding to the aromatic protons, CS-backbone and cyclam protons suggested the conjugation of CPTA on the backbone of CS. Subsequently, SEC trace (Figure 18) of C-CS displayed a shifting towards lower elution volume (with respect to CS) which revealed an increase of molecular weight from 56.7 (dispersity, Đ =1.91) to 72.3 kDa with dispersity Đ = 1.97. The increased molecular weight of C-CS (in comparison with CS) along with the coexistence of NMR signals (Figure 17) corresponding to cyclam and CS protons confirmed the successful synthesis of C-CS. The amount of CPTA conjugated to CS was calculated as 7.9 mol% of the Glc unit as determined from the NMR peak integrations. Both the CS and C-CS were tagged with a fluorescent dye Cy3 (0.7 wt%.)

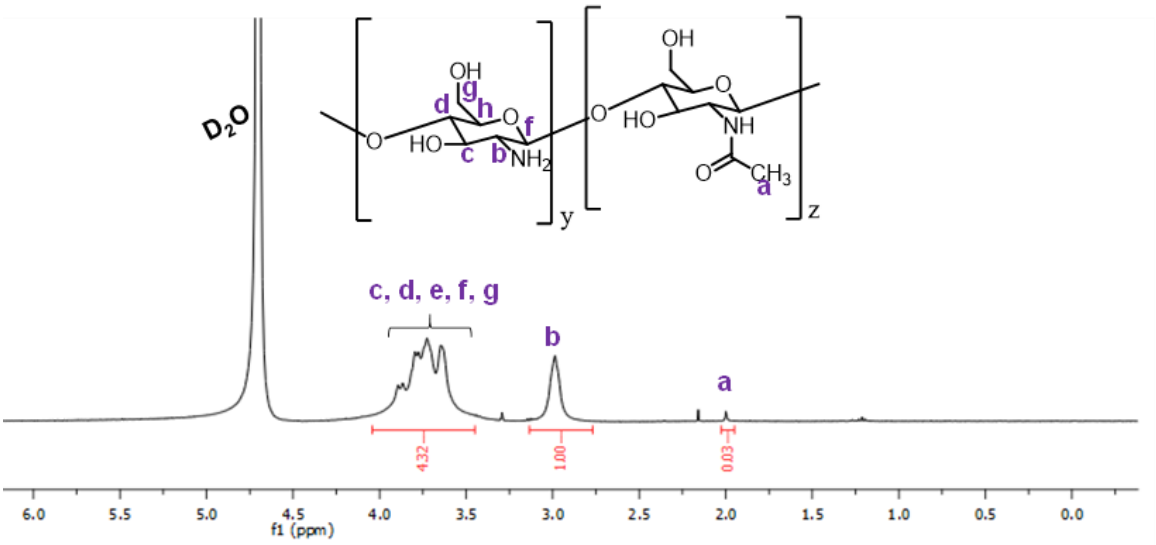

Figure 14. [1]H NMR spectrum of deacetylated chitosan (CS) in D2O, 25°C.

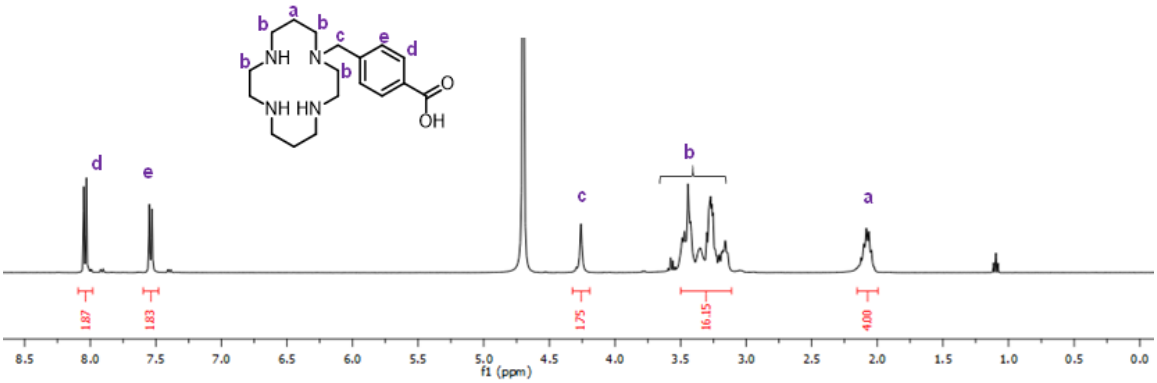

Figure 15. [1]H NMR spectrum of CPTA in D2O, 25°C.

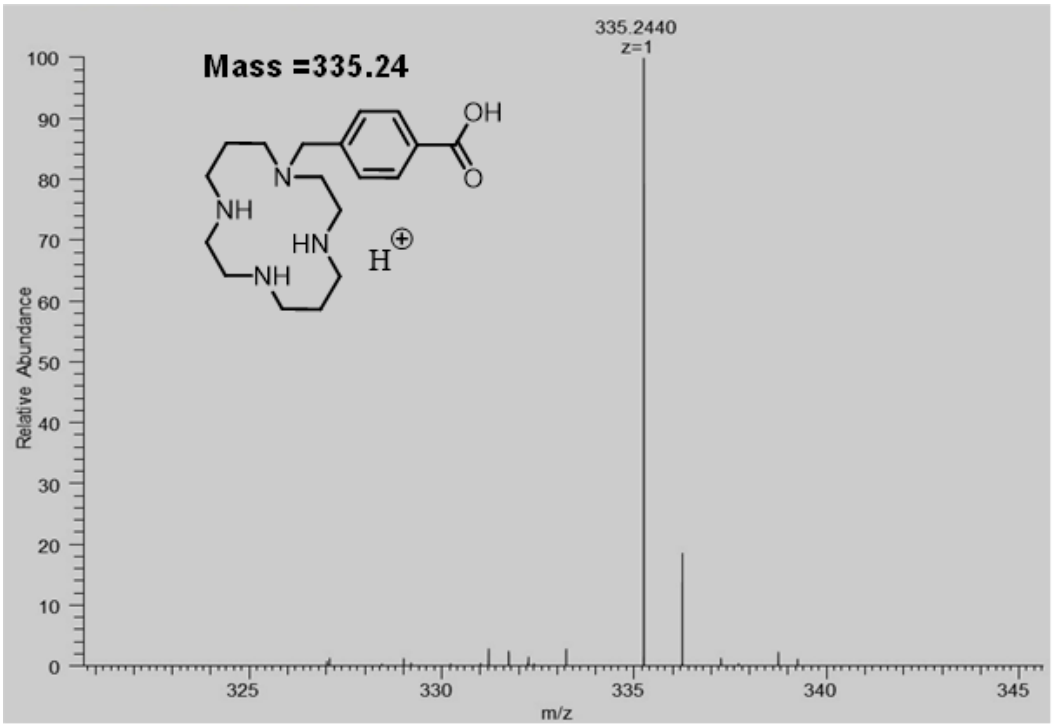

Figure 16. Mass spectroscopy of CPTA in D2O, 25°C

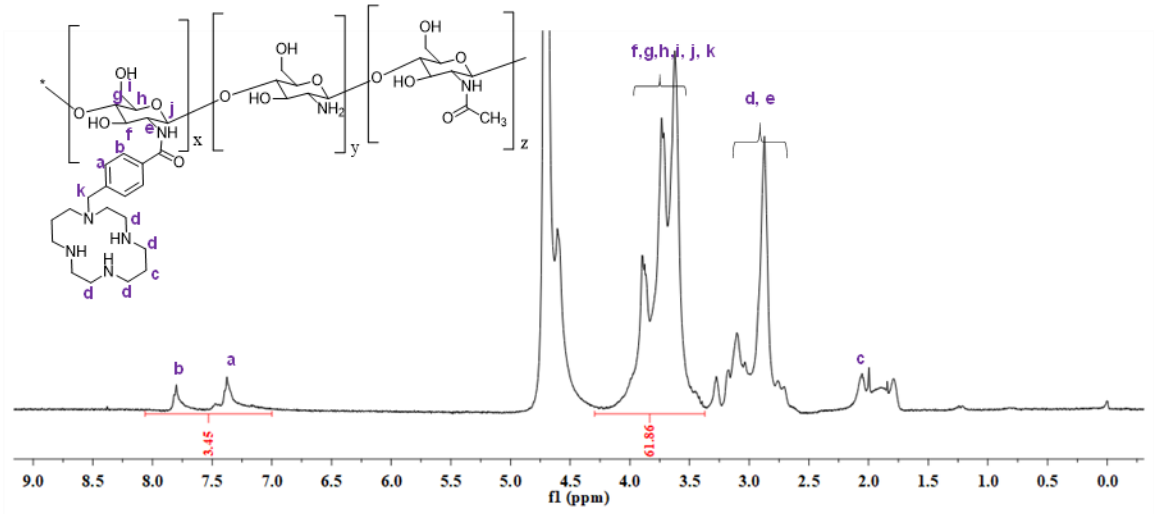

Figure 17. ^{1}H NMR spectrum of CPTA conjugated chitosan (C-CS) in D2O, 25°C

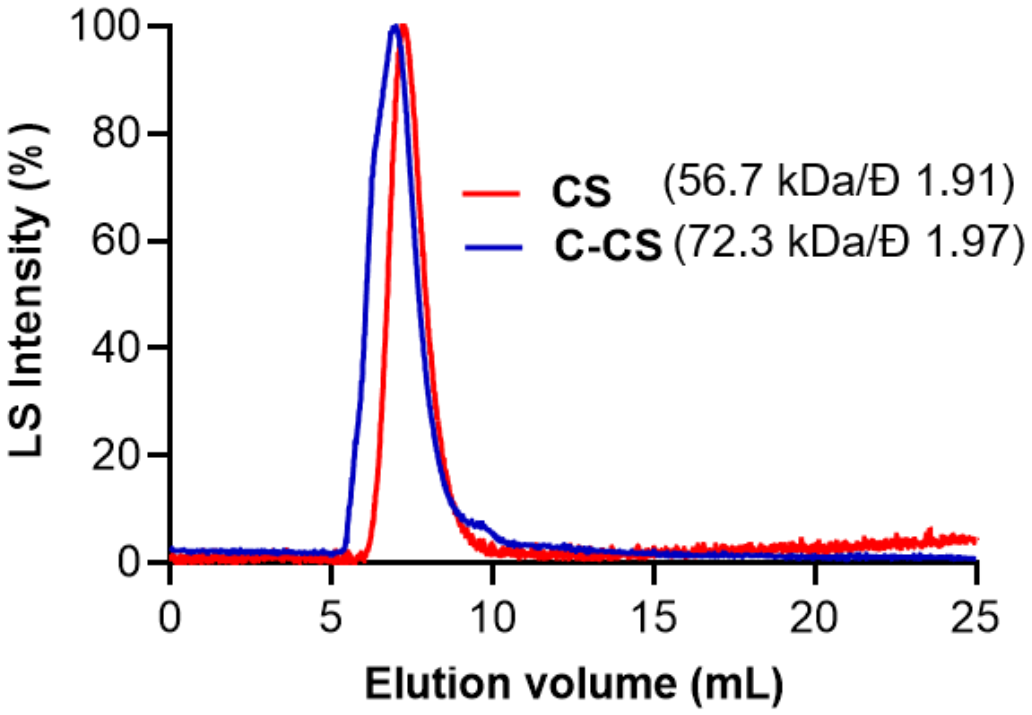

Figure 18. Size exclusion chromatography of deacetylated chitosan (CS) and CPTA conjugated chitosan (C-CS) in acetate buffer (pH 5) at 25 °C.

2.2. Formulation and characterization of polyplexes

The ability of C-CS and CS to bind siRNA was studied by gel retardation and SYBR-safe assays. Polyplexes were prepared by mixing polymer solutions with siRNA solution at increasing polymer/siRNA (w/w) ratios. In the gel retardation assay, partial retardation of siRNA movement was observed at w/w ratios of 0.5 and 1, as indicated by the siRNA smear. Both C-CS and CS fully complexed siRNA at and above w/w ratios of 2 (Figure 19B). In the SYBR-safe assay, the fraction of SYBR-safe stained free siRNA at different w/w ratios was quantified by a plate reader (excitation = 502 nm and emission = 530 nm), the result also showed the fully condensation of siRNA starting from w/w ratio of 2 (Figure 19C).

The hydrodynamic size and zeta potential of the CS and C-CS polyplexes at w/w ratios 2-12 were measured by dynamic light scattering (DLS) (Figure 20A, B, C). Polyplexes prepared at w/w ratio of 2 showed large particle size (>1000 nm) and lower positive zeta potential (< 5mV). As expected, the increase of polymer amount resulted in the formation of smaller sized particles with higher zeta potential. In particular, the w/w ratio of 8 gave the smallest unimodal size distribution for both C-CS/siRNA (~130 nm) and CS/siRNA (~200 nm) and with a PDI around 0.2. The zeta potential for both polyplexes was around 15 mV (Figure 19F). In comparison with CS, C-CS formed smaller sized particles. In TEM, the C-CS/siRNA polyplexes appeared as a spherically shaped nanoparticles with an average size ~110 nm that agreed well with the DLS results (Figure 19E).

We next measured the siRNA release from the polyplexes in a heparin displacement assay. The agarose gel results indicating that all polyplexes prepared at w/w ratios of 2-10 showed siRNA releasing with the heparin concentration increasing. Polyplexes prepared at higher w/w ratios required higher heparin concentrations to start siRNA release, for example 20 ug/ml of heparin for polyplexes prepared at w/w 2 and 100 ug/ml of heparin for polyplexes prepared at w/w 8. (Figure 20D). The percent of released siRNA were then quantified by SYBR-safe assay (Figure 20E), the results indicated that polyplexes prepared at higher w/w ratios showed less released siRNA at each concentrations of heparin.

Poor stability of polyplexes in the presence of serum may limit its in vivo applications as unstable delivery carriers might release drugs or genes by dissociation of polyplexes in the blood stream. The polyplexes were prepared at w/w 8 and incubated with 50% FBS for designated times, and the remaining encapsulated siRNA in polyplexes were released by using 400 ug/ml heparin and analyzed by gel electrophoresis. In comparison with free siRNA and CS/siRNA, C-CS/siRNA can protect the siRNA for at least 18 hours as indicating by the signal of SYBR-safe stained siRNA coming out from the wells, however CS/siRNA only can protect siRNA for around 6 hours (Figure 19G). This difference might indicate the CPTA modification could improve the siRNA protection ability of CS, which would be beneficial for in vivo applications.

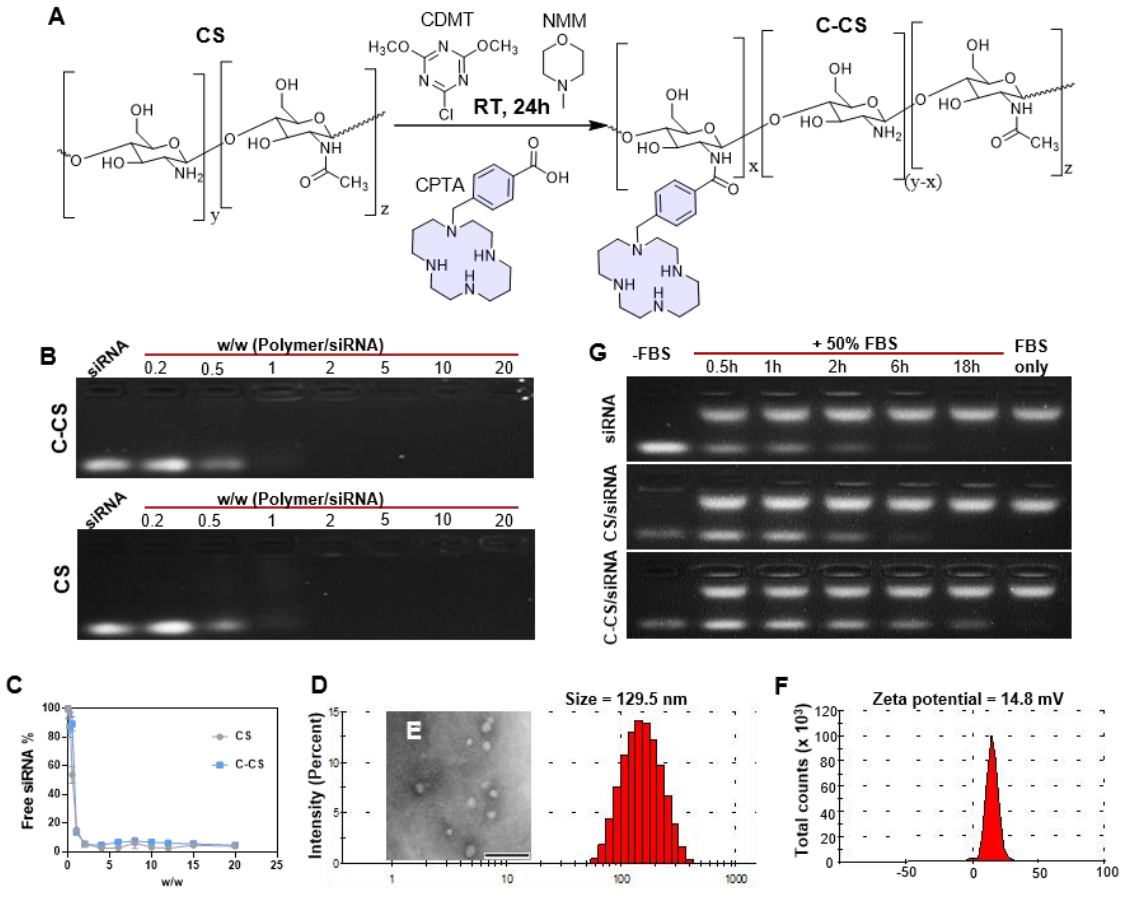

Figure 19. Characterization of C-CS/siRNA and CS/siRNA polyplexes. (A) Schematic presentation of the synthesis of cyclam (CPTA) modified chitosan (deacetylated) (C-CS). The coupling agents CDMT represents 2-Chloro-4,6-dimethoxy-1,3,5-triazine and NMM represents N-methylmorpholine. (B, C) siRNA condensation by C-CS and CS in 10 mM HEPES buffer (pH 7.4) using agarose gel electrophoresis and SYBR safe assay. (D) Representative hydrodynamic size distribution of C-CS/siRNA (w/w 8) polyplexes from DLS (n = 3). (E) Representative TEM image of C-CS/siRNA polyplexes (w/w8), scale bar = 500 nm. (F) Representative zeta potential of C-CS/siRNA polyplexes (w/w8) (n = 3). (G) siRNA stability study from C-CS/siRNA and CS/siRNA polyplexes (w/w8) in 50% FBS.

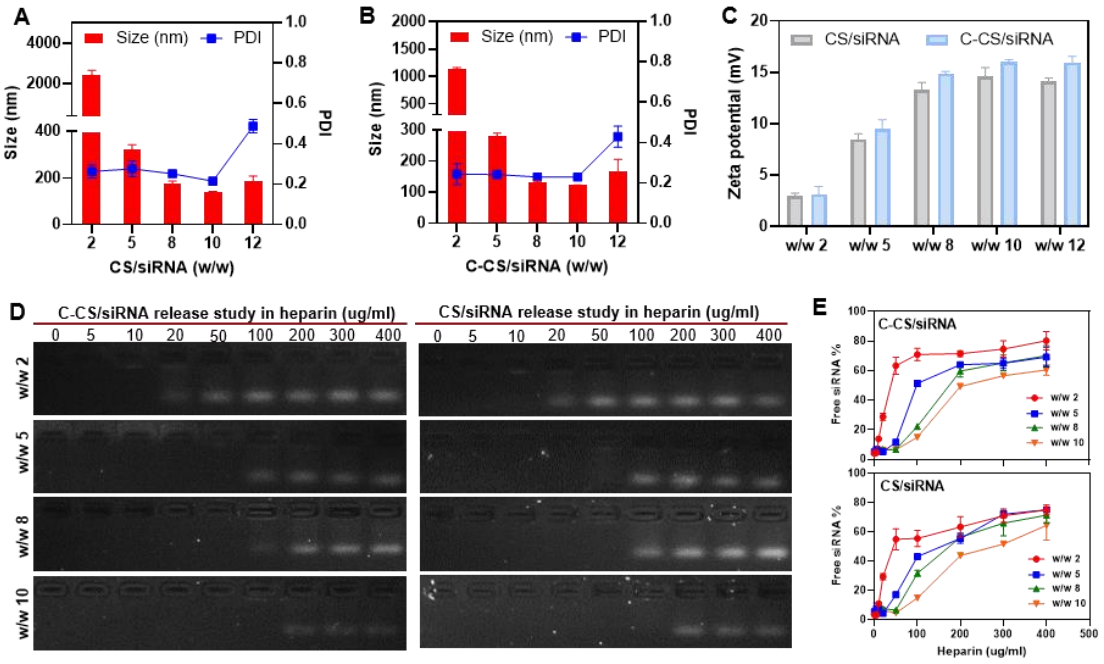

Figure 20. Characterization of C-CS/siRNA and CS/siRNA polyplexes. (A) Schematic presentation of the synthesis of cyclam (CPTA) modified chitosan (deacetylated) (C-CS). The coupling agents CDMT represents 2-Chloro-4,6-dimethoxy-1,3,5-triazine and NMM represents N-methylmorpholine. (B, C) siRNA condensation by C-CS and CS in 10 mM HEPES buffer (pH 7.4) using agarose gel electrophoresis and SYBR safe assay. (D) Representative hydrodynamic size distribution of C-CS/siRNA (w/w 8) polyplexes from DLS (n = 3). (E) Representative TEM image of C-CS/siRNA polyplexes (w/w8), scale bar = 500 nm. (F) Representative zeta potential of C-CS/siRNA polyplexes (w/w8) (n = 3). (G) siRNA stability study from C-CS/siRNA and CS/siRNA polyplexes (w/w8) in 50% FBS.

2.3. Cell compatibility and CXCR4 binding of the polyplexes

Cellular cytotoxicity was determined in human renal tubule cells (HK-2). The cells were incubated with increasing concentrations of free polymers for 24 h, then cell viability was measured by CellTiterBlue (CTB) assay and IC50 values were calculated as 42.1 μg/ml for C-CS (Figure 21B). Higher zeta potential of polycations usually associate with higher cellular toxicity [308]. And after C-CS/siRNA polyplexes formation, a part of the positive charge of polycations is neutralized by negative charged siRNA, which may decrease its cellular toxicity compared with the same amount of free polycation. Thus, the cellular toxicities of C-CS/siRNA polyplexes and free polymers were studied in HK-2 cells. As expected, starting from 50 nM siRNA onwards, polyplexes showed significantly higher cell viability than free C-CS (Figure 21C). Moreover, cells were treated with C-CS/siRNA and CS/siRNA (w/w 2, 5, 8, and 10) at 100 nM of p53 siRNA (sip53) and negative control siRNA (siNC) showed >85% cell viability at a w/w ratio up to 10 (Figure 21D). Those results indicating that C-CS/siRNA was safe for further biological studies.

Given the potential of CPTA conjugation could introduce the delivery systems with CXCR4 antagonism [264, 309, 310], we next performed a CXCR4 redistribution assay in human bone osteosarcoma epithelial cells (U2OS) to study the CXCR4 antagonism of C-CS as described in the methods part. As shown in Figure 22, C-CS and Cy3 labeled C-CS (C-CS-Cy3) treated group could block the internalization of cell surface CXCR4 receptors as AMD3100 treated group, indicating excellent CXCR4 antagonism of both C-CS and C-CS-Cy3. However, the same concentration of CS was unable to show any CXCR4

antagonism. The half maximal effective concentration (EC50) of tested compounds were then measured by using a plate reader to quantify the cellular GFP fluorescence intensity (Figure 23A). C-CS-Cy3 (7.4 ug/ml) had a slightly higher EC50 value than C-CS (5.5 ug/ml), indicating that the introduction of Cy3 on C-CS interfered with CXCR4 binding at some extend, this might because some of the fluorophores were conjugated directly to the cyclam moieties and blocked the binding of C-CS to CXCR4 receptors. Moreover, both EC50 values were much lower than their IC50 (Figure 21A),

This CXCR4 redistribution study indicating the great binding affinity of C-CS to CXCR4 receptors, and this might increase the chance for C-CS/siRNA endocytosis. We next performed cellular uptake study of C-CS/siRNA in U2OS cells to prove this hypothesis. Fluorescently labeled polyplexes were prepared with 50 nM siRNA at w/w ratios of 2, 5, 8 and 10, and incubated with U2OS cells for 3 h. As shown in Figure 24A, compared with free siRNA, both C-CS/siRNA and CS/siRNA treated cells showed >90% positive, indicating C-CS and CS improved the cellular uptake of siRNA. However, after quantification, C-CS/siRNA showed significantly higher cellular uptake than CS/siRNA at w/w ratios of 5, 8, and 10 (Figure 23B). The significantly higher cellular uptake of C-CS/siRNA in U2OS cells may be associated with the specific binding between cell surface CXCR4 receptors and CPTA moiety of C-CS. To further prove it, anti-CXCR4 antibody was used to block cell surface CXCR4 receptors. As shown in Figure 23C, after CXCR4 blocking, the cellular uptake of C-CS/siRNA was significantly decreased at 30 min, 1 h, and 2 h of incubation when compared with cells with no anti-CXCR4 antibody pretreatment. This might because the CXCR4 receptors intronization induced by anti-

CXCR4 antibodies reduced the amount of cell surface CXCR4 receptors [311], which gave less chance for the binding of C-CS/siRNA to the cells. This result was further confirmed by using confocal microscopy, fluorescence images showed that with the pretreatment of anti-CXCR4, the uptake of C-CS/siRNA was decreased as indicated by the less fluorescence intensity of siRNA-Cy5.5 (green) and C-CS-Cy3 (red) when compared with no anti-CXCR4 pretreated group (Figure 23D). Those studies indicated the specific binding between CXCR4 receptors and C-CS played a role in the enhanced endocytosis of C-CS/siRNA in U2OS cells. It worth to note that as a CXCR4 antagonism (Figure 23A), C-CS may would not induce the endocytosis of CXCR4 receptors. However, our study showed the improved cellular uptake of C-CS/siRNA, this might because the specific binding between CXCR4 and C-CS increased the chance for C-CS/siRNA to attach to cell membrane, which at the same time increased the chance for the endocytosis of polyplexes. Similar enhanced endocytosis were also been reported for other AMD3100 modified formulations in other CXCR4 expressed cell lines, like the PLGA nanoparticles [312, 313], lipoplexes and polyplexes [314].

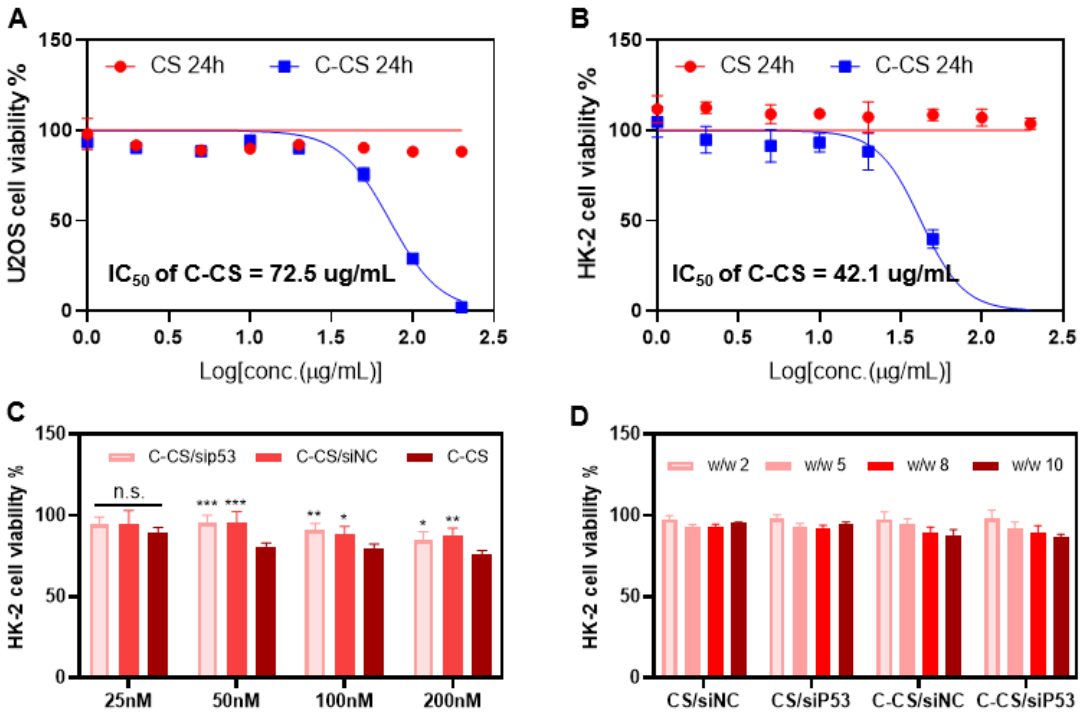

Figure 21. Cytotoxicity of CN, CC and CC/siRNA in U2OS and HK-2 cells. (**A, B**) Cellular toxicity of C-CS and CS in U2OS and HK-2 cells. (**C**) Cellular toxicity of CS/siRNA and C-CS/siRNA polyplexes in HK-2 cells. Polyplexes were prepared at w/w ratios of 2, 5, 8 and 10 at the siRNA concentration of 100nM. (**D**) Cellular toxicity of C-CS/siRNA (w/w 8) in HK-2 cells. Polyplexes were prepared at different concentrations of siRNA. All data are shown as n = 3, ∗P < 0.05, ∗∗P < 0.01, ∗∗∗P < 0.001, ns = no significance difference.

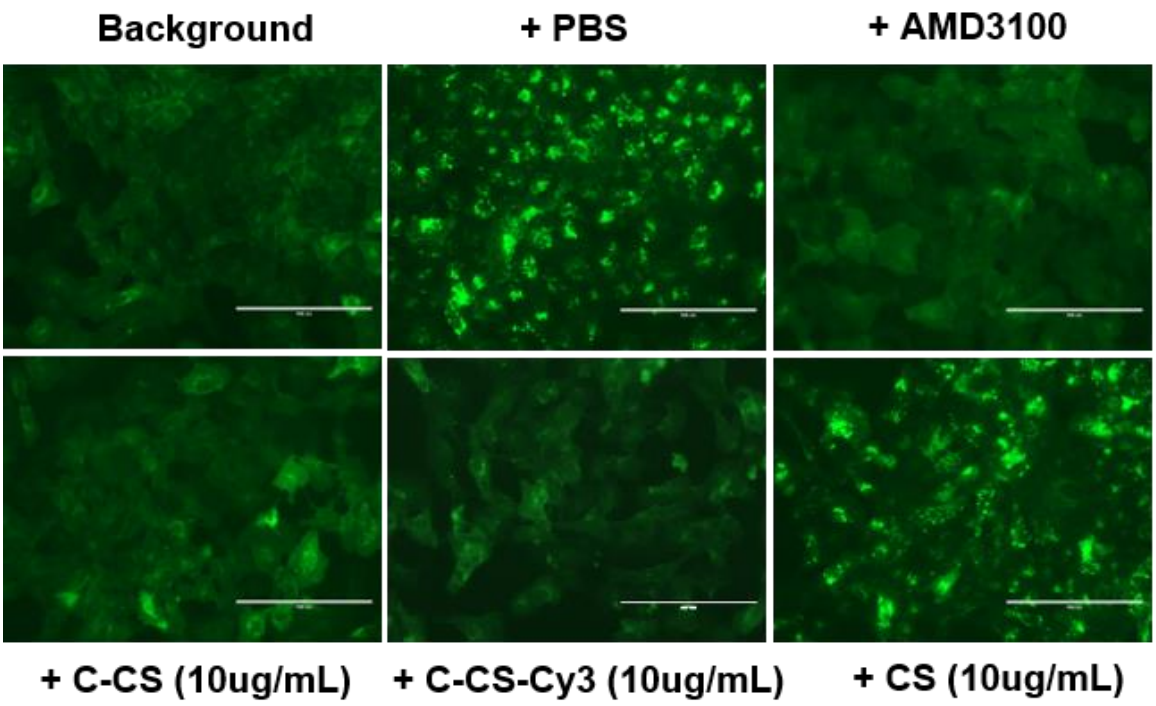

Compound	CXCR4 Antagonism (EC50, ug/mL)
AMD3100	0.005
CC	5.5
CC-Cy3	7.4
CN	-

Figure 22. CXCR4 antagonism of CC vs. AMD3100. CXCR4 receptor redistribution assay in U2OS cells expression GFP-tagged CXCR4 (green). AMD3100 (300 nM), C-CS and C-CS-Cy3 (10 μg/ml), CS (10 ug/ml). Scale bar = 100 μm.

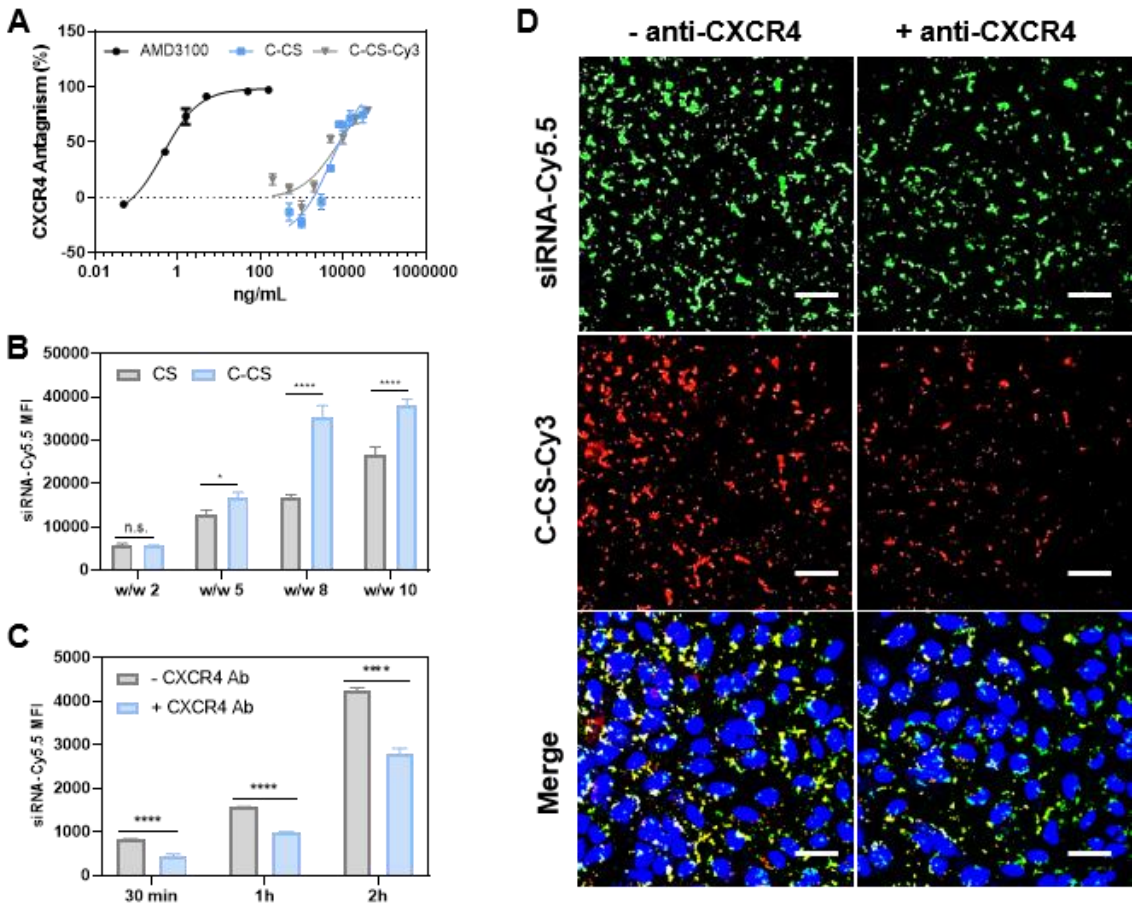

Figure 23. CXCR4 antagonism of C-CS vs. AMD3100 and CXCR4-associated endocytosis in vitro. (**A**) EC50 values of CXCR4 antagonism determined from receptor redistribution in U2OS cells (n = 3). (**B**) Flow cytometry assay to determine the cellular uptake of CS/siRNA-Cy5.5 and C-CS/siRNA-Cy5.5 in U2OS cells. Polyplexes were prepared at w/w ratios of 2, 5, 8, and 10 at the concentration of 50 nM of siRNA-Cy5.5 (n = 3). (**C**) Flow cytometry assay for the cellular uptake of C-CS/siRNA-Cy5.5 (w/w 8, 50 nM of siRNA-Cy5.5) in U2OS cells. The cells were pretreated with 10 μg/ml of CXCR4 antibody or equal amount of PBS, after washing with PBS, cells were incubated with polyplexes for 30 min, 1h, and 2h, then the uptake amount of polyplexes were determined

by flow cytometry (n = 3). (**D**) Representative confocal images from C-CS-Cy3/siRNA-Cy5.5 treated U2OS cells. The cells were pretreated with 10 μg/ml CXCR4 antibody or equal amount PBS for 30 min, after washed with PBS, further incubated with C-CS-Cy3/siRNA-Cy5.5 at the concentration of 50nM siRNA for another 4 hours, then visualized the uptake under a confocal microscopy. Scale bar = 50 μm. ∗P < 0.05, ∗∗∗∗P < 0.0001, ns = no significance difference. (Continued Figure 23)

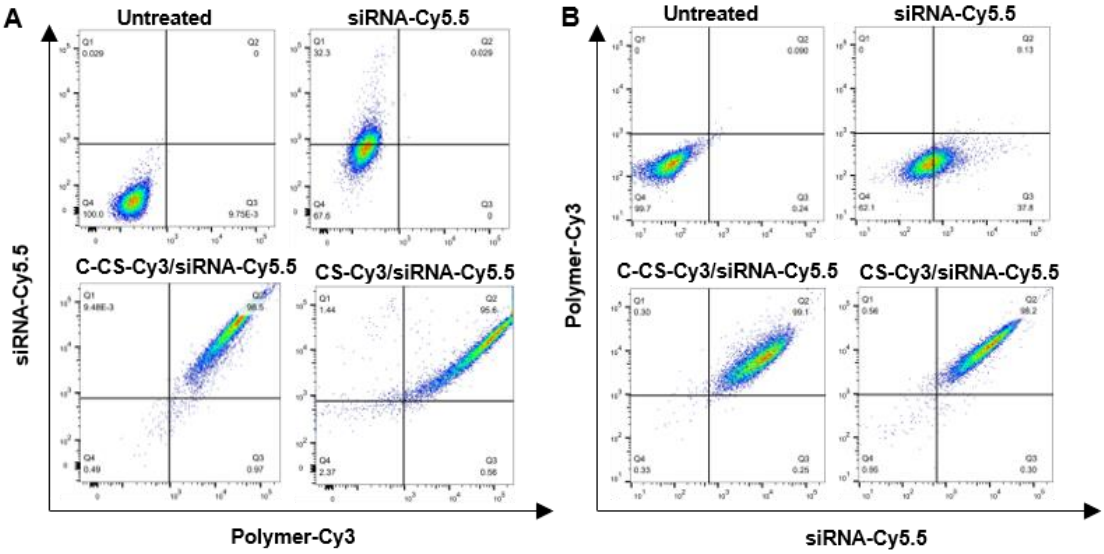

Figure 24. Cellular uptake of CC/siRNA and CS/siRNA in U2OS and HK-2 cells. (A, B) C-CS and CS enhanced siRNA uptake in U2OS (A) and HK-2 (B) cells. Polymers were labeled with Cy3 and siRNA were labeled with Cy5.5, cells were treated at 50nM of siRNA (w/w 8). Compared with free siRNA treated group, C-CS/siRNA and CS/**siRNA** treated cells showed over 90% cells were positive with Cy3 and Cy5.5.

2.4. Anti-apoptosis effects of C-CS/sip53 in vitro

The upregulation of renal CXCR4 in tubule cells has been reported from an ischemia-reperfusion induced AKI mice model [223], however, it hasn't been reported in vitro. Here, we used 5 μM cisplatin and 500 μM H2O2 as cell stressors. As shown in Figure 25B and C, treatment with cisplatin and H2O2, caused HK-2 cells to overexpress CXCR4. Moreover, with the longer times under stress, more CXCR4 were expressed. Confocal microscopy was used to visualize the expression of CXCR4 receptors. As shown in Figure 25A, CXCR4 (red) was specifically expressed on H2O2 and cisplatin stimulated cells surface while normal cells didn't show any CXCR4 expression. After confirming the CXCR4 expression on injured cells surface, we next performed cellular uptake experiment to determine if the expressed CXCR4 on HK-2 cells would enhance uptake of C-CS/siRNA like in U2OS cells. As shown in Figure 26, the siRNA (green) and C-CS (red) showed similar uptake in normal cells and in stimulated cells with anti-CXCR4 antibody pretreatment. However, for the stimulated cells without anti-CXCR4 antibody pretreatment showed higher siRNA and C-CS uptake. This result was consistent with the results from U2OS cells, which further confirmed the specific binding between C-CS and CXCR4 could enhance the endocytosis of C-CS/siRNA. Hence, it has been demonstrated that the use of CPTA as a potential CXCR4 binding moiety can specifically enhance the delivery of therapeutic siRNA in injured tubule cells.

As a well-known tumor suppress gene, p53 is markedly up-regulated when tubule cells are under stress and it plays an essential role in apoptosis induction after cell injury

[315]. As shown in Figure 25D, the Western blot results obtained in our study showed that the H2O2 and cisplatin stimulation significantly up-regulated the levels of p53 in HK-2 cells, which is consistent with previous report [316, 317]. Similar to the protein levels, the mRNA levels of CXCR4 and p53 were significantly increased after stimulation (Figure 25E and F). In vitro studies showed evidence that chemical or genetic inhibition of p53 protects renal tubule cells against cisplatin induced injury [121, 271, 318]. Polyplexes were prepared with 50 nM of p53 siRNA or negative control siRNA and incubated with HK-2 cells for 36 h. As shown in Figure 25G, C-CS/sip53 significantly downregulated around 70% of p53 mRNA as compared with untreated and C-CS/siNC control groups. Encouraged by the excellent transfection effect of C-CS/sip53 in HK-2 cells, we next studied its anti-apoptosis effect in vitro. HK-2 cells were pretreated with C-CS/sip53, C-CS/siNC, and PBS for 12 hours, after being stimulated with 5 uM of cisplatin for additional 20 hours, the apoptotic cells were quantified by using an Annexin V-FITC/PI apoptosis detection kit. The number of apoptotic cells in C-CS/sip53 treated group was significantly lower as compared with PBS and C-CS/siNC treated groups (Figure 25H and I), suggesting that silencing of p53 could relief cisplatin-induced apoptosis.

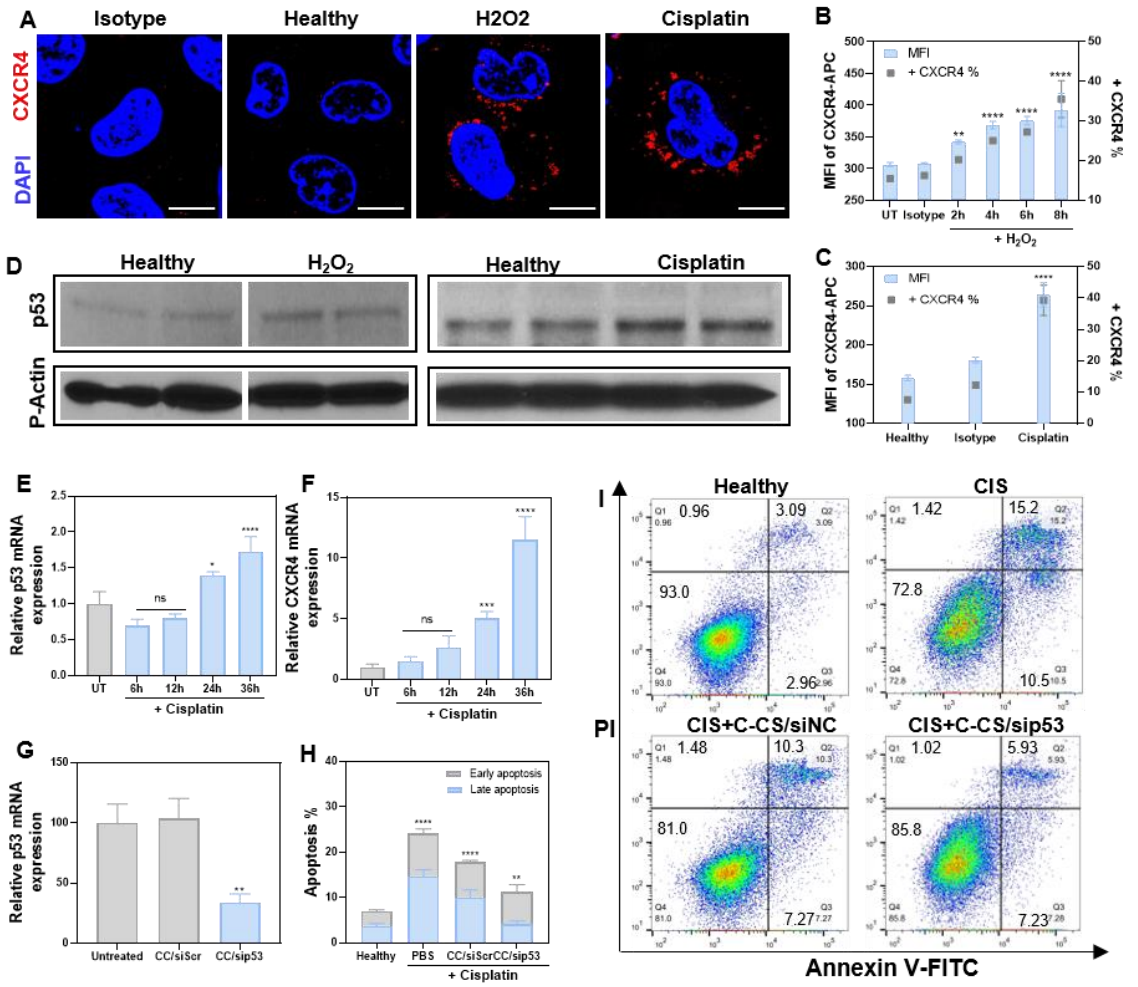

Figure 25. Upregulation of CXCR4, p53, and relief of apoptosis in vitro. (A) Representative confocal images of injured HK-2 cells surface CXCR4 expression. The cells were previously stimulated with H2O2 (500 μM) for 6 hours or cisplatin (5 μM) for 24 hours, then cells were incubated with APC labeled CXCR4 primary antibody at a concentration of 10 μg/ml for half hours, after wash with 3 times of PBS, the expression of CXCR4 was visualized under a confocal microscopy. Nuclei were stained with DAPI showing as blue and the expressed CXCR4 receptors were showing as red. Scale bars = 20 μm. (B, C) Determination of HK-2 cells surface CXCR4 expression by flow cytometry

assay in normal condition and H2O2 or cisplatin stimulated condition. (D) Western blotting analysis of p53 expression using lysates from healthy and H2O2 or cisplatin stimulated HK-2 cells. (E) Levels of p53 mRNA in HK-2 cells after stimulated by 5 μM of cisplatin for different time points. (F) Levels of CXCR4 mRNA in HK-2 cells after challenged with cisplatin for 6h, 12h, 24h and 36h. (G) Levels of p53 mRNA level in HK-2 cells after being treated with C-CS/siRNA nanoparticles (50 nM siRNA) for 48 hours. (H) The mean percentage of apoptotic cells in (I). (I) Flow cytometry-based apoptosis assay by the Annexin V-FITC Apoptosis Kit. Data are shown as n = 3, ∗P < 0.05, ∗∗P < 0.01, ∗∗∗P < 0.001, ∗∗∗∗P < 0.0001, ns = no significance difference, as compared with untreated or healthy group. (Continued Figure 25)

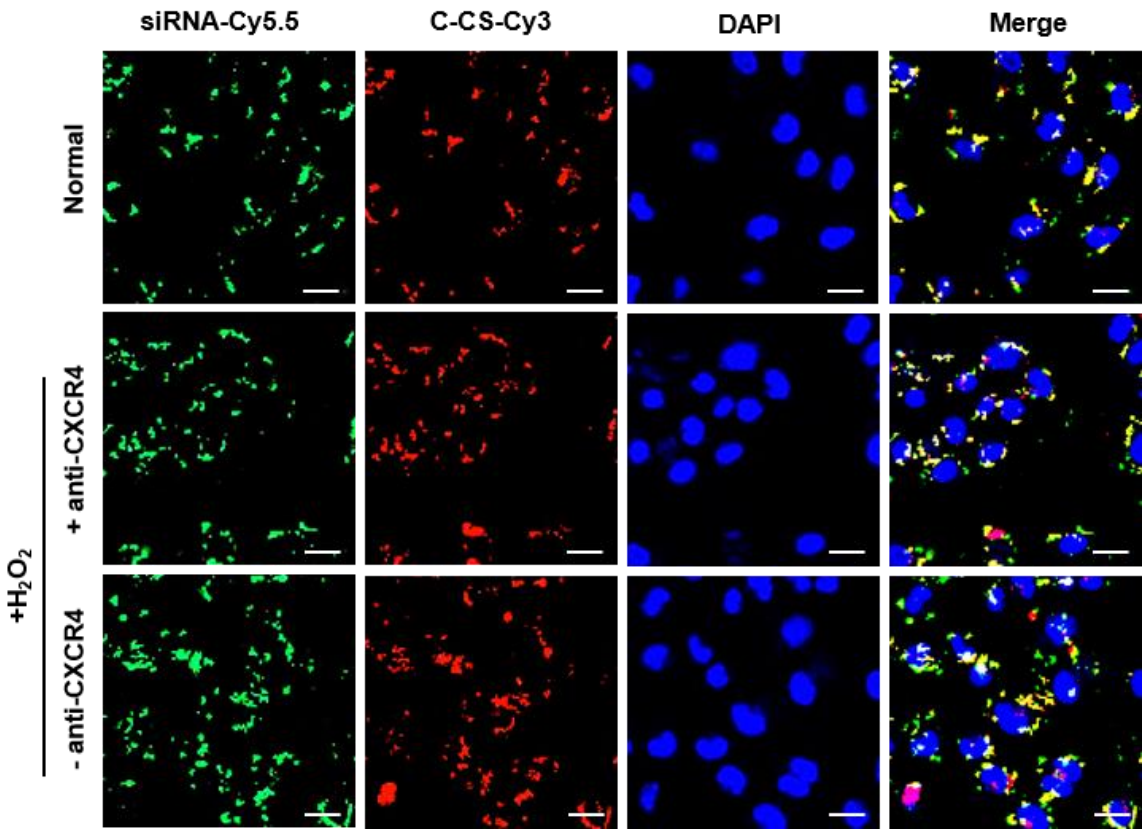

Figure 26. Representative confocal images of HK-2 cellular uptake of C-CS-Cy3/siRNA-Cy5.5 under normal and H_2O_2 induced injured conditions. The injured cells were pretreated with 5 μg/ml CXCR4 antibody or PBS for 30 min before further incubate with fluorescence labeled CC/siRNA polyplexes, then the uptake of C-CS/siRNA was visualized under a confocal microscopy. Scale bar = 50 μm.

2.5. Blood clearance kinetics of C-CS/siRNA

Intravital microscopy can be used to monitor the blood circulation of polyplexes and provide a more convenient way to discern the different pharmacokinetic parameters of nanoparticles in different animal models [319-322]. The blood circulation of C-CS/siRNA was studied in both normal (sham) and IRI-AKI mice by measuring changes in the fluorescence intensity of the polyplexes in an ear vein continuously imaged by intravital microscopy for 30 min [323]. Our results showed different pharmacokinetic properties in sham and AKI mice (Figure 27). As shown in Table 2, the area under the curve for C-CS/siRNA in sham was roughly three times higher than in AKI mice. Average circulation half-life of C-CS/siRNA in sham and AKI mice were 1.7 and 1.3 h, respectively. Those results indicating the quicker systemic clearance of C-CS/siRNA in AKI mice when compared with sham mice, and it might be because of the difference in renal structure of GFM between healthy and injured kidneys. Previous studies showed significant changes in the glomerular filtration membrane (GFM) structure and permeability in IRI-AKI mice during the initial injury phase. The injured GFM usually characterized by the enlarged fenestration of endothelium, enlarged gaps between podocytes, fewer crosslinks in GBM, enlarged gaps of endothelium, and fewer negative charges [4]. These changes induce large pores in GFM and can allow nanoparticles to freely pass through [252, 324-326]. However, the intact GFM in healthy kidneys gives nanoparticles less chance to pass through and the rest of them will join the systemic circulation again [4]. In addition, in the IRI-AKI stage, kidney loss their size and charge selectivity, which may further increase the chances of C-

CS/siRNA to reach to tubule areas and prolong its accumulation in the injured tubule cells through CXCR4 receptor binding and finally enhance its endocytosis (Scheme 8).

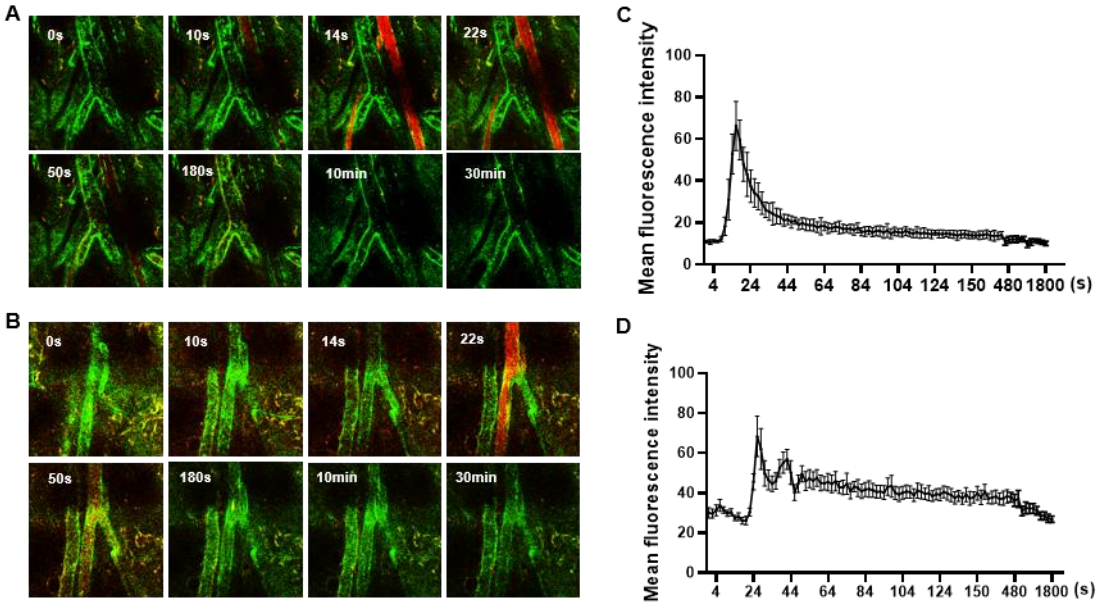

Figure 27. Pharmacokinetics of C-CS-Cy3/siRNA polyplexes in sham and IRI-AKI mice. (A, B) A panel of intravital microscopy images of mouse ear vein for visualization of pharmacokinetic differences of C-CS/siRNA in IRI-AKI (A) and sham (B) mice. (C, D) Quantified average intravascular fluorescence intensity curves from IRI-AKI (C) and sham (D) mouse ear vessel imaging.

Table 2

Non-compartmental blood pharmacokinetic analysis in sham and IRI-AKI mice.

Pharmacokinetic parameter	Sham	IRI-AKI
$t_{1/2}$ (h)	1.7 ± 0.7	1.3 ± 0.4
t_{max} (s)	29.6 ± 7	16.4 ± 0.9
AUC (mg·s)/(L)	57521.1 ± 9421.5	21868 ± 2211.2

2.6. Biodistribution of C-CS/siRNA

Since CXCR4 was upregulated in tubules of injured kidneys [223], and we have confirmed the excellent CXCR4 targeting ability of C-CS/siRNA in vitro, here we hypothesized that the specific interaction between C-CS/siRNA and CXCR4 may enhance the accumulation of C-CS/siRNA in the injured kidneys during systemic circulation. To confirm this hypothesis, in vivo biodistribution study of fluorescently labeled polyplexes was carried out in a bilateral IRI-AKI model. Fluorescence labeled polyplexes C-CS-Cy3/siRNA-Cy5.5 or CS-Cy3/siRNA-Cy5.5 were injected intravenously, and the biodistribution of polyplexes was assessed after 4 h of injection by using an IVIS imagining system. The ex vivo fluorescence images (Figure 28A and B) showed a preferential accumulation of C-CS-Cy3/siRNA-Cy5.5 in the injured kidneys as detected by the higher intensity of both C-CS and siRNA. In contrast, for CS/siRNA treated group, the CS and siRNA showed higher accumulation in the liver and kidney respectively, the poor colocalization of CS and siRNA in kidneys could be because of the poor serum stability of CS/siRNA polyplexes (Figure 19F), which may result in their dissociation during systemic circulation. After quantifying the fluorescence intensity from different organs, we found that C-CS-Cy3 showed a 4.8-fold higher kidney to liver ratio than CS-Cy3, indicating the targeting ability of C-CS to injured kidney (Figure 28C). Considering the targeting ability of C-CS to injured kidneys, one could assume that kidney to liver ratio of siRNA in the C-CS polyplexes should be similarly increased. However, the results revealed a similar kidney to liver ratio (Figure 28D) for both groups. We hypothesized that there must be a higher accumulation of C-CS/siRNA group in the kidney, but because

of the rapid dissociation of CS-Cy3/siRNA-Cy5.5 polyplexes followed by accumulation of free siRNA to the kidney, we are detecting a similar kidney to liver ratio of siRNA-Cy5.5.

To further investigate the targeting ability of C-CS/siRNA to injured kidneys, in vivo biodistribution of C-CS/siRNA was performed in sham and IRI-AKI mice. After injecting fluorescence labeled C-CS/siRNA nanoparticles, ex vivo images of major organs from the sham and IRI-AKI mice were captured at 24 h post injection. As shown in Figure 29A, compared with the sham mice, IRI-AKI mice displayed a significantly higher fluorescence intensity in the kidneys for both C-CS and siRNA. After quantifying the fluorescence intensity of each organ, we found that the accumulation of C-CS was ~2.5 times and accumulation of siRNA was ~1.5 times higher in the injured kidneys in comparison with healthy ones (Figure 29B, C). This study further suggested the targeting ability of C-CS/siRNA to the injured kidneys.

To identify the location of C-CS/siRNA in kidneys, we took the images of the frozen kidney section under confocal microscopy. As shown in Figure 29D, at post 4 hours of injection, C-CS (red) and siRNA (yellow) were mostly located in the tubules in the injured kidney; as for the sham kidneys, C-CS and siRNA were located in tubules and glomeruli. After 24 h of polyplexes injection, we found that most C-CS and siRNA were located in the tubules of the injured kidney; however, in the sham kidneys, the fluorescence signals of C-CS/siRNA were very weak and the rest of them were mostly accumulated in the glomeruli. The C-CS/siRNA polyplexes showed a significantly higher accumulation in the injured kidney than the sham kidney at 4 and 24 hours of post-injection, as indicated by

the fluorescent intensity and the positive areas. The different accumulation of C-CS/siRNA in sham and IRI kidneys might be because of the different size and charge selectivity of sham and injured kidneys as mentioned earlier. The enhanced accumulation of C-CS/siRNA in renal tubules in injured kidneys might be attributed to the CXCR4 helped endocytosis. To prove our hypothesis, frozen tissue slides were stained with anti-CXCR4-FITC and colocalization between C-CS/siRNA and CXCR4 was analyzed as merge them together (Figure 29D). The result reveled the CXCR4 expression was only in the injured kidney, which was consistent with our in vitro study (Figure 25A). More importantly, strong colocalization of CXCR4 and C-CS/siRNA was observed. In this study, we found that C-CS/siRNA polyplexes were mainly located in tubules in injured kidneys for at least 24 hours. However, in sham kidney, we could only see the tubule accumulation at earlier time point (4h), and most of the polyplexes were accumulated in glomeruli after 24 hours of injection. The enhanced accumulation of C-CS/siRNA in injured kidneys could be because of two main reasons: firstly, the loss of size and charge selectivity of GFM in injured kidneys [4, 275, 276] and secondly, the specific binding between CXCR4 and C-CS/siRNA. We hypothesized that the injured kidney with a large pore size of GFM may allow the C-CS/siRNA polyplexes to pass through followed by preferential accumulation of C-CS/siRNA polyplexes in the injured tubule cells through CXCR4 mediated endocytosis. These findings further suggesting the potential role of CXCR4 as a target for enhanced delivery of therapeutic siRNA to injured renal tubule cells for AKI treatment.

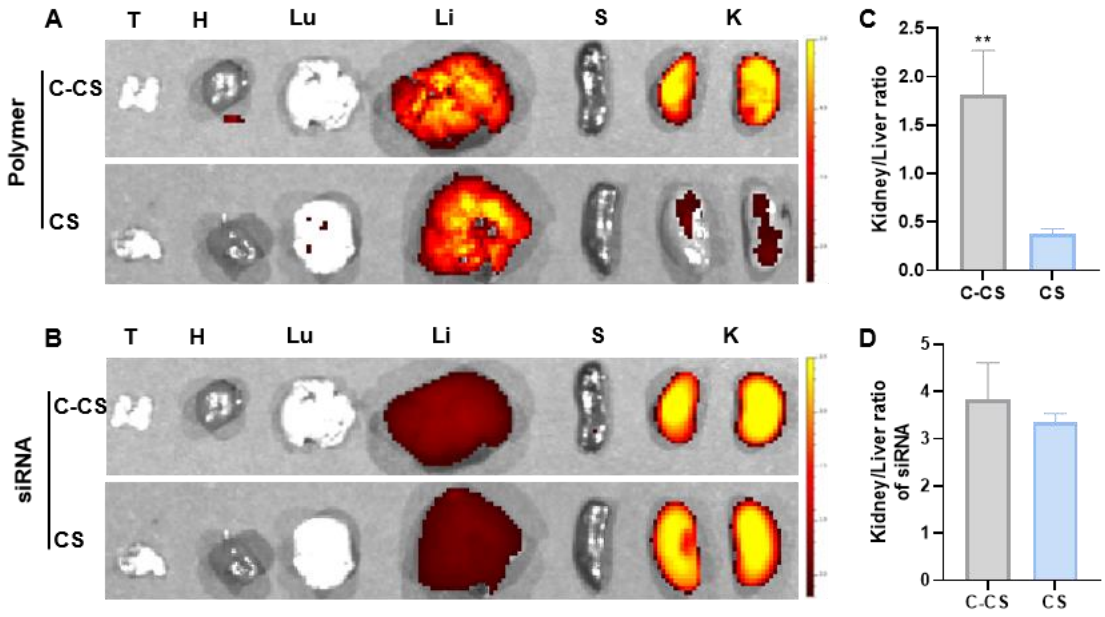

Figure 28. Biodistribution of polyplexes in IRI-AKI mice. Polymer were labeled with Cy3, and siRNA were labeled with Cy5.5. (A, B) Ex vivo fluorescence images of the main organs (from left to right, thymus, heart, lung, liver, spleen, kidneys) at 24 hours post intravenous injection of fluorescence labeled polyplexes. One of three independent experiments is shown. Renal ischemia was induced by clamping the bilateral renal pedicles for 30 min with a micro clamp and then removed clamping for reperfusion to induce IRI-AKI. After the induction of AKI, polyplexes (w/w 8, 0.5 mg/kg of siRNA) were administered intravenously. 4 hours later, the main organs were harvested for fluorescence visualization. (C, D) Kidney to liver ratios of polymer and siRNA fluorescence intensity. **p<0.01.

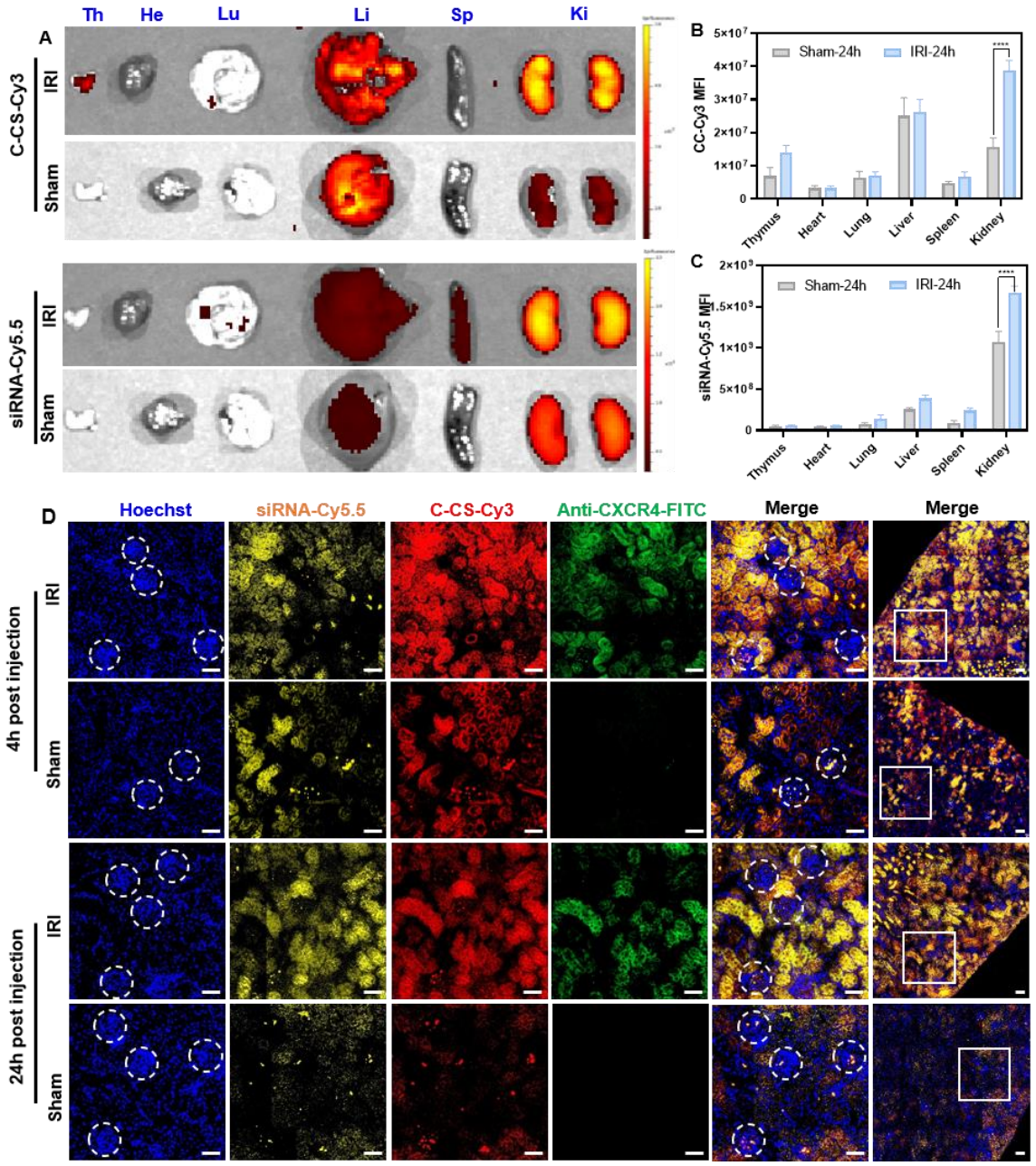

Figure 29. Biodistribution and renal accumulation of C-CS-Cy3/siRNA-Cy5.5 in IRI-AKI and sham mice. (A) Ex vivo fluorescence images of the main organs (thymus, heart, lung, liver, spleen, kidneys) at 24 hours post intravenous injection of C-CS-Cy3/siRNA-Cy5.5 polyplexes. One of three independent experiments is shown. Renal ischemia was

induced by clamping the bilateral renal pedicles for 30 min with a micro clamp and then removed clamping for reperfusion to induce IRI-AKI. Sham surgery was induced as the same procedures as IRI-AKI mice, but no renal vasal clamping. After the induction of AKI or sham, C-CS-Cy3/siRNA-Cy5.5 polyplexes (w/w 8, 0.5 mg/kg of siRNA) were administered intravenously. 24 hours later, the main organs were harvested for fluorescence visualization. (B, C) Region of interest analysis of the major organ uptake of C-CS-Cy3/siRNA-Cy5.5 polyplexes in sham and AKI mice at post 24 hours injection. n = 3 (sham) and 4 (BIRI) independent mice, ****$p<0.0001$ as compared with sham group. (D) Representative confocal images of kidney sections after 4 and 24 hours of C-CS-Cy3/siRNA-Cy5.5 injection. Sections were stained with FITC labeled CXCR4 antibody for the visualization of renal CXCR4 expression (green). The glomerular were indicated by the white circle dots. Scale bars = 50 μm. (Continued Figure 29)

2.7. Therapeutic effect of C-CS/sip53 in IRI-AKI model

We next investigated if the enhanced distribution of C-CS/siRNA in renal tubules would enhance the therapeutic effect of C-CS/sip53 in AKI. Prior to the animal study, the gene knockdown efficiency of three different p53 siRNA candidates was tested in mouse renal tubule cells (MCT), and the candidate (siRNA-3) with best gene knockdown effect (~92.5% gene silencing) was chosen for the following studies (Figure 30). The ability of the C-CS/sip53 polyplexes to alleviate AKI was studied in IRI-AKI mouse model. PBS, AMD3100 (1 mg/kg), C-CS/siNC and C-CS/sip53 (0.8 mg/kg of siRNA, w/w 8) were administrated through intravenous injection, then blood and major organs were collected for further analysis. It is worth mentioning that a high level of serum creatinine (Scr) and blood area nitrogen (BUN) usually indicates the loss of renal function [327, 328]. At this moment, to determine the level of Scr and BUN, serum was collected form the blood and detected by using a Scr and BUN detection kit. The results reveled a significantly lower Scr and BUN in C-CS/sip53 treated group (Figure 31B and C). We further analyzed the weight ratios between kidney and mice body for each treatment group (Figure 31D). The C-CS/sip53 treated group showed lowest ratio compared with other AKI mice, indicating less renal edema, which might be associated with decreased renal inflammation after treatment. P53 induced tubule cells apoptosis plays a pivotal role in the development of AKI. Kidney tissues were homogenized and levels of p53 mRNA were determined by using qRT-PCR. As shown in Figure 31E, AKI mice with PBS, AMD3100, and C-CS/siNC treatment showed significantly higher p53 levels when compared with sham mice, indicating that the treatment of CXCR4 antagonisms had no influence on p53 expression.

Whereas, after the treatment with C-CS/sip53, the renal p53 mRNA level was similar as sham mice, indicating the excellent gene knockdown efficiency of C-CS/sip53, which is consist with our in vitro study (Figure 25G). Moreover, downregulated p53 expression level by treatment with C-CS/sip53 was also revealed by immunofluorescence analysis of the kidney tissue sections (Fig 32E and I), and other AKI mice with different treatments did not show p53 downregulation, which was consist with our qRT-PCR result. We further analyzed H&E stained kidney slides for each group. Normal renal morphology was observed in the sham group. Several tubule damages were shown in AKI mice with PBS, AMD3100, and C-CS/siNC treatments, evidenced by that hyaline cast and sloughed cells filled in many tubules. However, the C-CS/sip53 treated AKI mice showed less cast formation and slough cells, indicating the great potential of C-CS/sip53 for AKI therapy (Figure 31G).

The number of macrophages increases in the ischemic kidneys soon after reperfusion, especially in the outer medulla [329]. The increased infiltration of macrophages facilitate the inflammatory condition in the injured kidneys through secretion of cytokines, induction of apoptosis and the recruitment of neutrophils, which finally establish renal injury [330]. As shown in Figure 32 (A and F), C-CS/sip53 treated AKI mice showed less macrophages infiltration, whereas there was an obvious increase of macrophages in other AKI mice, suggesting that C-CS/sip53 holds strong anti-inflammatory effect among all the treatment groups. As another inflammation player in IRI-AKI, neutrophils, also showed increased infiltration in the injured kidneys. However, C-CS/sip53 treated AKI mice showed decreased neutrophil infiltration (Figure 32B and G). We further evaluated the

apoptosis in injured kidneys by measuring their apoptotic cells using cleaved caspase 3 staining. The apoptotic cells were obviously decreased in C-CS/sip53 treated group when compared to other groups at 48 h after surgery (Figure 32C and H), indicating the favorable anti-apoptosis effect of C-CS/sip53 for IRI-AKI. We didn't see obviously change for CXCR4 expression in different treatment groups (Figure 32D).

At the end of treatment, we investigated whether C-CS/sip53 treatment had any adverse effect in other organs. Thus, the heart, liver, spleen and lung from each group were collected, weighted and tissue sections were conducted with H&E staining (Figure 33). By analyzing the H&E staining of tissue slides, we found that each group organs showed normal tissue structures and no obvious difference after different treatments. Also, the organ to body weight ratios showed no significant difference between each treatment group. Moreover, hematology analysis for each group showed the parameters were in normal ranges. These results clearly demonstrate biocompatibility of C-CS and indicate its potential as a siRNA carrier for AKI treatment.

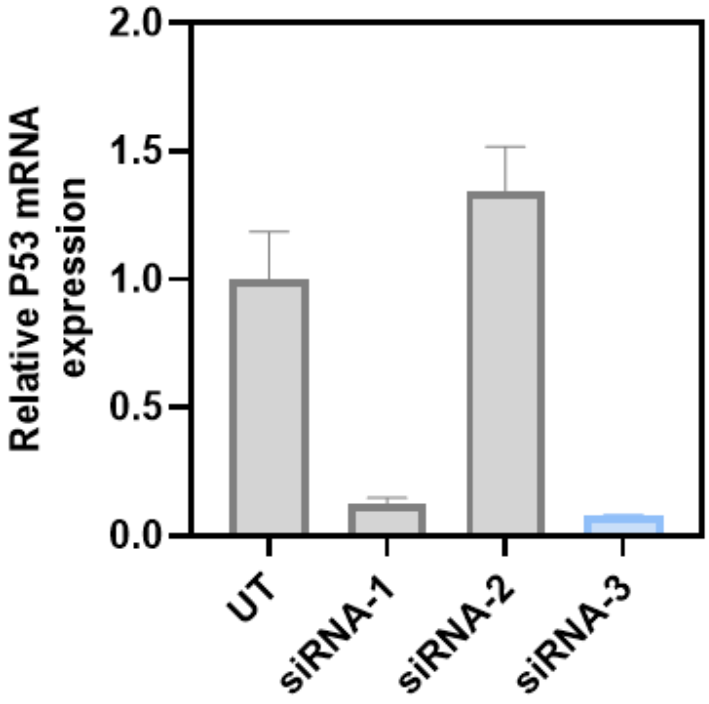

Figure 30. Screening of p53 siRNA candidates. 50nM of three mice p53 siRNAs were loaded by lipofectamine and incubated with MCT cells for 48 hours. Then the cells were harvested for RT-PCR analysis.

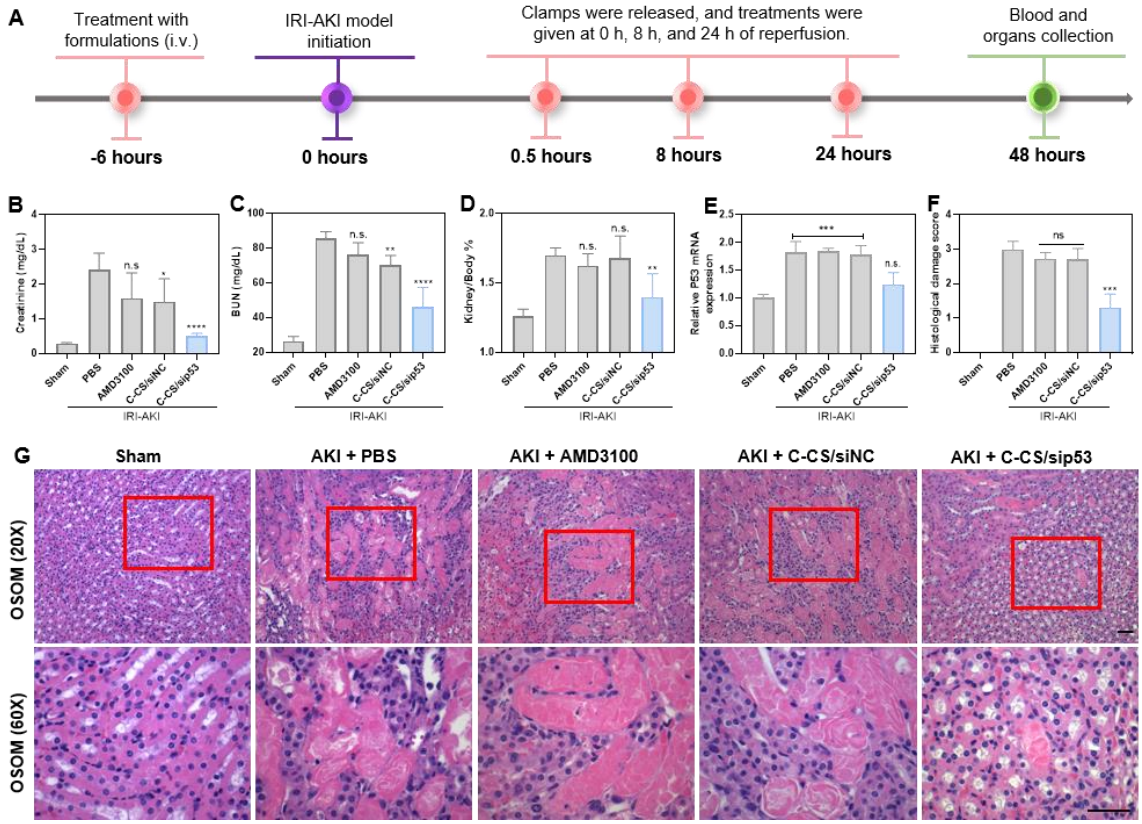

Figure 31. Attenuation of renal injury by CC/sip53 in vivo. (A) Six hours before the initiation of IRI-AKI, different treatment agents (PBS, AMD3100, C-CS/siNC, and C-CS/sip53) were administrated intravenously. After release clamps from kidney vessels, treatment agents were administrated intravenously at post 0 hour, 8 hours, and 24 hours of reperfusion. At post 48 hours of reperfusion, blood and major organs were collected for further evaluation. (B, C) Blood chemistry analysis for serum creatinine and BUN level after different treatments. (D) Kidney to body weight ratio (w/w %) from different treatment groups. (E) The mRNA level of p53 in the kidneys from different treatment groups. (F) Kidney damage scores for outer strip of the outer medulla (OSOM) in different treatment groups. (G) Representative H&E staining images for kidneys tissues in the

OSOM. The sham group showed normal tubules architecture and no evidences of injury. Serious injury was observed in kidneys of PBS, AMD3100, and C-CS/siNC treated mice. $*P < 0.05$, $**P < 0.01$, $***P < 0.001$, $****P < 0.0001$, ns = no significance difference, as compared with sham or PBS groups (n=4 or 5). Scale bar, 50 um. (Continued Figure 31)

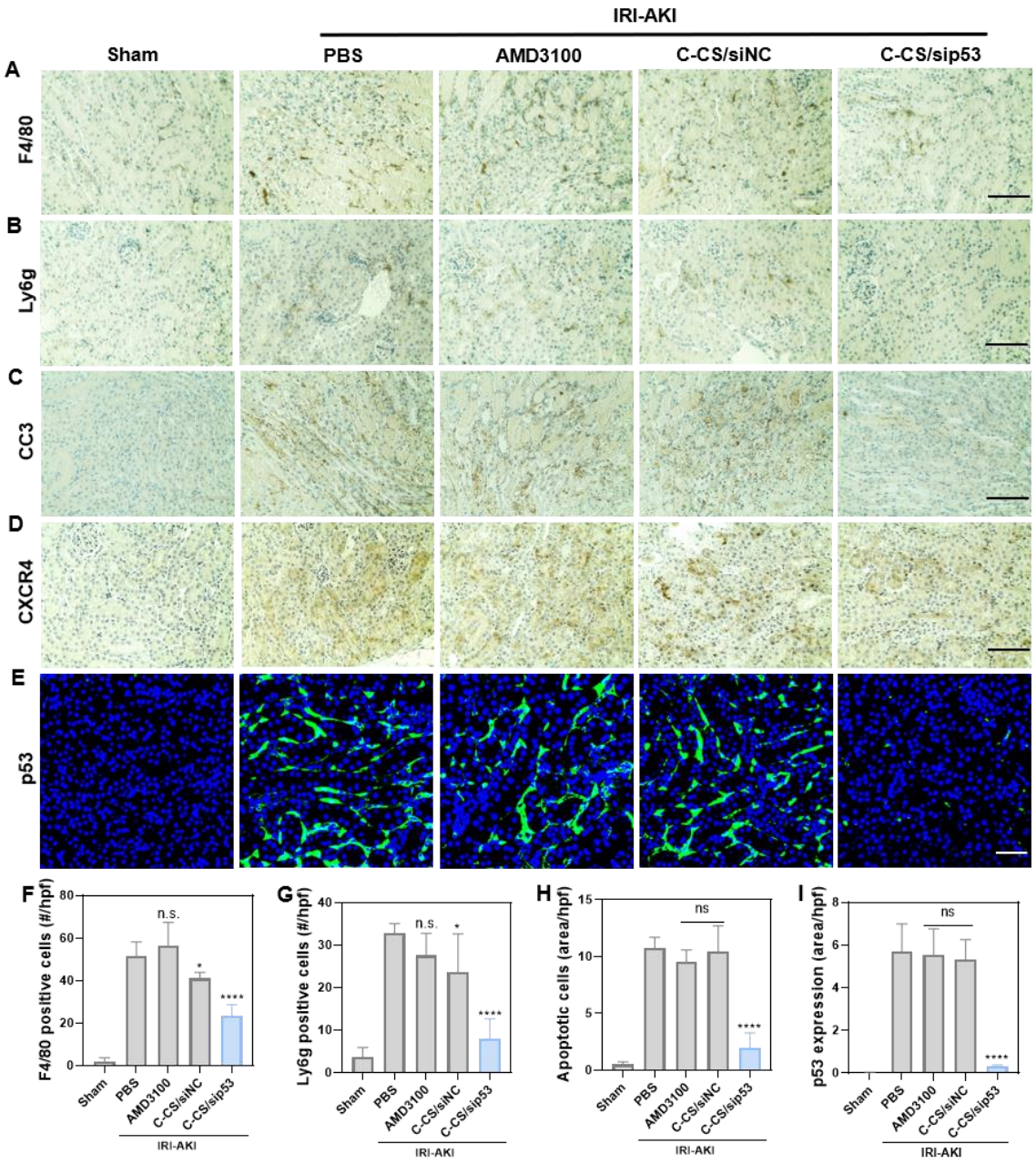

Figure 32. CC/sip53 treatment reduced renal immune cells infiltration, apoptotic cells, p53 expression in AKI mice. (**A**) Renal macrophage immunostaining using anti-F4/80 antibody. (**B**) Renal neutrophil immunostaining using anti-Ly6g antibody. Scale bar, 50um. (**C**) Renal cleaved caspase 3 immunostaining using anti-CC3 antibody. (**D**) Renal CXCR4 immunostaining using anti-CXCR4 antibody. (**E**) Renal p53 immunofluorescent

staining by using anti-p53 antibody. (**F**) The number of F4/80 positive cells per high-power field (hpf) in sham and AKI groups after different treatment. (**G**) The number of Ly6g positive cells per high-power field (hpf) in sham and AKI groups after different treatment. (**H**) The area percentage of apoptotic cells per high-power field (hpf) in sham and AKI groups after different treatment. (**I**) The area percentage of p53 positive cells per high-power field (hpf) in sham and AKI groups after different treatment. $*P < 0.05$, $****P < 0.0001$, ns = no significance difference, as compared with PBS group (n = 5). Scale bar, 50um. (Continued Figure 32)

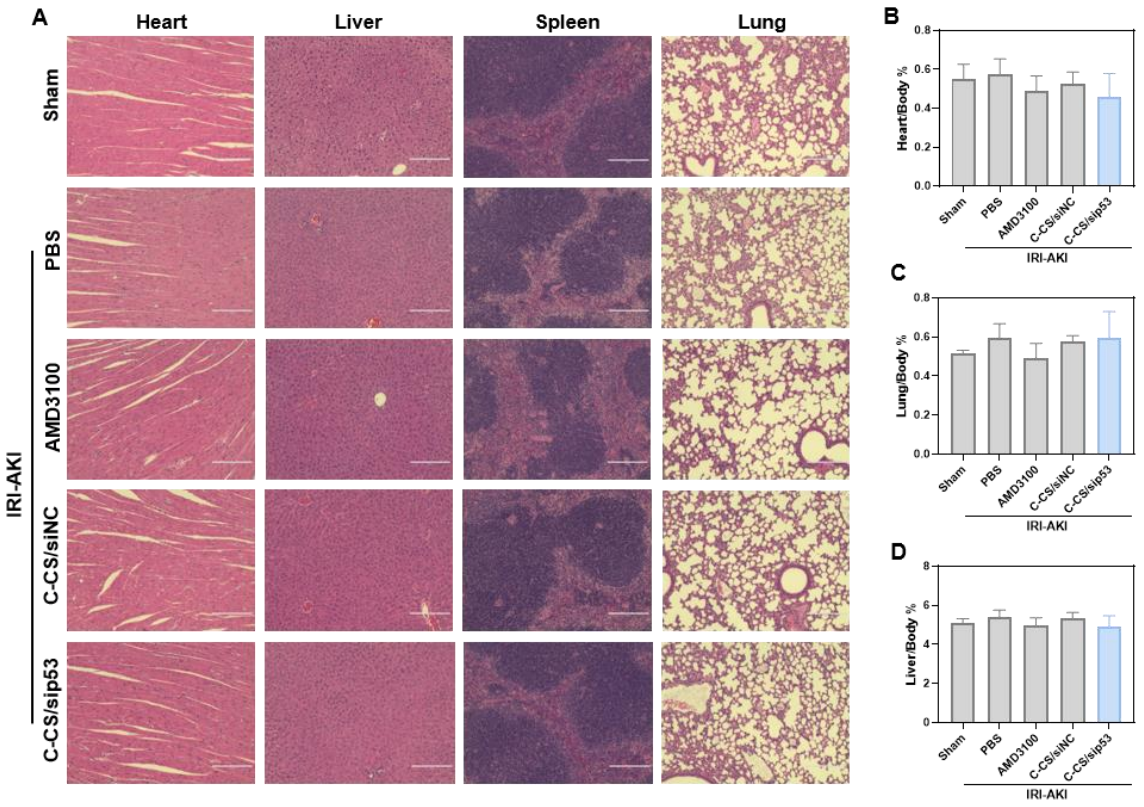

Figure 33. Assessment of treatment toxicity to major organs. (A) H&E staining of major organs (heart, liver, spleen, lung) from different treatment groups. (B - D) Organs (heart, lung, liver) to body weight ratio. Scale bars = 100 μm.

3. Conclusion

Here, we synthesized cyclam modified chitosan (C-CS) to deliver bioactive p53 siRNA to tubule cells in the injured kidneys as a pharmacological intervention to prevent IRI-AKI. We found that without cyclam modification, CS barely showed renal accumulation in AKI mice when compared with C-CS. Surprisingly, with the modification of cyclam, C-CS could effectively retain in the injured kidneys for at least 24 hours rather than be rapidly eliminated, which is essential to reach therapeutic effect and could effectively protect the kidney from serious damage. The enhanced renal accumulation and retention of C-CS/siRNA in the injured kidney is attributed to the preferential intronization by injured tubule cells through CXCR4 mediated endocytosis. The activation of CXCR4 in the pathology of IRI-AKI has been reported. However, use CXCR4 as a target for RNAi delivery is a new field. Our study showed the potential of combine CXCR4 targeting with p53 gene silencing as an effective treatment for IRI-AKI therapy.

4. Materials and methods

4.1. Materials

Chitosan (degree of deacetylation 85%, CAS# 9012-76-4) was purchased from Polyscience, Inc. Cyclam was purchased from ChemScene LLC. α-bromo-p-toluic acid was purchase from Sigma Aldrich. Chloro-4,6-dimethoxy-1,3,5-triazine (CDMT) and N-methylmorpholine (NMM) were purchased from TCI America, Inc. Cy3-NHS was purchased from Lumiprobe Corporation. All the chemicals were used without further purification unless it mentioned. FITC Annexin V Apoptosis Detection kit I, APC labeled anti-CXCR4, and IgG isotopy (Table 4) were purchased from BD Bioscience. SYBR-Safe DNA Gel Stain (S33102) was ordered from Thermo Fisher. Negative control siRNA (siNC) (Table 5) was ordered from Horizon Discovery. P53 siRNA (Table 5) and primers (Table 3) were ordered from Sigma-Aldrich. Serum creatinine (DICT-500) and BUN (DIUR-100) detection kit were ordered from BioAssay Systems. TrueBlack® Lipofuscin Autofluorescence Quencher (#23007) was ordered from Biotium. Micro clips (RS-5424) for ischemia reperfusion surgery were ordered from Roboz Surgical Instrument Co. The information about other used antibodies are listed in Table 4.

4.2. Synthesis of α-Cyclam-p-toluic acid (CPTA)

Cyclam derivative of p-toluic acid was synthesized by alkylation of α-bromo-p-toluic acid using LiOH as an alkylating agent [331]. Cyclam (5 g, 24.96 mmol) was taken in a 250 mL reaction flask and dissolved in 100 mL 80% ethanol. The reaction flask was then sat in an ice bath and LiOH (1.195 g, 49.87 mmol) was added in the flask with continuous stirring

for 30 min. Thereafter, α-bromo-p-toluic acid (1.073 g, 4.98 mmol) was added in the reaction flask and continue to stir until get homogenize. Flask was then connected with reflux condenser and placed in preheated oil bath for overnight reflux. Thereafter, reaction mixture was cool down to room temperature and ethanol was removed under reduced pressure followed by washing with excess volume of chloroform to remove any unreacted cyclam. Reaction mixture was then concentrated under reduced pressure to 1/10 of its initial volume followed by recrystallization from ethanol/water/con. HCl. The product in the form of white solid was then characterized by ^{1}H NMR and mass spectrometry. ^{1}H NMR (400 MHz, D2O, 25°C): δ 8.05 (-C**H**-; d), δ 7.55 (-C**H**-; e), δ 4.26 (-C**H**$_2$-N; c), δ 3.44 to 3.14 (-C**H**$_2$-NH-, and-C**H**$_2$-N-; b), δ 2.08 (-C**H**$_2$-CH$_2$-NH; a). HRMS (m/z): $[M+H]^+$ calculated for $C_{18}H_{31}N_4O_2$, 335.2442; found, 335.2440.

4.3. Deacetylation of chitosan (CS)

In brief, 1 g of CS was taken in 50 mL flask followed by addition of 15 mL NaOH solution (40 wt%) [305, 332]. The reaction flask was then connected with reflux-condenser and placed on a preheated oil bath at 100 °C. After two days, reaction mixture was cooled down to room temperature and the precipitated CS was collected by filtration through a filter paper followed by multiple water washes to remove the remaining NaOH. Finally, CS precipitate was dissolved in 20 mL of 1 M HCl followed by dialysis using regenerated cellulose acetate membrane (cut off 3.5 kDa) against deionized water for 4 days with frequent water changes. The solution was then lyophilized to achieve solid deacetylated CS. Deacetylated CS was then characterized by ^{1}H NMR and SEC. ^{1}H NMR chemical shifts:

(400 MHz, D2O, 25°C) δ 3.89-3.65 (-C**H**-O; f), (-C**H**-CH_2OH; h), (-C**H**$_2$OH; g), (-C**H**(O-); d), (-C**H**(OH); c), δ 2.99 (-C**H**(NH_2)-; b), δ 2 (-CH_3). The molecular weight of the polymer was analyzed by Agilent 1260 Infinity LC system equipped with a miniDAWN TREOS multi-angle light scattering (MALS) detector, a Optilab T-rEX refractive index detector, and a column (TSKgel G5000PWXL-CP). Sodium acetate buffer (0.1 M, pH 5.0) was used as an eluent at a flow rate 0.5mL/min. Results were analyzed using Astra 6.1 software from Wyatt Technology.

4.4. Synthesis of CPTA conjugated chitosan (C-CS)

CPTA was conjugated with pendant amine group of deacetylated CS by acid-amine coupling (Scheme S1) [333]. CPTA (0.165 g, 0.49 mmol) was taken in 100 mL reaction flask and dissolved with 10 mL of water. CDMT (0.0866 g, 0.49 mmol) was separately dissolved in 10 mL acetonitrile and added into the reaction flask. The flask was then set in ice bath and N-methylmorpholine (0.0749 g, 0.74 mmol) was directly added. After 1 h, reaction flask was allowed to come to room temperature followed by addition of 10 mL aqueous solution of CS (10 mg/mL) and continued the reaction for overnight under stirring. Thereafter, the reaction mixture was purified by dialysis (cellulose acetate, 3.5 kDa molecular weight cut-off) against water over 4 days. The solution was then lyophilized, and solid product was characterized by SEC and ^{1}H NMR. The mol% of CPTA conjugation was calculated by using the ratio of NMR peak integration areas corresponding to the aromatic protons of CPTA and backbone protons of CS. ^{1}H NMR (400 MHz, D2O, 25°C): δ 7.80 (-C**H**-; b), δ 7.38 (-C**H**-; a), δ 4.00 to 3.32 (-C**H**-O; j), (-C**H**-CH_2OH; h), (-C**H**$_2$OH; i),

(-C**H**(O-); g), (-C**H**(OH); f), (-C**H**$_2$-N-, k), δ3.28 to 2.67 (-C**H**$_2$-NH-, and-C**H**$_2$-N-; d), δ 2.08 (-C**H**$_2$-CH$_2$-NH; c).

4.5. Synthesis of Cy3-labeled C-CS

C-CS was fluorescently labeled with Cy3 using NHS activated esterification reaction [334]. C-CS (50 mg) was dissolved with 5 mL DI-water followed by addition of 0.5 mg of DMSO-dissolved Cy3-NHS. The reaction was continued with overnight stirring at room under dark condition. The reaction mixture was then dialyzed (cellulose acetate, 3.5 kDa cut off) over 7 days and lyophilized under dark to get Cy3-C-CS. Amount of Cy3 conjugated in the polymer was determined by UV-visible absorption spectroscopy using a calibration curve.

4.6. Polyplex formulation and characterization

Gel retardation assay in was used to determine siRNA binding to CS and C-CS. Polyplexes were prepared at increasing w/w ratios (0-20) by mixing equal volume of polymer and siRNA solution in 10 mM HEPES buffer (pH7.4) and running at 15 min at 110 V in 0.5 × Tris/Borate/EDTA buffer. E-Gel® Imager System with blue light base was then used to visualize the gel. In the heparin displacement assay, the polyplexes were prepared at w/w ratio of 2, 5, 8, 10 and incubated with increasing concentrations of heparin for 30 min at room temperature. Then 30 ul of each sample were analyzed by agarose gel electrophoresis. In the serum stability assay, polyplexes were prepared at w/w of 8, after being incubated with 50% FBS for determined time points, 400 ug/mL of heparin was used to release siRNA and analyzed by using agarose gel electrophoresis. Dynamic

light scattering (DLS) using a ZEN3600 Zetasizer Nano-ZS was used to determine the hydrodynamic size and zeta potential of the polyplexes. TEM was used to determine the morphology of polyplexes prepared at w/w 8.

4.7. CXCR4 antagonism and binding

U2OS cell line based CXCR4 redistribution assay was used to determine the CXCR4 antagonism of C-CS, C-CS-Cy3 and CS. The CXCR4 receptors on U2OS cells is tagged with green fluorescent protein (GFP), and this cell line has been widely used to determine the CXCR4 antagonism of potential compounds [259, 335, 336]. Briefly, cells were seeded in black 96-well plates for 24 h. After washing with assay buffer for three times, the cells were treated with tested compounds for 30 min, then SDF-1 was added for 1 h incubation. Finally, cells were fixed, and the fluorescence intensity of internalized CXCR4 were measured by a plate reader as described from previous study [336]. To investigate the CXCR4 binding of C-CS/siRNA, U2OS cells were seeded into 12-well plates and cultured overnight. The cells were pretreated with CXCR4 antibody (30 ug/mL) for 30 min before incubating with fluorescently labeled C-CS/siRNA for 30 min, 1 h, and 2 h, then cells were detached for flow cytometry.

4.8. Cytotoxicity

Human proximal tubule cells HK-2 were cultured in the Keratinocyte Serum Free Medium (K-SFM) suspended with 0.05 mg/ml of bovine pituitary extract (BPE) and 5 ng/ml of human recombinant epidermal growth factor (EGF). Human epithelial osteosarcoma U2OS cells stably expressing functional EGFP-CXCR4 fusion protein were

purchased from Fisher Scientific and were cultured in DMEM supplemented with 2 × 10−3 M L-glutamine, penicillin (100 U/mL), streptomycin (100 μg/mL), G418 (0.5 mg/mL), and 10% FBS. All cells were maintained in an incubator at 37 °C and 5% CO2. Cytotoxicity was measured in cells seeded in 96-well plates for overnight and treated with C-CS, CS and polyplexes for 24 h. Cell viability was determined by the CellTiter-Blue assay. Apoptosis was evaluated by staining with PI and Annexin V-FITC.

4.9. Western blot

HK-2 cells stimulated by H2O2 and cisplatin were lysed with a buffer containing Protease Inhibitor Cocktail (1:100) on ice for 30 min. The concentration of protein was determined by a BCA protein assay kit. Equal amounts of proteins for each group were loaded on a Midi Protein Gel. Following electrophoresis at 120 V for 2 h and gel transfer, the membrane was then probed overnight at 4 °C with primary antibody for p53 (1:300). After washing, the membrane was incubated with secondary antibody (anti-rabbit IgG HRP-linked antibody 1:2000) for 2 h at room temperature and the secondary antibody was imaged using Pierce ECL Western Blotting Substrate.

4.10. Real-time PCR

Total RNA from cells or kidney tissues was extracted using the TRIzol reagent (Invitrogen, USA). Then 0.5 ug of total RNA from each group was reverse-transcribed to cDNA with the QuantiTect reverse transcription kit (Qiagen). The relative level of mRNA was quantified by RT-PCR with QuantiFast SYBR Green PCR kit (Qiagen) on a Rotor-

Gene Q (Qiagen). Relative levels of mRNA were calculated based on the Ct values. Primers sequences used are provided in Table 3.

4.11. IRI-AKI mouse model

C57BL/6J mice (male, 8 weeks) were ordered from Jackson Laboratories. Male mice were used in all the animal experiments due to the female mice are generally more resistant to ischemia AKI than male mice [57]. Animal experiment protocols have been approved by the University of Nebraska Medical Center Institutional Animal Care and Use Committee. To establish the IRI-AKI model, mice were anesthetized by intraperitoneal administration of ketamine (15 mg/kg) and xylazine (5 mg/kg). Shortly after anesthesia, 50 μg/kg of buprenorphine was administered subcutaneously for pain relief. After buprenorphine injection, the hair on both side of the mice were removed with hair remover. Then the skin in the surgical area were wiped with povidone-iodine prep pad and clean with 70% alcohol pad. After skin preparation, the mice are immediately placed on a heating table for 20 minutes before surgery to stabilize body temperature and make sure they are in deep anesthesia. Then the left side skin and muscle were cut open firstly with an incision (size around 1 to 1.5 cm), the kidney was then pushed out from the incision with a sterile cotton swap, and the tissue around renal pedicle was removed by using a fine-point tweezer to expose the blood vessel for renal pedicle clamping. The right-side renal pedicle was prepared by a similar procedure. Renal ischemia was then induced by clamping of both renal pedicles with micro clips. During the ischemic period, mouse body temperature was maintained by placing on a 37 °C heating table. After 30 min of

clamping, both micro clips was released for reperfusion. The sham mice underwent the same surgery process as IRI-AKI mice, but without the clamping.

4.12. Blood clearance by intravital microscopy

An upright, Olympus FVMPE-RS Multiphoton Laser Scanning Microscope equipped with a Spectra Physics Dual line InSight X3 near infrared laser and 25x (1.05 NA) water-immersion objective was used to obtain real-time intravital images of vasculature within the inner ear and clearance of fluorescently labeled polyplexes. Vasculature was identified using 920 nm excitation of FITC-labeled tomato lectin (8 mg/kg, Vector Laboratories) injected intravenously into the proximal tail vein 30 min prior to the onset of imaging. A tail vein catheter was used to perform a single, timed injection of 100 ul of C-CS-Cy3/siRNA (w/w 8, 0.5 mg/kg of siRNA) through the tail vein and obtain time-dependent measurements of C-CS-Cy3/siRNA fluorescence intensity (1040 nm excitation) changes post polyplex injection. Matched diameter blood vessels, image acquisition, and analysis settings were used for all samples. Changes in fluorescence intensity were quantified by using NIH ImageJ. Mice were prepared for intravital imaging according to approved Institutional Animal Care and Use Committee protocols and NIH guidelines. Briefly, mice were anesthetized by intraperitoneal administration of ketamine (15 mg/kg) and xylazine (5 mg/kg). Once anesthetized, a depilatory cream was used to remove hair on the left ear, a tail vein catheter was inserted, and the ear was gently embolized in vacuum grease sealed imaging chamber using a custom stage platform and #1 coverslip. Mice were supplemented with 1% isoflurane during imaging and a temperature-controlled heating

system was used to maintain a body temperature of 37 °C for the duration of the experiment.

4.13. Biodistribution

Fluorescently labeled polyplexes (w/w 8, 0.5 mg/kg of siRNA) were injected intravenously and the animals were sacrificed at predetermined time points. The fluorescence intensity of major organs was measured by a Xenogen IVIS 200 system. To observe the locations of polyplexes in kidneys, kidney tissues were embedded in an OCT compound, cut into 10 μm frozen sections, stained with DAPI, and observed using a confocal microscope. The frozen kidney sections were applied with TrueBlack® Lipofuscin Autofluorescence Quencher then stained with FITC-labeled anti-CXCR4 antibody.

4.14. Treatment of IRI-AKI

C57BL/6J mice (male, 8 weeks) were randomly assigned to five groups with five animals per group (n = 5). The groups IRI-AKI animal groups were treated with PBS, AMD3100 (30 ug/mouse), C-CS/siNC (16ug siNC/mouse, w/w 8), and C-CS/sip53 (16ug sip53/mouse, w/w 8). PBS, AMD3100 and polyplexes were intravenously injected 8 h before renal ischemia. Another dose was given immediately after clamp removal and 8 and 24 h post-reperfusion. At the end of the experiment, blood was collected from the retro-orbital venous plexus for serum biochemistry tests. Mice were sacrificed, and kidneys and major organs were harvested, fixed in 4% paraformaldehyde solution, embedded in paraffin, and sectioned for histological analysis. Part of the kidney tissues

was set aside for RT-PCR analysis. The tissue slides were stained with hematoxylin and eosin (H&E) and the histological damage scores were blindly evaluated by a renal pathologist. Five fields of approximately 100 tubules from cortex area were counted at 200X by using a Lumenera Infity3 equipped microscopy. The cast formation, tubule dilation, and sloughed cells were counted as evidence of injury. Score 0 indicated normal kidney, score 1 indicate injury between 10% and 25%, score 2 indicate injury between 26% to 50%, score 3 indicate injury between 51% to 75%, and score 4 indicate injury over 75%. The tissue slides were also stained with F4/80, Ly6G, cleaved caspase 3 for the observation of macrophages, neutrophiles, and apoptotic cells, respectively. Immunofluorescence staining was performed to analyze the expression of p53, with the autofluorescence quencher applied before the staining.

4.15. Statistical Analysis

Results are presented as mean ± standard deviation. The differences among multiple groups analyzed by ANOVA and followed by Tukey's multiple comparison test. The statistical significance between the two groups were analyzed by using student's t test. A minimal level of significance was considered as $P < 0.05$. GraphPad Prism 9 was used to perform all statistical analyses.

Table 3. The information of primers used in studies.

Primer name	Forward	Reverse
Human CXCR4	5'-AACTTCAGTTTGTTGGCTG-3'	5'-GTGTATATACTGATCCCCTCC-3'
Human p53	5'-ACCTATGGAAACTACTTCCTG-3'	5'-ACCATTGTTCAATATCGTCC-3'
Mice p53	5'-TAGGTAGCGACTACAGTTAG-3'	5'-GGATATCTTCTGGAGGAAGTAG-3'
Human GAPDH	5'-ACAGTTGCCATGTAGACC-3'	5'-TTGAGCACAGGGTACTTTA-3'
Mice GAPDH	5'-CAATGACCCCTTCATTGACC-3'	5'-GATCTCGCTCCTGGAAGATG-3'

Table 4. Information of antibodies used in this study.

Antibody name	Catalog number	Vender
APC Anti-CXCR4 Antibody	558644	BD Biosciences
IgG2a, k Isotopy-APC	555576	BD Biosciences
Anti-p53 Antibody	Sc-126	Santa Cruz Biotechnology
Anti-F4/80 Antibody	ab6640	Abcam
Anti-Ly6G Antibody	ab25377	Abcam
Anti-CXCR4 Antibody	PA1237	Boster Biological Technology

Table 5. Information of siRNA used in this study.

siRNA name	Sense	Anti-sense
Human p53 siRNA	5'-GAGGUUGGCUCUGACUGUA-3'	5'-UACAGUCAGAGCCAACCUC-3'
Mouse p53 siRNA-1	5'-CCACUACAAGUACAUGUGU-3'	5'-ACACAUGUACUUGUAGUGG-3'
Mouse p53 siRNA-3	5'-AGGAGUCACAGUCGGAUAUCAGCCU-3'	5'-AGGCUGAUAUCCGACUGUGACUCCUCC-3'
Scrambled siRNA	5'-AUGAACGUGAAUUGCUCAAUU-3'	5'-UUGAGCAAUUCACGUUCAUUU-3'

Chapter 4. Determinations of Renal Targeted Accumulation of Polymeric Plerixafor Derivatives in Acute Kidney Injury

1. Introduction

Acute kidney injury (AKI) is characterized by a rapid reduction in renal function with high morbidity and mortality [337]. As one of the global healthcare burdens, AKI is impacting 13.3 million people around the world, and around 1.7 million people die from it annually [338-340]. Clinically, AKI is mainly triggered by sepsis, kidney ischemia-reperfusion injury (IRI), and nephrotoxins [341-343], and it has been recognized as a common complication of coronavirus disease 2019 (COVID-19) [344]. The incidence of AKI has a higher chance for the development of chronic kidney disease (CKD) and end-stage renal disease (ESRD) [337, 345]. Despite the progress in renal replacement therapy and the growing understanding of the pathophysiology, AKI remains an unmet medical need and without any effective pharmacological treatment available [19]. Hence, it is necessary to develop alternative pharmacological treatments for AKI alleviation.

The pathogenesis of AKI is complicated and is associated with inflammation, oxidative stress, vascular damage, and so on [33, 346, 347]. Among them, inflammation has been considered to play a pivotal role in the development of AKI [33, 130, 330, 348]. The pro-inflammatory cytokines and chemokines were released by leukocytes and renal tubular cells during AKI, and they are the important components both in the initiation and extension of inflammation in AKI [349]. The greatly increased expression of C-X-C chemokine receptor 4 (CXCR4) and its ligand stromal cell-derived factor (SDF-1) are

found in the injured kidneys [125] and their interaction is considered as a critical mediator of renal injury due to the recruitment of leucocytes [293-295]. Either by local anti-inflammatory effects or by systemic stem cells mobilization, treatment with CXCR4 antagonists to disrupt the interaction between CXCR4 and SDF-1 has been shown potentials for the alleviation of AKI [139, 140, 350-354]. Thus, CXCR4 holds excellent potentials in AKI treatment, either by inhibiting inflammatory immune cells renal infiltration and mobilizing stem cells in circulation or act as a target for therapeutic reagents delivery to the injured renal tubule cells for combinational therapy to attenuate AKI.

As the predominant cell type in the mammalian kidney, proximal tubule cells (PTCs) are the primary target of injury and progression of renal disease [355, 356]. Thus, renal tubule is an ideal target for AKI treatment. Drug targeting to injured PTCs could enhance the therapeutic effect to AKI by lower the doses and undesired side effects in other organs. Several native or synthetic polymers have been shown the renal tubule cells targeting ability [357]. Either by chemically conjugation or physically encapsulation of therapeutic reagents, those polymer candidates may could be used as drug carriers for targeted drug delivery for AKI treatment. Among them, a natural cationic polysaccharide, low molecular weight chitosan (LMWC) has been widely used as a drug carrier for targeted renal drug delivery to treat AKI based on its megalin targeting ability [206, 358, 359] and the excellent biocompatibility and biodegradation [360]. L-serine modified chitosan showed extensively improved accumulation in the injured kidneys due to the specific interaction between l-serine and KIM-1, and the delivery of therapeutic peptide SS31 by

this carrier showed an excellent therapeutic effect in an IRI mouse model [192]. Hyaluronic acid (HA) is another commonly used anionic natural polymer and based on the expression of CD44 in injured kidneys [361], the role of HA as a drug carrier for targeted AKI therapy has been exploited. Either by electronically coated on the surface of payload [189, 191], or by chemically conjugation with small therapeutic molecules [188], HA plays an important role in the enhancement accumulation of payloads in injured kidneys due to the specific interaction between HA and CD44. Moreover, several synthetic polymers have also been shown great renal targeting ability. Like the polyvinylpyrrolidone-co-dimethyl maleic an-hydride reported by Kamada er al [362], and the negatively charged 21 kDa HPMA copolymer reported by Mitra et al [363]. Our recent study reported that two synthetic polymers, the negatively charged pMAA and neutral pHPMA, showed the most selective accumulation in the injured kidneys at 24 h of reperfusion (about 4 times higher than normal kidneys) [364]. These studies suggest that polymers with specific targeting ability to receptors or modified with specific molecular weight or charges could influence their renal accumulation, which may provide ideas for the development of novel polymeric materials for targeted drug delivery in the injured kidney.

In this report, we synthesized a panel of polymeric CXCR4 antagonists with different modification moieties, like hydrophilicity, hydrophobicity, negatively charged, and positively charged moieties. We hypothesized that compared with PEI, those polymers with CXCR4 binding ability might show higher accumulation in the injured kidneys due to the overexpression of CXCR4 in injured renal tubules [125]. Furthermore, the different

properties of those modifications might influence their renal accumulation (Scheme 9). To prove our hypothesis, we first characterized the zeta potentials of those polymers, tested their CXCR4 binding ability and cellular uptake in vitro, and measured their protein binding amount in mice serum. Finally, the biodistribution study of those polymers was conducted in a unilateral IRI mice model.

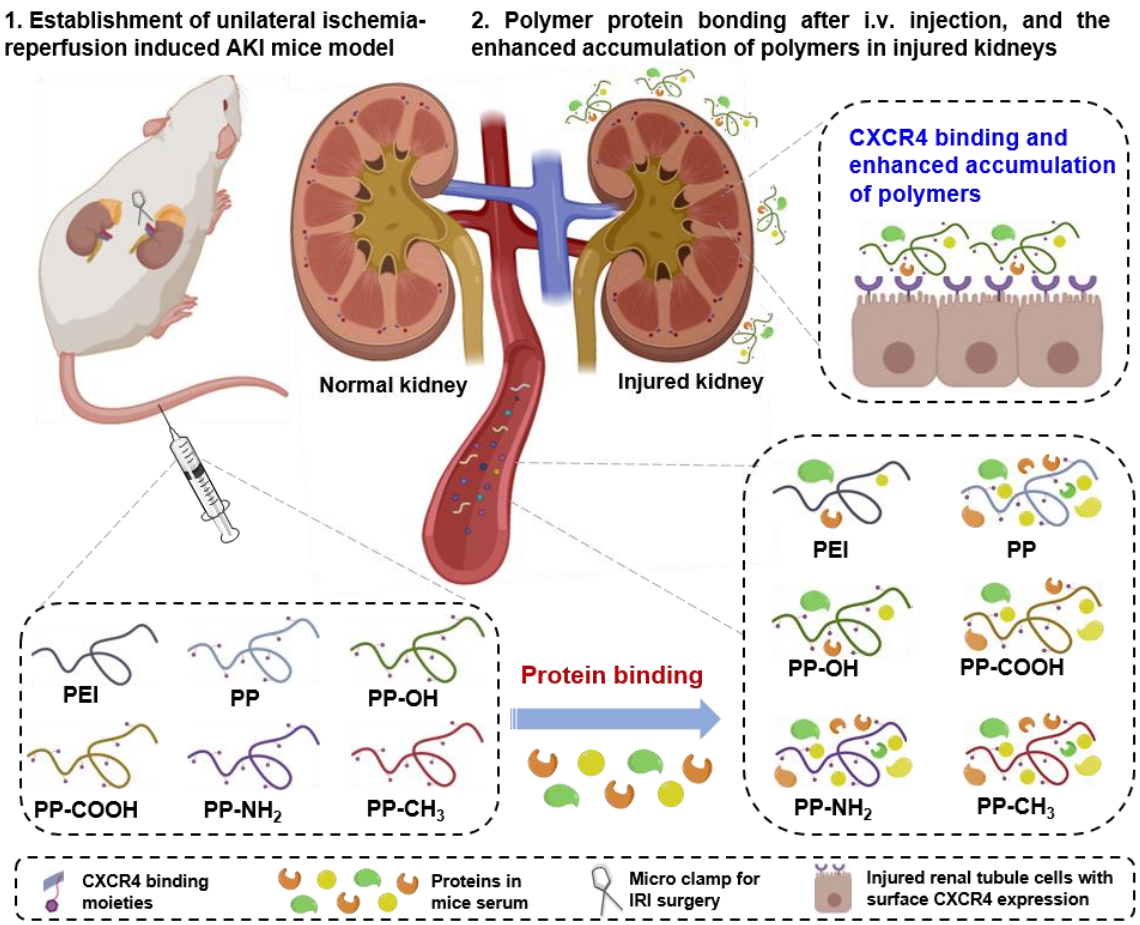

Scheme. 9. Proposed schematic illustration showing the protein absorption and renal accumulation of polymeric plerixafor and its derivatives. After establishing the unilateral ischemia-reperfusion induced AKI mouse model, fluorescently labeled polymers were intravenously administrated. At post 24 h of injection, the hydrophilic modified polymers (PP-OH) showed the greatest accumulation in the injured kidneys due to its CXCR4 binding ability and less surface protein absorption.

2. Results and discussion

2.1. Polymer synthesis and characterization

Polymeric materials have been widely applied in the field of nanomedicine for drug delivery to treat various diseases, including AKI. Either by chemically conjugation or physically encapsulation/coating of therapeutic payload or targeting moieties, polymeric carriers have been shown great advantages in the improvement of stabilities, pharmacokinetics, and biodistribution of payloads.[365-371] Moreover, polymeric pharmacophore as drug delivery carriers have been shown great potentials for combinational therapy, such as the polymeric plerixafor (PP) as gene delivery carriers for cancer treatments.[259, 372] Based on the facts that CXCR4 overexpressed on injured renal tubule cells, and the renal infiltration of immune cells during AKI, here we hypothesized that PP and its derivatives might be considered as promising drug delivery carriers candidates for combinational AKI therapy as they might have the potentials like AMD3100 for reducing renal leukocyte infiltration, and mobilizing stem cells circulation due to their CXCR4 antagonism. Moreover, it might be modified to deliver therapeutic cargo to the injured kidneys through the specific binding with CXCR4. Properties like molecular weight, charge, hydrophilicity, and hydrophobicity usually influence the distribution of polymeric carriers. For drug delivery carriers equipped with targeting moieties, those properties might play a role in decreasing or enhancing their accumulation in the target.

In this report, we synthesized a panel of nine polymeric CXCR4 antagonisms and evaluated their candidacy as drug carriers for targeted delivery in injured kidneys. One (PP) without modification as previously reported[373], and another eight ones were co-polymerized through Michael polyaddition with different moieties which have hydrophilicity (PP-OH), hydrophobicity (PP-CH_3), negatively charge (PP-COOH), and positively charge (PP-NH_2) properties (Figure 34). Table 6 shows the polymerization conditions in which polymers were prepared by copolymerization of the predetermined molar ratios of monomers (HMBA/ AMD3100/ modification moieties). All polymers were characterized by GPC and ^{1}H-NMR (Figure 35). The molecular weight range was from 11kDa to 20kDa, with a low dispersity (Đ) in a range from 1.3 to 1.6. The GPC curves of synthesized polymers were shown in Figure 36, in which well-defined, monomodal, and symmetric peaks were observed. Cy3-NHS was used to label the polymers with fluorescence to track the subcellular fate and the distribution of the polymers both in vitro and in vivo. The content of Cy3 was quantified for each polymer based on a predetermined standard curve (Table 6). Since the introduction of other copolymerized moieties decreased the feed ratio of AMD3100, and the negatively charged moieties can neutralize part of the positive charge, we next measured the zeta-potential values for all the polymers. As expected, without any modification, PP showed the highest zeta-potential value (~11mV), and other polymers with different moieties copolymerization showed lower zeta-potential values, especially the one modified with higher in feed ratio of negatively charged moieties (PP-$COOH_{(H)}$) showed the lowest zeta-potential (~1mV).

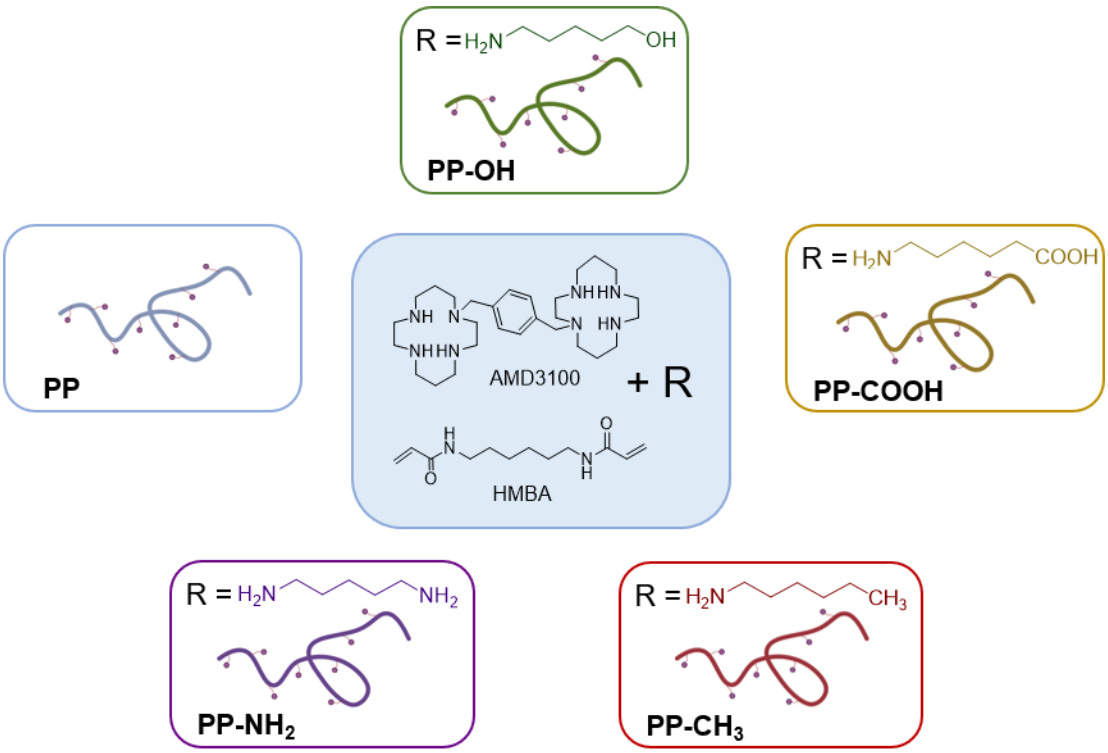

Figure 34. Synthesis and modification of polymeric CXCR4 antagonists. AMD3100, HMBA, and different modification moieties were reacted at predetermined molar ratios; reactions were carried out in methanol and water (7/3 v/v) under 37 °C for 3days. (A) PP. (B) PP-OH. (C) PP-COOH. (D) PP-NH2. (E) PP-CH3.

Table 6

Polymer characterization.

Polymer	Feed ratio [a]	Mn	Mw	Đ [b]	Polymer/Cy3 (w/w)
PEI10k	-	-	-	-	158:1
PP	1:1:0	8.316*10^3	1.304*10^4	1.57	278:1
$PP\text{-}OH_{(L)}$ [c]	1:0.8:0.2	1.158*10^4	1.653*10^4	1.43	276:1
$PP\text{-}OH_{(H)}$ [c]	1:0.5:0.5	9.336*10^3	1.174*10^4	1.26	335:1
$PP\text{-}COOH_{(L)}$	1:0.8:0.2	1.262*10^4	2.019*10^4	1.60	312:1
$PP\text{-}COOH_{(H)}$	1:0.5:0.5	1.144*10^4	1.553*10^4	1.36	298:1
$PP\text{-}NH_{2(L)}$	1:0.8:0.2	9.526*10^3	1.343*10^4	1.41	250:1
$PP\text{-}NH_{2(H)}$	1:0.5:0.5	8.871*10^3	1.107*10^4	1.25	191:1
$PP\text{-}CH_{3(L)}$	1:0.8:0.2	1.127*10^4	1.736*10^4	1.54	280:1
$PP\text{-}CH_{3(H)}$	1:0.5:0.5	1.075*10^4	1.537*10^4	1.43	223:1

Reactions were carried out in methanol and water (methanol/H_2O = 7/3 v/v) under 37 °C for 3 days.

[a] Feed molar ratio of HMBA/ AMD3100/ modification moieties.

[b] Mw = weight-average molecular wright, Mn = number-average molecular weight.

[c] L = lower feed ratio of modification moieties, H = higher feed ratio of modification moieties.

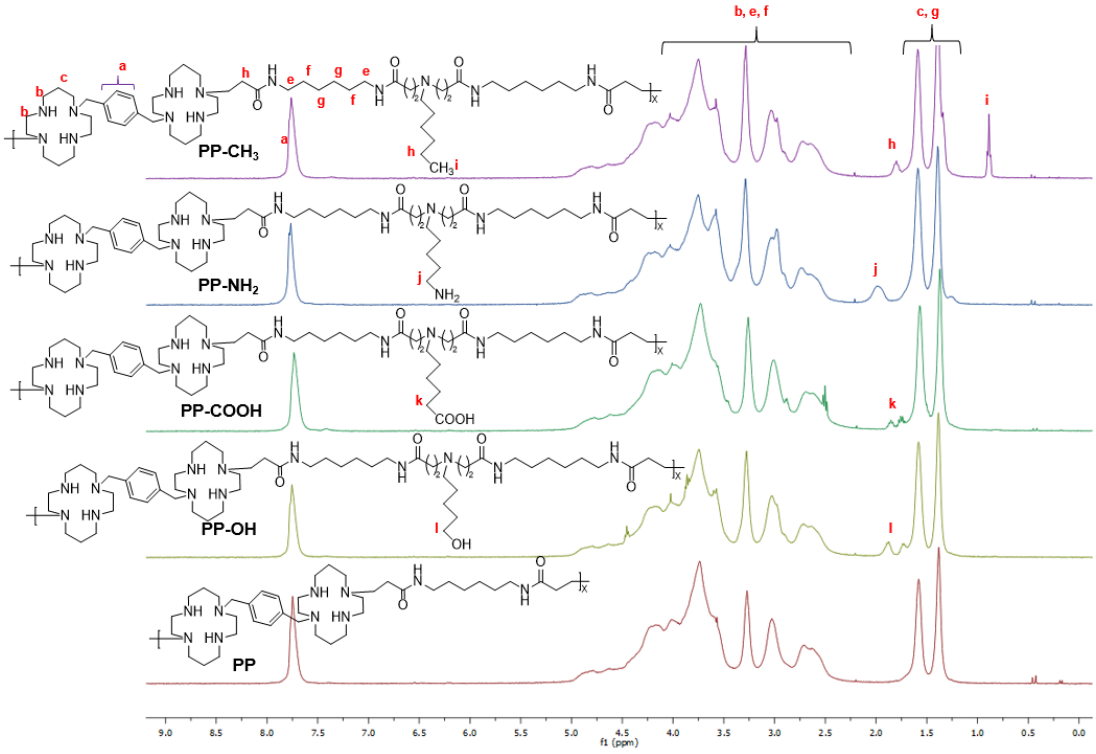

Figure 35. Representative ^1H NMR spectrum of PP, PP-OH, PP-COOH, $PP\text{-}NH_2$, and $PP\text{-}CH_3$ in D-TFA, 25°C

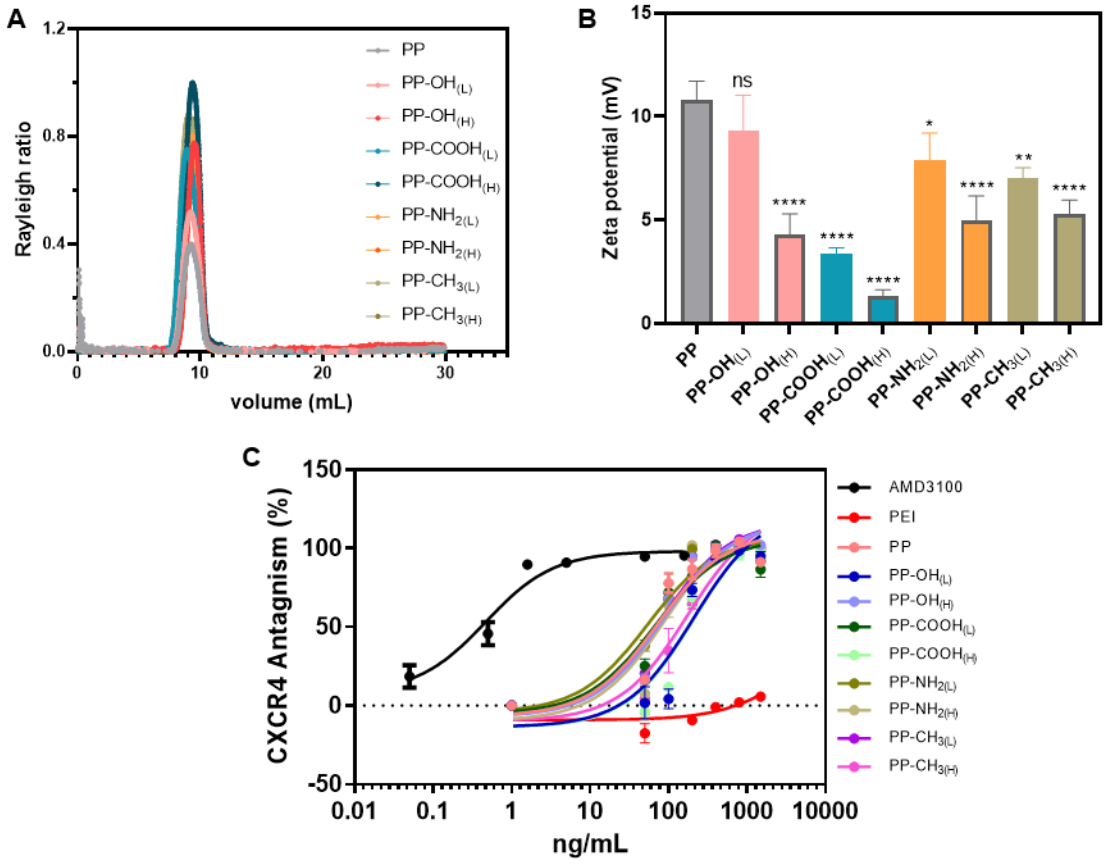

Figure 36. Characterization and CXCR4 antagonism assessment of synthesized polymers. (A) GPC curves of each polymer. (B) Zeta potential values of each polymer (n = 3). Polymers were dissolved in HEPES buffer (pH = 7.4) at 5 mg/mL. (C) Dose response curve of CXCR4 antagonism of synthesized polymers vs. AMD3100 and PEI (n = 3).

2.2. Cytotoxicity and CXCR4 antagonism of polymers

As drug delivery carriers, the safety is paramount important, especially in the condition like AKI. Cellular cytotoxicity for all the polymers was determined in mice tubule cells (MCT) and human tubule cells (HK-2), PEI was used as control. The cells were incubated with increasing concentrations of polymers for 24 h, then the cell viabilities were measured by CellTiterBlue (CTB) assay (Figure 37), and the calculated IC50 values for each polymer were in the range of 6-14 ug/mL for HK-2 cells and 12-18 ug/mL for MCT cells (Table 7).

Given those modifications may decrease the containing of AMD3100 in the polymers and might influence their CXCR4 antagonism at some extend. We next performed a CXCR4 redistribution assay in human bone osteosarcoma epithelial cells (U2OS) to study the CXCR4 antagonism of all the synthesized polymers. As shown in Figure 38, the PP and its derivatives treated cells could block the internalization of cell surface CXCR4 receptors like cells treated with AMD3100, indicating that after being introduced with different moieties, derivatives of PP remain their CXCR4 antagonism. However, the same concentration of PEI was unable to show and CXCR4 antagonism. Then, the half-maximal effective concentrations (EC50) of tested polymers were measured by quantifying the internalized EGFP-CXCR4 fluorescence intensity (Figure 36C). The EC50 values for all the AMD3100 containing polymers were located in the range from 0.05 to 0.22 ug/mL (0.004 to 0.014 uM) (Table 7).

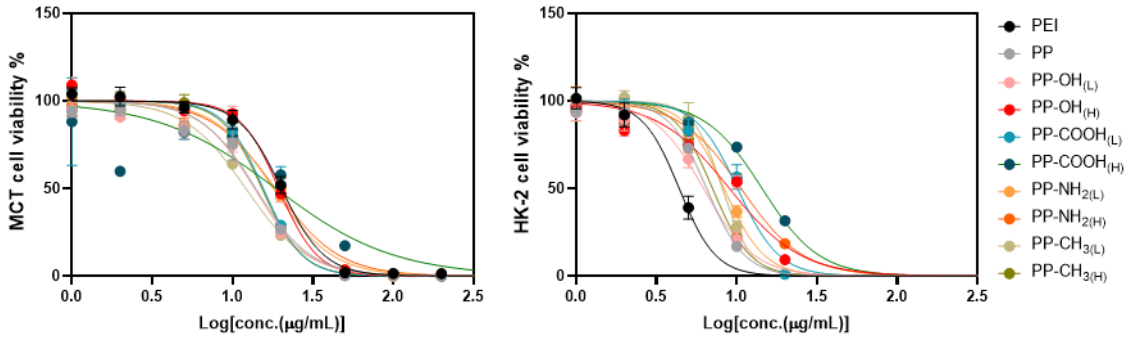

Figure 37. Cell viability responsible curve of MCT and HK-2 cells for different polymers. Polymers at different concentrations were incubated with MCT and HK-2 cells for 24 hours, then cell viabilities were determined by CTB assay (n=3).

Table 7

Cellular toxicity and CXCR4 antagonism of different polymers

Compound	CXCR4 Antagonism (EC50, ug/mL)	CXCR4 Antagonism (EC50, uM)	IC_{50} in HK-2 cells (ug/mL)	IC_{50} in MCT cells (ug/mL)
AMD3100	0.005	0.01	-	-
PEI10k	NA	NA	4.4	20.2
PP	0.07	0.005	6.5	14.0
$PP\text{-}OH_{(L)}$	0.21	0.013	6.2	13.7
$PP\text{-}OH_{(H)}$	0.09	0.008	9.0	19.4
$PP\text{-}COOH_{(L)}$	0.07	0.003	10.1	15.6
$PP\text{-}COOH_{(H)}$	0.22	0.014	14.4	18.7
$PP\text{-}NH_{2(L)}$	0.05	0.004	8.3	18.0
$PP\text{-}NH_{2(H)}$	0.09	0.008	10.7	18.4
$PP\text{-}CH_{3(L)}$	0.08	0.005	8.1	12.1
$PP\text{-}CH_{3(H)}$	0.18	0.012	7.1	15.3

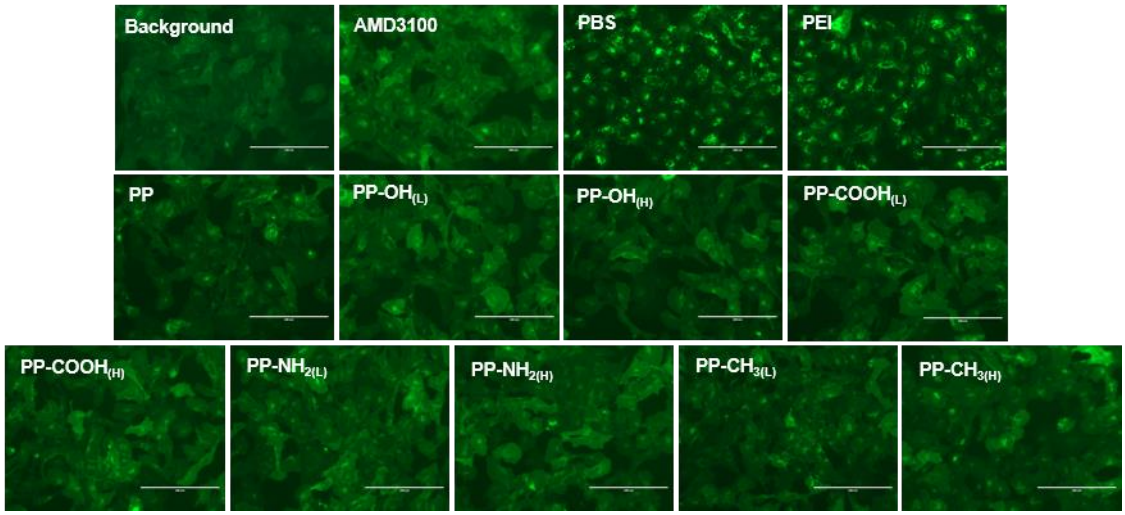

Figure 38. CXCR4 antagonism of synthesized polymers vs. AMD3100 and PEI in vitro. CXCR4 receptor redistribution assay was performed in U2OS cells with EGFP-tagged CXCR4 (green), the endocytosis of CXCR4 receptors was observed in PBS and PEI treated groups. AMD3100 (300 nM), each polymer (0.5 ug/mL). Scale bar = 100 μm.

2.3. Cellular uptake and intracellular trafficking

The results from the CXCR4 redistribution study indicate the remarkable binding affinities of all the synthesized polymers to the CXCR4 receptor. This may enhance their intracellular uptake in the CXCR4 expressing tubule cells in injured kidneys. To mimic the ischemia-reperfusion induced injury in vitro, a widely used hypoxia-reoxygenation cell culture method was performed. Basically, MCT cells were cultured in serum-free medium under hypoxia for 24 h, then replaced with fresh medium containing 10% FBS and cultured in normal condition for 6 h before studies. We first tested if the hypoxia-reoxygenation would stimulate the expression of CXCR4 receptors on the surface of MCT cells by flow cytometry. After staining with anti-CXCR4-APC antibody, we found that the hypoxia-reoxygenation condition was able to significantly stimulate cell surface CXCR4 expression as indicated by the significantly increased fluorescence intensity of APC and the percent of CXCR4 positive cells (Figure 39A). Confocal fluorescence images have further confirmed the expression of CXCR4 on the hypoxia-reoxygenation stimulated MCT cells, as indicated by the pink fluorescence signals located at the cell surface area (Figure 40).

Having confirmed MCT cells surface CXCR4 expression, we next investigated if the specific binding between CXCR4 and AMD3100 containing polymers would enhance their cellular uptake in the hypoxia-reoxygenation stimulated MCT cells, and if the modified moieties would influence their intracellular uptake amount. Cy3 labeled polymers (2 ug/mL) were incubated with hypoxia-reoxygenation stimulated and normal

MCT cells for 3 h under normal cell culture conditions. Then flow cytometry was used to quantify the cellular uptake of polymers, then fluorescence intensity ratios of hypoxia to normoxia were calculated for each polymer (Figure 39B). All the AMD3100 containing polymers showed significantly higher ratios than PEI, indicating their specific CXCR4 binding abilities play a role in their enhanced cellular uptake. Similar results were observed by confocal microscopy, and fluorescence images showed that the uptake of all the AMD3100 containing polymers in hypoxia-reoxygenation stimulated MCT cells were increased as indicated by the higher fluorescence signals of polymers when compared with normal cells (Figure 39C). Due to the lack of CXCR4 binding moieties, PEI didn't show significantly improved uptake in hypoxia-reoxygenation stimulated cells. In particular, polymers containing hydrophilic moieties (PP-OH) showed the highest hypoxia to normoxia uptake ratios, indicating hydrophilic moieties somehow enhanced the cellular uptake of PP-OH. It might be because of less protein absorption on their surface due to the hydrophilic modification[374] and therefore allowed more CXCR4 antagonism moieties exposed to cell surface CXCR4 receptors. However, further studies are needed to investigate if the introduced modification moieties would influence the surface protein absorption of those polymers.

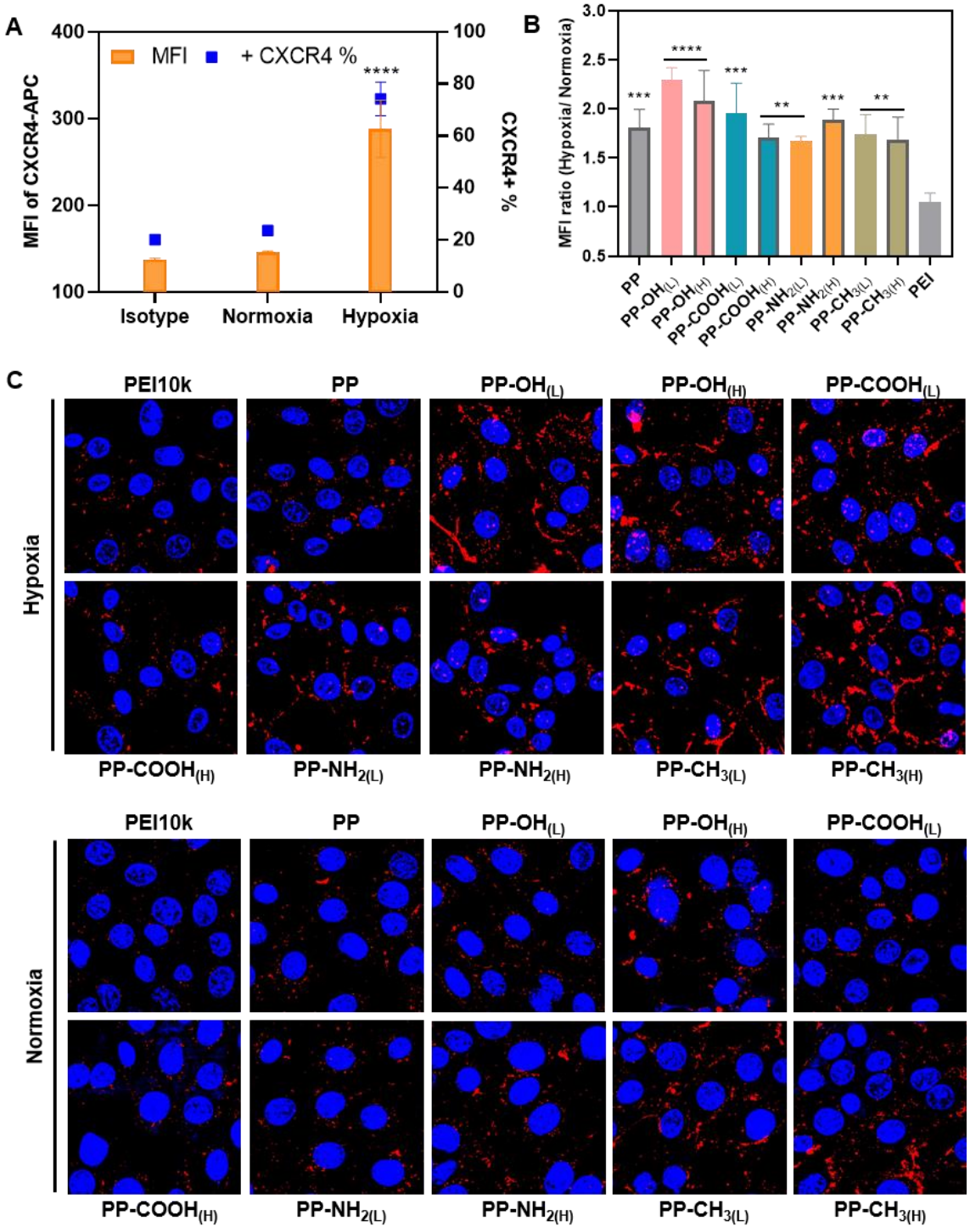

Figure 39. Cellular uptake and intracellular trafficking of synthesized polymers in hypoxia stimulated and normal MCT cells. (A). Expression of CXCR4 on hypoxia

stimulated MCT cells. (B). Cellular uptake study of Cy3 labeled polymers by using flow cytometry to quantify the mean fluorescence intensity ratios from hypoxia stimulated to normal MCT cells. (C). Intracellular trafficking of polymers in hypoxia stimulated and normal MCT cells by using confocal microscopy, one of three studies for each polymer was presented. For all the hypoxia related cell culture studies, MCT cells were incubated in a hypoxia chamber (1% O2, 94% N2, and 5% CO2) for 24 h, then cells were transferred to a normal incubator for 6 hours before other studies. Data are shown as mean ± SD (n = 3). ****P < 0.0001, ***P < 0.001, **P < 0.01. (Continued Figure 39)

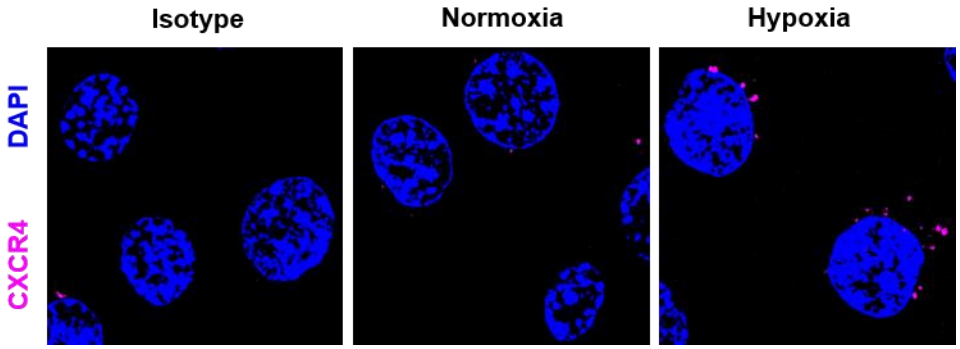

Figure 40. Confocal microscopy for the determination of MCT cell surface CXCR4 expression. MCT cells were stimulated with hypoxia for 24 h in a hypoxia cell culture chamber, then cells were transferred to normal incubator for another 6 h before anti-CXCR4-APC staining. The expression of CXCR4 (pink) on hypoxia stimulated MCT cells was observed.

2.4. Polymer protein binding

The primary function of the kidney is for blood filtration and reabsorption. Every day, around 180 liters of primary urine without macromolecules are formed in the kidneys. After the reabsorption and excretion performed by renal tubular systems, the final daily excretion is around 1-1.5 liter [375]. Thus, the intravenous injection might be the best way for the administration of renal targeted delivery systems, as they can travel with a large volume of blood and reach to the kidneys, and release their payload at the target. However, there are several biological barriers that may limit the functionality of polymeric carriers for effective drug delivery, such as the formation of the protein corona, the opsonization by the mononuclear phagocyte system (MPS), nonspecific distribution, and so on [376]. In our case, nonspecific surface protein absorption may hinder the CXCR4 binding ability of polymeric carriers, and it may therefore limit their following applications. Hence, to understand the impacts of polymer with different properties modification on the formation of the protein corona, we analyzed adsorbed proteins by polymers. First, the protein corona from each polymer was analyzed using SDS-PAGE after proteins were dissociated from polymers (Figure 41A). After staining with Coomassie brilliant blue, the proteins bands were appeared, indicating that various serum proteins were adsorbed to the surface of polymers. The protein identities were represented by the molecular weight of each band, and the intensity of each band indicated amounts of absorbed proteins. In particular, proteins around 55kDa were the most absorbed ones for each polymer, which might be hemopexin [377]. After quantifying the intensity of absorbed proteins with ImageJ, we observed that PEI, PP-$OH_{(L)}$, and PP-

$OH_{(H)}$ showed relatively lower absorbed proteins amounts; and the polymers containing hydrophobic moieties (PP-CH_3) showed the highest protein binding amounts among all the polymers (Figure 41B and C). In a more quantitative measurement, the BCA protein assay was performed to measure the concentrations of isolated proteins. As shown in Figure 41D, the PEI, PP-$OH_{(L)}$, and PP-$OH_{(H)}$ absorbed about 0.22 mg, 0.28 mg, and 0.31 mg proteins per milligram of polymers, respectively. While the amounts of absorbed proteins increased with introducing hydrophobicity to polymers, PP-$CH_{3(L)}$ and PP-$CH_{3(H)}$ absorbed about 1.09 mg and 0.91 mg proteins per milligram of polymers, respectively, which might be because the higher surface energy of hydrophobic polymers allows stronger hydrophobic interactions between polymers and proteins, thus resulted in the increased protein adsorption [378].

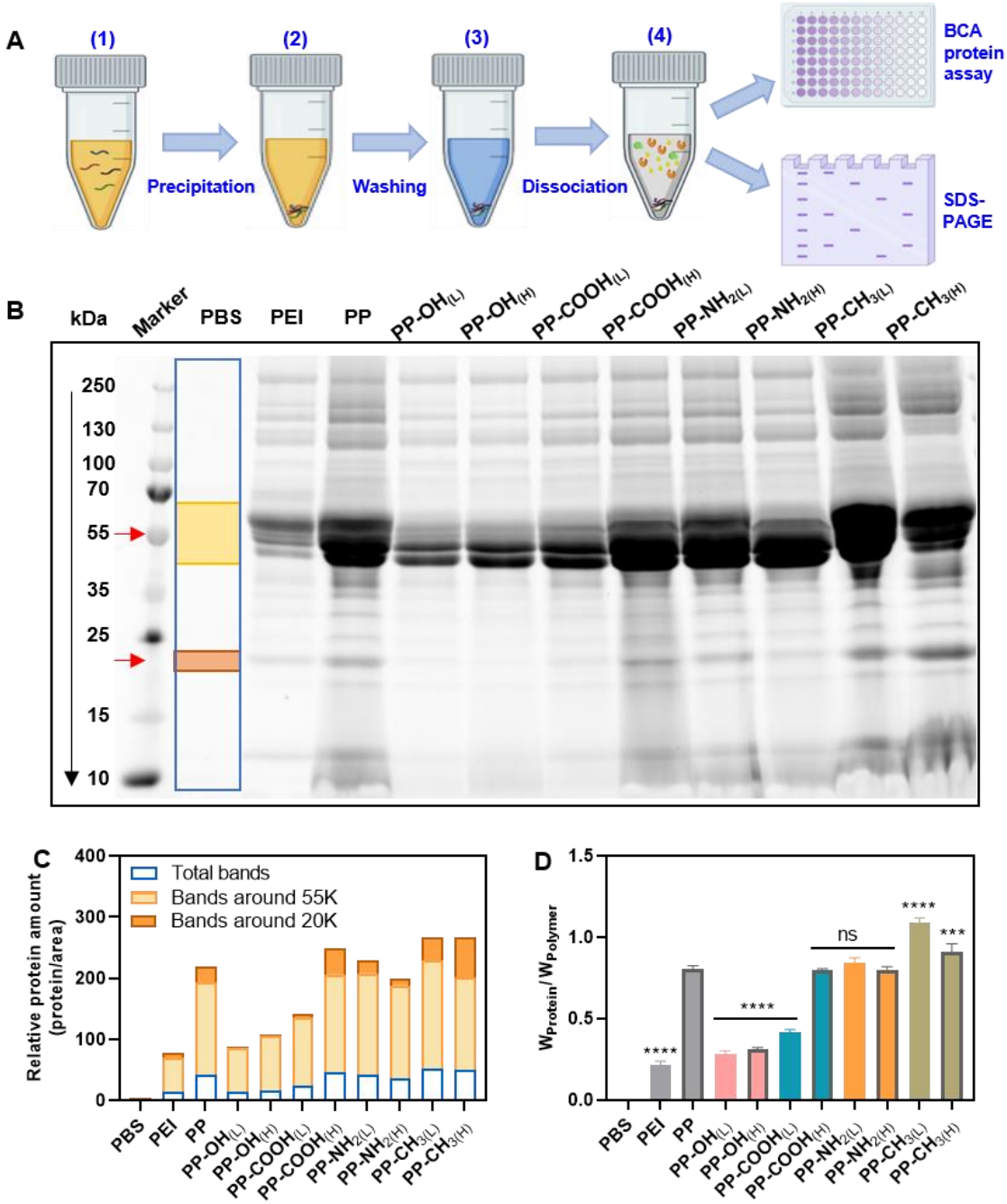

Figure 41. Protein absorption of synthesized polymers in mouse serum. (A) Scheme illustration of polymers surface absorbed protein analysis. Polymers (2 mg/mL) were mixed with 200 ul of mice serum at 37 °C for 1 h (1), after precipitation (2), the polymer and protein mixtures were washed with cold PBS for 3 times (3), then after dissociation with cell lysis RIPA buffer and precipitation, the absorbed proteins were obtained from

the supernatants (4). Finally, the amounts of proteins were quantified by BCA protein assay and SDS-PAGE. (B) The absorbed proteins were determined by SDS-PAGE. (C) Quantification the intensity of absorbed proteins in SDS-PAGE by ImageJ. (D) Protein binding to polymers was determined by BCA protein assay (Wprotein/Wpolymer = protein (mg)/polymer (mg). (Continued Figure 41)

2.5. Biodistribution

In the previous studies, we have confirmed the CXCR4 binding ability of PP and its derivatives in the CXCR4 redistribution assay (Figure 36C). Moreover, we have confirmed that the hydrophilic modified polymers (PP-OH) showed less surface protein binding (Figure 41) and higher hypoxia to normoxia ratio in the cellular uptake study (Figure 39). Those advantages of PP-OH from in vitro studies might make it a promising carrier for targeted drug delivery to the injured kidney for AKI therapy. However, further in vivo studies are needed to confirm it. Hence, to understand how different modifications affect renal accumulation, we conducted the biodistribution study for all the polymers in an unliteral ischemia-reperfusion induced AKI mouse model, where the renal injury was induced in the left kidney with left renal artery clamping (I/R), while the right kidneys were performed as left kidneys without clamping (Sham). Mice were sacrificed at 24 h after intravenous administration with Cy3 labeled polymers, and major organs were collected for ex vivo fluorescence imaging by an IVIS system (Figure 42A), and the fluorescence intensities of the region of interest (ROI) from each organ were quantified for each group (Figure 43). Generally, we found that all the polymers were mainly accumulated in the liver and injured kidneys. In particular, PP, PP-OH, PP-$COOH_{(L)}$, and PP-CH_3 showed relatively more selective accumulation in the injured kidneys. However, PEI, PP-$COOH_{(L)}$, and PP-NH_2 showed higher selective accumulation in the liver when compared with other organs in the same group. Using ROI ratios between I/R kidney to the liver in the same mouse, we found that PP-$OH_{(L)}$ and PP-$OH_{(H)}$ showed the highest I/R kidney to liver ratios, and it is around 2.4 times higher than PEI. Other polymers like PP,

PP-$COOH_{(L)}$, and PP-$CH3_{(L)}$ also showed a significant higher I/R kidney to liver ratio than PEI. However, PP-$COOH_{(H)}$, PP-HN_2, and PP-$CH3_{(H)}$ didn't show any difference with PEI (Figure 42B). Moreover, after quantifying the I/R kidney to sham kidney ROI ratios and compared with the PEI group, we found that PP-OH(L) and PP-CH3(H) showed the highest ratio. The PP, PP-$OH_{(H)}$, and PP-$CH3_{(L)}$ showed relatively significantly higher ratios; however, PP-COOH and PP-NH_2 didn't show any difference with PEI (Figure 42C). Based on those results, we found that polymers with hydrophilic modification showed great selectivity accumulation ability in the injured kidneys as indicated by the significantly higher ratios of both I/R kidney to the liver and I/R kidney to the sham kidney. This further enhances the role of PP-OH as a potential renal drug delivery carrier for AKI treatment. The favorable accumulation of PP-OH in injured kidneys might be because of the less surface protein absorption on PP-OH. In this way, more CXCR4 targeting moieties are exposed on the surface and increase their chance to bind to CXCR4 receptors in the injured renal tubule cells. As for PEI, even less protein absorption was observed. It showed low I/R kidney to the liver and I/R kidney to sham kidney ROI ratios, which might be because of the lack of CXCR4 targeting ability due to no CXCR4 binding moieties on it.

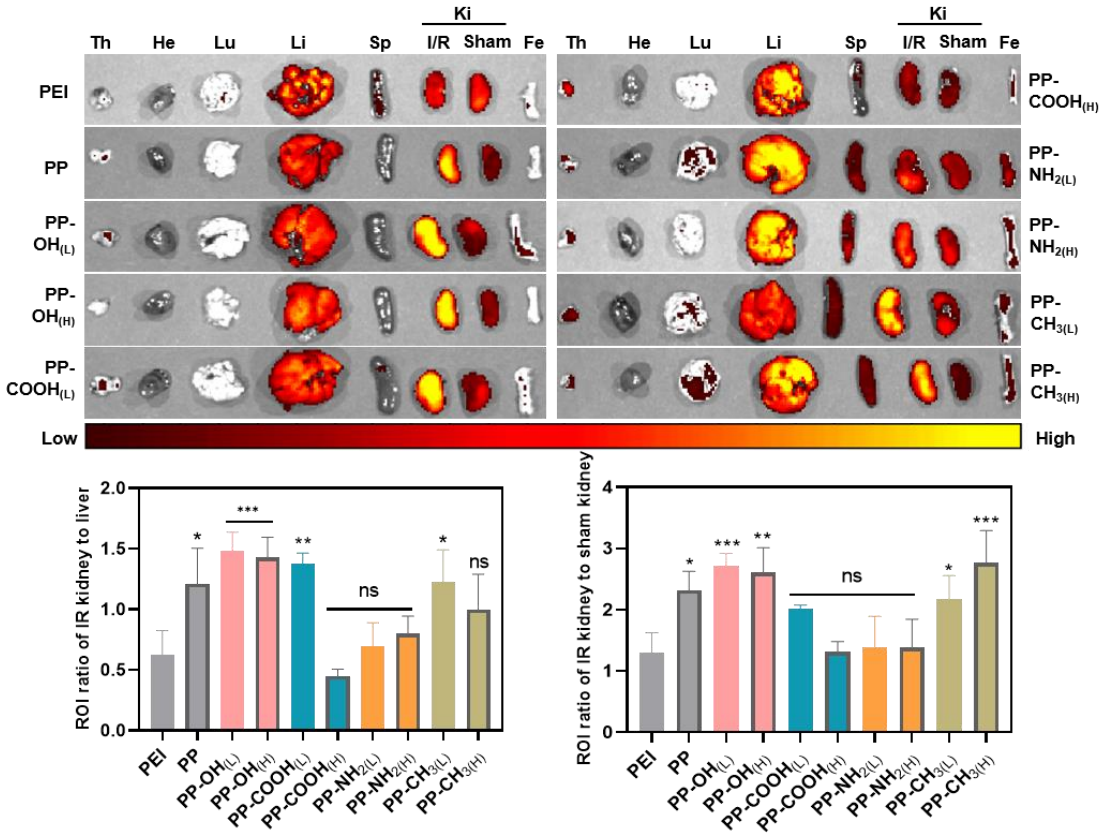

Figure 42. Biodistribution study of synthesized polymers in unilateral IRI-AKI mice. (A) Represent ex vivo imaging of detected organs at 24 hours post intravenously injection. From left to right: thymus, heart, lung, liver, spleen, injured kidney, normal kidney, femur. (B, C) Region-of-interest (ROI) ratios of injured kidney to liver (B), and ROI ratios of injured kidney to normal kidney (C) at post 24 hours post injection. Data are shown as the mean ± SD (n = 3). *** $p < 0.001$, ** $p < 0.01$, * $p < 0.05$, ns = no significant difference.

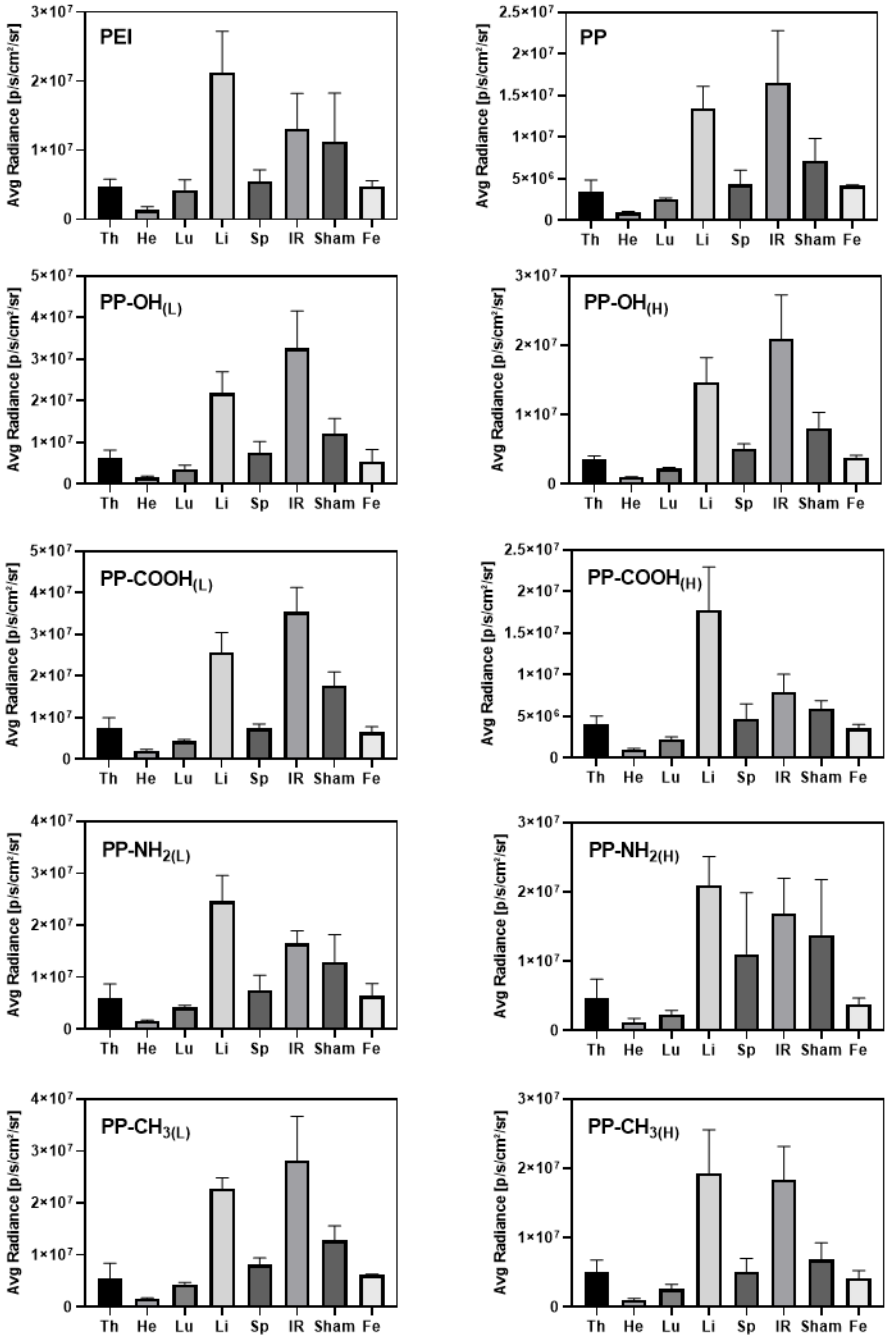

Figure 43. Region of interest analysis of the major organ uptake of synthesized polymers at post 24 hours injection in unilateral IRI-AKI mice, PEI was used as control (n=3).

3. Conclusions

In this study, we have synthesized a panel of nine polymers. One is polymeric plerixafor and another eight were based on polymeric plerixafor, introduced with different modifications moieties. Those polymers were showed excellent CXCR4 binding effects either in the CXCR4 redistribution assay or in the cellular uptake study in MCT cells. Moreover, we found that after introducing hydrophilic moieties, PP-OH showed less protein absorption, which might relate to their enhanced accumulation in the injured kidneys. These findings not only enhance our fundamental understanding the relationship between the surface modification of polymers and their transportation in normal and injured kidneys, but also provide us initial insights into improved CXCR4 targeted drug delivery system to AKI.

4. MATERIALS AND METHODS

4.1. Materials

5-Amino-1-pentanol, 6-Aminocaproic acid (EACA), 1,5-Diaminopentane, 1-Aminohexane, and N,N′-Diacetyl-1,6-hexanediamine (HMBA) were purchased from Sigma-Aldrich. AMD3100 was obtained from BioChemPartner. Cy3-NHS was purchased from Lumiprobe Corporation. APC labeled anti-CXCR4, and IgG isotopy were purchased from BD Bioscience. RPMI-1640 medium and Fetal bovine serum (FBS) were obtained from Hyclone. CellTiter-Blue reagent was purchased from Promega. Mouse renal tubular epithelial cells (MCT) and human tubular cells (HK-2) provided by Dr. Padanilam.

4.2. Polymer synthesis and characterization

Polymers were synthesized by Michael polyaddition of predetermined ratio of AMD3100, HMBA, and modification moieties as previously reported [373] (Figure 34). In a typical reaction, HMBA (112.2 mg, 0.5 mmol), AMD3100 (200.8 mg, 0.4 mmol), and EACA (13.1 mg, 0.1 mmol) were added into a glass vial containing methanol/water mixture (4 mL, 7/3 v/v). Polymers were synthesized under nitrogen atmosphere in dark at 37 °C for 3 days. Then, additional 20 mg of plerixafor was added to and the mixture was stirred for another 6 h to consume any residual acrylamide groups. The reaction mixture was then added dropwise to excess of 1.25M HCl in ethanol to keep pH was around 3. The resulting precipitated HCl salt of polymers was isolated by centrifugation. The polymers were washed twice in ethanol, dried in vacuum, and dissolved in water and dialyzed (MWCO 3.5 kDa) against water for 2 days before freeze-drying. The feed ratio,

reagent, and reaction time were according to Table 1. The weight- and number- average molecular weights and dispersity (Đ) were determined by size exclusion chromatography using Viscotek GPCmax chromatography system equipped with a refractive index detector and a low- and right-angle light scattering detector (Malvern Instruments, UK). A single pore AquaGelTM columns (cat# PAA-202 and PAA-203) from PolyAnalytik (London, ON, Canada) was used in this study. Sodium acetate buffer (0.1 M, pH 5.0) was used as an eluant with flow rate of 0.3 mL/min.

4.3. Synthesis of Cy3-labeled polymers

PEI and synthesized polymers were fluorescently labeled with Cy3 using NHS activated esterification reaction [334]. Briefly, 50 mg polymers were dissolved in 5 mL DI water, then 0.5 mg of Cy3-NHS in DMSO were dropwise into the polymer solutions followed by overnight stirring at room temperature under dark condition. The reaction mixtures were then dialyzed for 7 days to remove the unreacted Cy3-NHS. Then the Cy3 labeled polymers were obtained after lyophilization, and the amount of conjugated Cy3 was determined by UV-visible absorption spectroscopy using a calibration curve.

4.4. Cell culture

MCT cells were cultured in RPMI-1640 medium with 10% fetal bovine serum (FBS) and 1% penicillin/streptomycin. HK-2 cells were cultured in Keratinocyte Serum Free Medium (K-SFM) with 0.05 mg/ml bovine pituitary extract (BPE) and 5 ng/ml epidermal growth factor (EGF) supplements. Human bone osteosarcoma U2OS cells stably expressing human CXCR4 receptor fused to the N-terminus of enhanced green fluorescent

protein (EGFP) were cultured in DMEM supplemented with 2 mM L-Glutamine, 10% FBS, 1% penicillin/streptomycin and 0.5 mg/mL G418. All the cells were cultured in 37 °C cell incubator with 5% CO2.

4.5. In vitro cytotoxicity

The Cell Titer Blue assay was used to determine the cytotoxicity of the polymers. Briefly, mice tubule cells (MCT) and human tubule cells (HK-2) were seeded in 96-well plates at 8000 cells/well for 24 hours. Then polymers were suspended in fresh cell culture medium with different concentrations and incubated with cells. After 24 h of incubation, the medium was replaced with a mixture of 100 ul of serum-free medium and 20 ul of CellTiter-Blue reagent for 2 h. Then the fluorescence (560/590 nm) was measured by using a SpectraMax iD3 Multi-Mode Microplate Reader (MolecularDevices, CA). The relative cell viability (%) was determined as [fluorescence]sample/[fluorescence]untreated× 100%.

4.6. CXCR4 redistribution assay

CXCR4 redistribution assay was used to determine the CXCR4 antagonism of all the synthesized polymers as described before[373], PEI, PBS, and AMD3100 were used as controls. Briefly, U2OS cells expressing EGFP-CXCR4 receptors were seeded in black 96-well plates at the density of 8000 cells per well for 24 h. Cells were washed twice with assay buffer (DMEM supplemented with 2 mM L-Glutamine, 1% FBS, 1% Pen-Strep and 10 mM HEPEs) and then incubated with polymers and controls in assay buffer containing 0.25% DMSO at 37 °C for 30 min. SDF-1 was then added to each well with a final concentration of 10 nM for 1h. Then cells were fixed with 4% formaldehyde at room

temperature for 20 min and washed 3 times with PBS. Then cell nuclei were stained with 1 uM Hoechst in PBS containing 0.5% Triton X-100. Images were taken by EVOS fluorescence microscope at 20 X. Then high-content analysis was performed to quantify the CXCR4 antagonistic activity according to the internalized EGFP-CXCR4 receptors.

4.7. Cell hypoxia-reoxygenation and CXCR4 expression

The MCT cells were plated in 6-well plates at a density of $3x10^6$ cells per well and incubated until they reached approximately 90% confluence for experiment. To mimic the ischemia-reperfusion injury in vitro, the cells were cultured for 24 h under hypoxic conditions (1% O2, 94% N2, and 5% CO2) in serum free medium to induce hypoxic injury. After hypoxic treatment, the cells were transferred back to regular culture medium with oxygen for 6 h for reoxygenation. Control cells were incubated in complete culture medium in a regular incubator (5% CO2 and 95% air). Then cells were detached from the plate and sained with anti-CXCR4-APC antibody or control IgG isotype according to manufacturer's protocol. After washing three times with could PBS, flow cytometry was used to quantify the expression of cell surface CXCR4 receptors, and the results were processed using FlowJo software.

4.8. Cellular uptake and intracellular trafficking of polymers

Flow cytometry was conducted to study the cellular uptake of polymers. MCT cells were seeded in 12-well plates at the density of 3×10^4 per well and cultured to approximately 80% confluence. Then cells were incubated with Cy3 labeled polymer (2μg/mL) at 37 °C for 3 h. After washing with PBS twice, cells were detached and subjected

to analysis using a BD FACS Calibur flow cytometer (BD Bioscience, Bedford, MA). The results were processed by using FlowJo software. The intracellular trafficking was observed by LSM 800 Laser Scanning Microscope (Zeiss, Jena, Germany). Briefly, MCT cells were cultured in an 8-well cell culture chamber with coverslip glass at 2×10^4 cells per well for overnight. After 24 h, cell culture medium was replaced with fresh medium suspended with Cy3 labeled polymers at the concentration of 2 μg/mL for 3 h. After washing with cold PBS three times, the cells were fixed with 4% formaldehyde at room temperature for 20 min, then stained with 1 uM Hoechst in PBS for another 10 min.

4.9. Protein binding affinity

Polymers at the concentration of 2 mg/mL were incubated with 200 ul of mice serum on a shaker at 37 °C for 1 h. Then the mixtures were centrifuged at $1.4x10^4$ g for 1 h at 4 °C. After washing three times with cold PBS, the protein pellets were resuspended in 50 ul of RIPA lysis buffer containing 1% HaltTM Protease Inhibitor Cocktail to release proteins from the surface of polymers. Then the mixtures were centrifuged at $1.4x10^4$ g for 30 min at 4 °C, and the supernatants were collected. After collection, 5 ul of each supernatant was diluted 20 times with 95 ul saline, and 25 ul of each diluted solution was applied in the protein BCA assay to determine their concentrations. To visualize the molecular weight distribution of absorbed proteins by the polymers, 25 ul of the supernatant was loaded to SDS-PAGE for protein separation. After staining with Coomassie Brilliant Blue for 30 min and washing with DI water for 24 h, the proteins in the gel were visualized by ChemiDoc

Imaging Systems (BIO-RAD). Finally, ImageJ was used to quantify the relative protein amount from the gel image.

4.10. Induction of unilateral ischemia-reperfusion kidney injury

Male mice were used in this study due to female mice are generally more resistant to ischemia AKI than male mice [57]. Animal experiment protocols have been approved by the University of Nebraska Medical Center Institutional Animal Care and Use Committee (IACUC). To establish the unilateral ischemia-reperfusion kidney injury model, mice were anesthetized by intraperitoneal administration of ketamine (15 mg/kg) and xylazine (5 mg/kg). After anesthesia, 50 μg/kg of buprenorphine was given subcutaneously for pain relief. Then both side hair of the mice was removed with hair remover, and the skin in the surgical area was wiped with a povidone-iodine prep pad and clean with a 70% alcohol pad. Mice were placed on a heating table immediately after skin preparation for 20 minutes before surgery to stabilize body temperature and allow them are in deep anesthesia. The left side skin and muscle were then cut open with an incision (around 1 to 1.5 cm), and the left kidney was then pushed out from the incision by using a sterile cotton swap. Then the tissue around the renal pedicle was removed by a fine-point tweezer to expose the blood vessel for renal pedicle clamping. The right-side renal pedicle was prepared by a similar procedure without clamping. After 30 min clamping for the left side kidney, the micro clamps were released for renal reperfusion. The body temperature of mice was maintained at 37 °C on a heating plate until they were fully awake.

4.11. In vivo biodistribution study

Biodistribution of polymers in unilateral IRI-AKI mice was analyzed by ex vivo fluorescence imaging. After 24 hours of reperfusion, Cy3 labeled polymers were administrated to mice via tail vein injection at the concentration of 2 mg/kg. Then mice were sacrificed at 24 h after administration, and major organs were isolated and imaged using a Xenogen IVIS 200 system. Emission wavelength of 569 nm and excitation wavelength of 555 was used to image the organs. The fluorescence intensities of organs were quantified by using Living Image® 4.5 software, and the radiant efficiency was measured as (photons/sec/cm^2/sr)/($\mu W/cm^2$). Finally, the fluorescent ratios of injured kidney to sham kidney, and injured kidney to liver were studied.

4.12. Statistical analysis

Results are showed as mean ± SD. ANOVA was used to analyze the differences between multiple groups followed by Tukey's multiple comparison test. $P < 0.05$ was considered as a minimal significance. All statistical analysis was processed with GraphPad Prism v9.

Chapter 5. Summary and Future Directions

Acute kidney injury affects over 13 million people worldwide and leads to about 2 million deaths each year. Patients who survive from AKI are in the high risk to develop chronic kidney disease or end stage renal disease, and ultimately result in kidney failure. Despite the extensive basic research and the growing understanding of the underlying pathophysiology, AKI remains a significant unmet medical requirement, and no effective pharmacological treatments are available. Due to the complicate pathophysiology of AKI, it may be necessary to develop combinational treatment methods to simultaneously treat AKI for better treatment outcomes.

As one of the most well-known tumor suppressor proteins, p53 has been attracted increasing attentions as a therapeutic target in AKI. p53 induced cell death has been considered as the major contributor for the development of AKI. Inhibition of p53 by siRNA has been demonstrated the beneficial effect both in IRI-AKI and CIS-AKI animal models. However, large amount of free siRNA was required to achieve desired therapeutic outcomes due to the lack of renal targeted siRNA delivery systems. Growing evidence shows that CXCR4/SDF-1 axis is involved in the pathology of AKI, and block CXCR4 by antagonism could inhibit renal immune cells infiltration and improve renal function. Moreover, CXCR4 has been reported overexpression on injured tubules, which could be used as a target for therapeutic reagents delivery to the injured renal tubule cells.

Taking advantage of the role of CXCR4 and p53 in AKI, we have developed two polycations, one is PCX and another one called C-CS. Both polymers were showed

excellent CXCR4 binding ability and siRNA condensation ability. In our in vitro studies, the PCX/siRNA and C-CS/siRNA showed excellent gene silencing effect. Moreover, the enhanced cellular uptake in the injured renal tubule cells which expressing CXCR4 receptors were observed. In the biodistribution studies, both polycations showed enhanced siRNA delivery in the injured kidneys as indicated by the higher fluorescence intensity and longer retention times when compare with normal kidneys, and the sub-organ images showed polymer and siRNA were mainly located in tubule areas, which might because the specific CXCR4 binding of polyplexes. In the study from C-CS/siRNA, the CXCR4 staining was further confirm the CXCR4 targeting ability of C-CS. The favorable accumulation of PCX/siRNA and C-CS/siRNA in the injured kidneys encouraged us to test their therapeutic effect. As expected, PCX/sip53 and C-CS/sip53 successfully downregulated the expression of p53 in the injured kidneys and showed great therapeutic for CIS-AKI and IRI-AKI respectively, as indicated by the improved renal functions, less immune cells infiltration, and less renal damage. Our studies showed we have successfully used CXCR4-directed delivery with PCX and C-CS to enhance the renal accumulation of therapeutic siRNA for p53 silencing. This is the first report showed the potential of combined CXCR4 inhibition with p53 gene silencing for AKI therapy.

Based on our previous studies, we proposed to develop polymer-siRNA conjugates for effective AKI treatment in our future directions. The polymer will be equipped with CXCR4 binding ability and the siRNA can be any therapeutic siRNA which benefit for AKI. The use of sample polymer-siRNA conjugates could enhance the stability and activity of siRNA, meanwhile decrease the amount of polymers injection. Thus, an pilot

study was conducted with the aim to find a polymer candidate for future siRNA conjugation. In our pilot study, a panel of polymeric CXCR4 antagonists with different modification moieties were synthesized. All the polymers showed enhanced cellular uptake in the CXCR4 overexpressed MCT cells. Moreover, the hydrophilic moiety modified polymer (PP-OH) showed the lowest protein binding in mice serum and the best accumulation ability in the injured kidneys. This polymer might be suitable for future siRNA conjugations.

Bibliography

[1] V.G. Puelles, W.E. Hoy, M.D. Hughson, B. Diouf, R.N. Douglas-Denton, J.F. Bertram, Glomerular number and size variability and risk for kidney disease, Current opinion in nephrology and hypertension 20(1) (2011) 7-15.
[2] H.W. Smith, The kidney: structure and function in health and disease, Oxford University Press, USA1951.
[3] L. Bankir, C. De Rouffignac, Urinary concentrating ability: insights from comparative anatomy, American Journal of Physiology-Regulatory, Integrative and Comparative Physiology 249(6) (1985) R643-R666.
[4] B. Du, M. Yu, J. Zheng, Transport and interactions of nanoparticles in the kidneys, Nature Reviews Materials 3(10) (2018) 358-374.
[5] G. Jarad, J.H. Miner, Update on the glomerular filtration barrier, Current opinion in nephrology and hypertension 18(3) (2009) 226.
[6] M.C. Menon, P.Y. Chuang, C.J. He, The glomerular filtration barrier: components and crosstalk, International journal of nephrology 2012 (2012).
[7] M.G. Farquhar, The primary glomerular filtration barrier—basement membrane or epithelial slits?, Kidney international 8(4) (1975) 197-211.
[8] B. Haraldsson, J. Nyström, W.M. Deen, Properties of the glomerular barrier and mechanisms of proteinuria, Physiological reviews (2008).
[9] A. Singh, S.C. Satchell, C.R. Neal, E.A. McKenzie, J.E. Tooke, P.W. Mathieson, Glomerular endothelial glycocalyx constitutes a barrier to protein permeability, Journal of the American Society of Nephrology 18(11) (2007) 2885-2893.
[10] S. Reitsma, D.W. Slaaf, H. Vink, M.A. Van Zandvoort, M.G. oude Egbrink, The endothelial glycocalyx: composition, functions, and visualization, Pflügers Archiv-European Journal of Physiology 454(3) (2007) 345-359.
[11] J. Tencer, I.-M. Frick, B.W. Öquist, P. Alm, B. Rippe, Size-selectivity of the glomerular barrier to high molecular weight proteins: upper size limitations of shunt pathways, Kidney international 53(3) (1998) 709-715.
[12] W.D. Comper, E.F. Glasgow, Charge selectivity in kidney ultrafiltration, Kidney international 47(5) (1995) 1242-1251.
[13] D.C. Eaton, J.P. Pooler, Vander's renal physiology, Mc Graw Hil Medicall2009.
[14] S.K. Mallipattu, J.C. He, A new mechanism for albuminuria-induced podocyte injury, Am Soc Nephrol, 2013.
[15] N. Lameire, W. Van Biesen, R. Vanholder, The changing epidemiology of acute renal failure, Nature clinical practice Nephrology 2(7) (2006) 364-377.
[16] E.A. Hoste, J.A. Kellum, N.M. Selby, A. Zarbock, P.M. Palevsky, S.M. Bagshaw, S.L. Goldstein, J. Cerdá, L.S. Chawla, Global epidemiology and outcomes of acute kidney injury, Nature Reviews Nephrology 14(10) (2018) 607-625.
[17] A. Zuk, J.V. Bonventre, Acute kidney injury, Annual review of medicine 67 (2016) 293-307.
[18] R.L. Mehta, J. Cerdá, E.A. Burdmann, M. Tonelli, G. García-García, V. Jha, P. Susantitaphong, M. Rocco, R. Vanholder, M.S. Sever, International Society of Nephrology's 0by25 initiative for acute kidney injury (zero preventable deaths by 2025): a human rights case for nephrology, The Lancet 385(9987) (2015) 2616-2643.

[19] E.A.J. Hoste, J.A. Kellum, N.M. Selby, A. Zarbock, P.M. Palevsky, S.M. Bagshaw, S.L. Goldstein, J. Cerdá, L.S. Chawla, Global epidemiology and outcomes of acute kidney injury, Nat Rev Nephrol 14(10) (2018) 607-625.
[20] P. Susantitaphong, D.N. Cruz, J. Cerda, M. Abulfaraj, F. Alqahtani, I. Koulouridis, B.L. Jaber, World incidence of AKI: a meta-analysis, Clinical Journal of the American Society of Nephrology 8(9) (2013) 1482-1493.
[21] F.B. Rodrigues, R.G. Bruetto, U.S. Torres, A.P. Otaviano, D.M. Zanetta, E.A. Burdmann, Incidence and mortality of acute kidney injury after myocardial infarction: a comparison between KDIGO and RIFLE criteria, PloS one 8(7) (2013) e69998.
[22] X. Luo, L. Jiang, B. Du, Y. Wen, M. Wang, X. Xi, A comparison of different diagnostic criteria of acute kidney injury in critically ill patients, Critical care 18(4) (2014) 1-8.
[23] T. Fujii, S. Uchino, M. Takinami, R. Bellomo, Validation of the Kidney Disease Improving Global Outcomes criteria for AKI and comparison of three criteria in hospitalized patients, Clinical Journal of the American Society of Nephrology 9(5) (2014) 848-854.
[24] S.M. Bagshaw, C. George, R. Bellomo, Changes in the incidence and outcome for early acute kidney injury in a cohort of Australian intensive care units, Critical care 11(3) (2007) 1-9.
[25] R.K. Hsu, C.E. McCulloch, R.A. Dudley, L.J. Lo, C.-y. Hsu, Temporal changes in incidence of dialysis-requiring AKI, Journal of the American Society of Nephrology 24(1) (2013) 37-42.
[26] R. Bellomo, The epidemiology of acute renal failure: 1975 versus 2005, Current opinion in critical care 12(6) (2006) 557-560.
[27] D.N. Cruz, C. Ronco, Acute kidney injury in the intensive care unit: current trends in incidence and outcome, Critical care 11(4) (2007) 1-2.
[28] G.M. Chertow, E. Burdick, M. Honour, J.V. Bonventre, D.W. Bates, Acute kidney injury, mortality, length of stay, and costs in hospitalized patients, Journal of the American Society of Nephrology 16(11) (2005) 3365-3370.
[29] L.S. Chawla, P.W. Eggers, R.A. Star, P.L. Kimmel, Acute kidney injury and chronic kidney disease as interconnected syndromes, New England Journal of Medicine 371(1) (2014) 58-66.
[30] S.G. Coca, S. Singanamala, C.R. Parikh, Chronic kidney disease after acute kidney injury: a systematic review and meta-analysis, Kidney international 81(5) (2012) 442-448.
[31] A. Ishani, J.L. Xue, J. Himmelfarb, P.W. Eggers, P.L. Kimmel, B.A. Molitoris, A.J. Collins, Acute kidney injury increases risk of ESRD among elderly, Journal of the American Society of Nephrology 20(1) (2009) 223-228.
[32] R. Thadhani, M. Pascual, J.V. Bonventre, Acute renal failure, N Engl J Med 334(22) (1996) 1448-60.
[33] D.P. Basile, M.D. Anderson, T.A. Sutton, Pathophysiology of acute kidney injury, Compr Physiol 2(2) (2012) 1303-1353.
[34] C. Altmann, A. Andres-Hernando, R.H. McMahan, N. Ahuja, Z. He, C.J. Rivard, C.L. Edelstein, L. Barthel, W.J. Janssen, S. Faubel, Macrophages mediate lung inflammation in a mouse model of ischemic acute kidney injury, Am J Physiol Renal Physiol 302(4) (2012) F421-32.

[35] S. Balasubramanian, M. Jansen, M.T. Valerius, B.D. Humphreys, T.B. Strom, Orphan nuclear receptor Nur77 promotes acute kidney injury and renal epithelial apoptosis, J Am Soc Nephrol 23(4) (2012) 674-86.
[36] C.R. Amura, B. Renner, T. Lyubchenko, S. Faubel, P.L. Simonian, J.M. Thurman, Complement activation and toll-like receptor-2 signaling contribute to cytokine production after renal ischemia/reperfusion, Mol Immunol 52(3-4) (2012) 249-57.
[37] N. Arfian, N. Emoto, N. Vignon-Zellweger, K. Nakayama, K. Yagi, K. Hirata, ET-1 deletion from endothelial cells protects the kidney during the extension phase of ischemia/reperfusion injury, Biochem Biophys Res Commun 425(2) (2012) 443-9.
[38] D.P. Basile, J.L. Friedrich, J. Spahic, N. Knipe, H. Mang, E.C. Leonard, S. Changizi-Ashtiyani, R.L. Bacallao, B.A. Molitoris, T.A. Sutton, Impaired endothelial proliferation and mesenchymal transition contribute to vascular rarefaction following acute kidney injury, Am J Physiol Renal Physiol 300(3) (2011) F721-33.
[39] J.W. Celie, K.K. Katta, S. Adepu, W.B. Melenhorst, R.M. Reijmers, E.M. Slot, R.H. Beelen, M. Spaargaren, R.J. Ploeg, G. Navis, J.J. van der Heide, M.C. van Dijk, H. van Goor, J. van den Born, Tubular epithelial syndecan-1 maintains renal function in murine ischemia/reperfusion and human transplantation, Kidney Int 81(7) (2012) 651-61.
[40] J. Chen, J.K. Chen, R.C. Harris, Deletion of the epidermal growth factor receptor in renal proximal tubule epithelial cells delays recovery from acute kidney injury, Kidney Int 82(1) (2012) 45-52.
[41] T.M. El-Achkar, R. McCracken, M. Rauchman, M.R. Heitmeier, Z. Al-Aly, P.C. Dagher, X.R. Wu, Tamm-Horsfall protein-deficient thick ascending limbs promote injury to neighboring S3 segments in an MIP-2-dependent mechanism, Am J Physiol Renal Physiol 300(4) (2011) F999-1007.
[42] W. Yu, S. Beaudry, H. Negoro, I. Boucher, M. Tran, T. Kong, B.M. Denker, H2O2 activates G protein, α 12 to disrupt the junctional complex and enhance ischemia reperfusion injury, Proc Natl Acad Sci U S A 109(17) (2012) 6680-5.
[43] R.A. Zager, A. Vijayan, A.C. Johnson, Proximal tubule haptoglobin gene activation is an integral component of the acute kidney injury "stress response", Am J Physiol Renal Physiol 303(1) (2012) F139-48.
[44] D. Zhou, Y. Li, L. Lin, L. Zhou, P. Igarashi, Y. Liu, Tubule-specific ablation of endogenous β-catenin aggravates acute kidney injury in mice, Kidney Int 82(5) (2012) 537-47.
[45] M.A. Alikhan, C.V. Jones, T.M. Williams, A.G. Beckhouse, A.L. Fletcher, M.M. Kett, S. Sakkal, C.S. Samuel, R.G. Ramsay, J.A. Deane, C.A. Wells, M.H. Little, D.A. Hume, S.D. Ricardo, Colony-stimulating factor-1 promotes kidney growth and repair via alteration of macrophage responses, Am J Pathol 179(3) (2011) 1243-56.
[46] H. Braun, B.M. Schmidt, M. Raiss, A. Baisantry, D. Mircea-Constantin, S. Wang, M.L. Gross, M. Serrano, R. Schmitt, A. Melk, Cellular senescence limits regenerative capacity and allograft survival, J Am Soc Nephrol 23(9) (2012) 1467-73.
[47] D.A. Ferenbach, T.A. Sheldrake, K. Dhaliwal, T.M. Kipari, L.P. Marson, D.C. Kluth, J. Hughes, Macrophage/monocyte depletion by clodronate, but not diphtheria toxin, improves renal ischemia/reperfusion injury in mice, Kidney Int 82(8) (2012) 928-33.
[48] N. Huang, L. Tan, Z. Xue, J. Cang, H. Wang, Reduction of DNA hydroxymethylation in the mouse kidney insulted by ischemia reperfusion, Biochem Biophys Res Commun 422(4) (2012) 697-702.

[49] A. Kirov, M. Duarte, J. Guay, M. Karolak, C. Yan, L. Oxburgh, I. Prudovsky, Transgenic expression of nonclassically secreted FGF suppresses kidney repair, PLoS One 7(5) (2012) e36485.
[50] M.P. Schneider, J.C. Sullivan, P.F. Wach, E.I. Boesen, T. Yamamoto, T. Fukai, D.G. Harrison, D.M. Pollock, J.S. Pollock, Protective role of extracellular superoxide dismutase in renal ischemia/reperfusion injury, Kidney Int 78(4) (2010) 374-81.
[51] A.M. Siedlecki, X. Jin, W. Thomas, K.A. Hruska, A.J. Muslin, RGS4, a GTPase activator, improves renal function in ischemia-reperfusion injury, Kidney Int 80(3) (2011) 263-71.
[52] C. Brooks, Q. Wei, S.G. Cho, Z. Dong, Regulation of mitochondrial dynamics in acute kidney injury in cell culture and rodent models, J Clin Invest 119(5) (2009) 1275-85.
[53] R. Lan, H. Geng, A.J. Polichnowski, P.K. Singha, P. Saikumar, D.G. McEwen, K.A. Griffin, R. Koesters, J.M. Weinberg, A.K. Bidani, W. Kriz, M.A. Venkatachalam, PTEN loss defines a TGF-β-induced tubule phenotype of failed differentiation and JNK signaling during renal fibrosis, Am J Physiol Renal Physiol 302(9) (2012) F1210-23.
[54] M. Liu, D.N. Grigoryev, M.T. Crow, M. Haas, M. Yamamoto, S.P. Reddy, H. Rabb, Transcription factor Nrf2 is protective during ischemic and nephrotoxic acute kidney injury in mice, Kidney Int 76(3) (2009) 277-85.
[55] Q. Ma, P. Devarajan, Induction of proapoptotic Daxx following ischemic acute kidney injury, Kidney Int 74(3) (2008) 310-8.
[56] Q. Wei, K. Bhatt, H.Z. He, Q.S. Mi, V.H. Haase, Z. Dong, Targeted deletion of Dicer from proximal tubules protects against renal ischemia-reperfusion injury, J Am Soc Nephrol 21(5) (2010) 756-61.
[57] Q. Wei, Z. Dong, Mouse model of ischemic acute kidney injury: technical notes and tricks, American journal of physiology. Renal physiology 303(11) (2012) F1487-F1494.
[58] A. Ozkok, C.L. Edelstein, Pathophysiology of cisplatin-induced acute kidney injury, Biomed Res Int 2014 (2014) 967826-967826.
[59] M. Schetz, J. Dasta, S. Goldstein, T. Golper, Drug-induced acute kidney injury, Curr Opin Crit Care 11(6) (2005) 555-65.
[60] A. Kodama, H. Watanabe, R. Tanaka, M. Kondo, V.T. Chuang, Q. Wu, M. Endo, Y. Ishima, M. Fukagawa, M. Otagiri, T. Maruyama, Albumin fusion renders thioredoxin an effective anti-oxidative and anti-inflammatory agent for preventing cisplatin-induced nephrotoxicity, Biochim Biophys Acta 1840(3) (2014) 1152-62.
[61] D. Lebwohl, R. Canetta, Clinical development of platinum complexes in cancer therapy: an historical perspective and an update, Eur J Cancer 34(10) (1998) 1522-34.
[62] F. Shiraishi, L.M. Curtis, L. Truong, K. Poss, G.A. Visner, K. Madsen, H.S. Nick, A. Agarwal, Heme oxygenase-1 gene ablation or expression modulates cisplatin-induced renal tubular apoptosis, Am J Physiol Renal Physiol 278(5) (2000) F726-36.
[63] R. Safirstein, J. Winston, M. Goldstein, D. Moel, S. Dikman, J. Guttenplan, Cisplatin nephrotoxicity, Am J Kidney Dis 8(5) (1986) 356-67.
[64] H. Rabb, M.D. Griffin, D.B. McKay, S. Swaminathan, P. Pickkers, M.H. Rosner, J.A. Kellum, C. Ronco, Inflammation in AKI: Current Understanding, Key Questions, and Knowledge Gaps, J Am Soc Nephrol 27(2) (2016) 371-9.
[65] R. Medzhitov, Inflammation 2010: new adventures of an old flame, Cell 140(6) (2010) 771-6.

[66] S. Dellepiane, J.S. Leventhal, P. Cravedi, T Cells and Acute Kidney Injury: A Two-Way Relationship, Front Immunol 11 (2020) 1546.
[67] H. Chiao, Y. Kohda, P. McLeroy, L. Craig, I. Housini, R.A. Star, Alpha-melanocyte-stimulating hormone protects against renal injury after ischemia in mice and rats, J Clin Invest 99(6) (1997) 1165-72.
[68] T. Nemoto, M.J. Burne, F. Daniels, M.P. O'Donnell, J. Crosson, K. Berens, A. Issekutz, B.L. Kasiske, W.F. Keane, H. Rabb, Small molecule selectin ligand inhibition improves outcome in ischemic acute renal failure, Kidney Int 60(6) (2001) 2205-14.
[69] K. Solez, L. Morel-Maroger, J.D. Sraer, The morphology of "acute tubular necrosis" in man: analysis of 57 renal biopsies and a comparison with the glycerol model, Medicine (Baltimore) 58(5) (1979) 362-76.
[70] J.J. Friedewald, H. Rabb, Inflammatory cells in ischemic acute renal failure, Kidney Int 66(2) (2004) 486-91.
[71] S. Bolisetty, A. Agarwal, Neutrophils in acute kidney injury: not neutral any more, Kidney Int 75(7) (2009) 674-6.
[72] S. Tanaka, T. Tanaka, T. Kawakami, H. Takano, M. Sugahara, H. Saito, Y. Higashijima, J. Yamaguchi, R. Inagi, M. Nangaku, Vascular adhesion protein-1 enhances neutrophil infiltration by generation of hydrogen peroxide in renal ischemia/reperfusion injury, Kidney Int 92(1) (2017) 154-164.
[73] B. Deng, Y. Lin, S. Ma, Y. Zheng, X. Yang, B. Li, W. Yu, Q. Xu, T. Liu, C. Hao, R. He, F. Ding, The leukotriene B(4)-leukotriene B(4) receptor axis promotes cisplatin-induced acute kidney injury by modulating neutrophil recruitment, Kidney Int 92(1) (2017) 89-100.
[74] D.K. Ysebaert, K.E. De Greef, S.R. Vercauteren, M. Ghielli, G.A. Verpooten, E.J. Eyskens, M.E. De Broe, Identification and kinetics of leukocytes after severe ischaemia/reperfusion renal injury, Nephrol Dial Transplant 15(10) (2000) 1562-74.
[75] H.R. Jang, H. Rabb, Immune cells in experimental acute kidney injury, Nat Rev Nephrol 11(2) (2015) 88-101.
[76] S.K. Jo, S.A. Sung, W.Y. Cho, K.J. Go, H.K. Kim, Macrophages contribute to the initiation of ischaemic acute renal failure in rats, Nephrol Dial Transplant 21(5) (2006) 1231-9.
[77] S. Lee, S. Huen, H. Nishio, S. Nishio, H.K. Lee, B.S. Choi, C. Ruhrberg, L.G. Cantley, Distinct macrophage phenotypes contribute to kidney injury and repair, J Am Soc Nephrol 22(2) (2011) 317-26.
[78] S. Swaminathan, M.D. Griffin, First responders: understanding monocyte-lineage traffic in the acutely injured kidney, Kidney Int 74(12) (2008) 1509-11.
[79] H.J. Anders, M. Ryu, Renal microenvironments and macrophage phenotypes determine progression or resolution of renal inflammation and fibrosis, Kidney Int 80(9) (2011) 915-925.
[80] J. Yamate, A. Ishida, K. Tsujino, M. Tatsumi, S. Nakatsuji, M. Kuwamura, T. Kotani, S. Sakuma, Immunohistochemical study of rat renal interstitial fibrosis induced by repeated injection of cisplatin, with special reference to the kinetics of macrophages and myofibroblasts, Toxicol Pathol 24(2) (1996) 199-206.
[81] L.H. Lu, D.J. Oh, B. Dursun, Z. He, T.S. Hoke, S. Faubel, C.L. Edelstein, Increased macrophage infiltration and fractalkine expression in cisplatin-induced acute renal failure in mice, J Pharmacol Exp Ther 324(1) (2008) 111-7.

[82] C.L. Schlichting, W.D. Schareck, M. Weis, Renal ischemia-reperfusion injury: new implications of dendritic cell-endothelial cell interactions, Transplant Proc 38(3) (2006) 670-3.
[83] R.K. Tadagavadi, W.B. Reeves, Renal dendritic cells ameliorate nephrotoxic acute kidney injury, J Am Soc Nephrol 21(1) (2010) 53-63.
[84] R.K. Tadagavadi, W.B. Reeves, Endogenous IL-10 attenuates cisplatin nephrotoxicity: role of dendritic cells, J Immunol 185(8) (2010) 4904-11.
[85] T.A. Fleisher, J.B. Oliveira, Functional and molecular evaluation of lymphocytes, J Allergy Clin Immunol 114(2) (2004) 227-34; quiz 235.
[86] H. Shau, M.D. Roth, S.H. Golub, Regulation of natural killer function by nonlymphoid cells, Nat Immun 12(4-5) (1993) 235-49.
[87] L. Chiche, J.M. Forel, G. Thomas, C. Farnarier, F. Vely, M. Bléry, L. Papazian, E. Vivier, The role of natural killer cells in sepsis, J Biomed Biotechnol 2011 (2011) 986491.
[88] Z.X. Zhang, S. Wang, X. Huang, W.P. Min, H. Sun, W. Liu, B. Garcia, A.M. Jevnikar, NK cells induce apoptosis in tubular epithelial cells and contribute to renal ischemia-reperfusion injury, J Immunol 181(11) (2008) 7489-98.
[89] M.J. Burne, F. Daniels, A. El Ghandour, S. Mauiyyedi, R.B. Colvin, M.P. O'Donnell, H. Rabb, Identification of the CD4(+) T cell as a major pathogenic factor in ischemic acute renal failure, J Clin Invest 108(9) (2001) 1283-90.
[90] M. Liu, C.C. Chien, M. Burne-Taney, R.R. Molls, L.C. Racusen, R.B. Colvin, H. Rabb, A pathophysiologic role for T lymphocytes in murine acute cisplatin nephrotoxicity, J Am Soc Nephrol 17(3) (2006) 765-74.
[91] A. Linkermann, N. Himmerkus, L. Rölver, K.A. Keyser, P. Steen, J.H. Bräsen, M. Bleich, U. Kunzendorf, S. Krautwald, Renal tubular Fas ligand mediates fratricide in cisplatin-induced acute kidney failure, Kidney Int 79(2) (2011) 169-78.
[92] M.T. Gandolfo, H.R. Jang, S.M. Bagnasco, G.J. Ko, P. Agreda, M.J. Soloski, M.T. Crow, H. Rabb, Mycophenolate mofetil modifies kidney tubular injury and Foxp3+ regulatory T cell trafficking during recovery from experimental ischemia-reperfusion, Transpl Immunol 23(1-2) (2010) 45-52.
[93] H. Lee, D. Nho, H.S. Chung, H. Lee, M.K. Shin, S.H. Kim, H. Bae, CD4+CD25+ regulatory T cells attenuate cisplatin-induced nephrotoxicity in mice, Kidney Int 78(11) (2010) 1100-9.
[94] K. Eller, T. Weber, M. Pruenster, A.M. Wolf, G. Mayer, A.R. Rosenkranz, A. Rot, CCR7 deficiency exacerbates injury in acute nephritis due to aberrant localization of regulatory T cells, J Am Soc Nephrol 21(1) (2010) 42-52.
[95] E.T. Chouchani, V.R. Pell, A.M. James, L.M. Work, K. Saeb-Parsy, C. Frezza, T. Krieg, M.P. Murphy, A Unifying Mechanism for Mitochondrial Superoxide Production during Ischemia-Reperfusion Injury, Cell Metab 23(2) (2016) 254-63.
[96] B.J. Padanilam, Cell death induced by acute renal injury: a perspective on the contributions of apoptosis and necrosis, Am J Physiol Renal Physiol 284(4) (2003) F608-27.
[97] A. Kezić, N. Stajic, F. Thaiss, Innate Immune Response in Kidney Ischemia/Reperfusion Injury: Potential Target for Therapy, J Immunol Res 2017 (2017) 6305439.
[98] W. Jassem, S.V. Fuggle, M. Rela, D.D. Koo, N.D. Heaton, The role of mitochondria in ischemia/reperfusion injury, Transplantation 73(4) (2002) 493-9.

[99] J.L. Martin, A.V. Gruszczyk, T.E. Beach, M.P. Murphy, K. Saeb-Parsy, Mitochondrial mechanisms and therapeutics in ischaemia reperfusion injury, Pediatr Nephrol 34(7) (2019) 1167-1174.
[100] E.T. Chouchani, V.R. Pell, E. Gaude, D. Aksentijević, S.Y. Sundier, E.L. Robb, A. Logan, S.M. Nadtochiy, E.N.J. Ord, A.C. Smith, F. Eyassu, R. Shirley, C.H. Hu, A.J. Dare, A.M. James, S. Rogatti, R.C. Hartley, S. Eaton, A.S.H. Costa, P.S. Brookes, S.M. Davidson, M.R. Duchen, K. Saeb-Parsy, M.J. Shattock, A.J. Robinson, L.M. Work, C. Frezza, T. Krieg, M.P. Murphy, Ischaemic accumulation of succinate controls reperfusion injury through mitochondrial ROS, Nature 515(7527) (2014) 431-435.
[101] Q. Wei, G. Dong, J.K. Chen, G. Ramesh, Z. Dong, Bax and Bak have critical roles in ischemic acute kidney injury in global and proximal tubule-specific knockout mouse models, Kidney Int 84(1) (2013) 138-48.
[102] F. Kruiswijk, C.F. Labuschagne, K.H. Vousden, p53 in survival, death and metabolic health: a lifeguard with a licence to kill, Nat Rev Mol Cell Biol 16(7) (2015) 393-405.
[103] D.W. Meek, C.W. Anderson, Posttranslational modification of p53: cooperative integrators of function, Cold Spring Harb Perspect Biol 1(6) (2009) a000950.
[104] R. Saldaña-Meyer, F. Recillas-Targa, Transcriptional and epigenetic regulation of the p53 tumor suppressor gene, Epigenetics 6(9) (2011) 1068-77.
[105] C. Tang, Z. Ma, J. Zhu, Z. Liu, Y. Liu, Y. Liu, J. Cai, Z. Dong, P53 in kidney injury and repair: Mechanism and therapeutic potentials, Pharmacol Ther 195 (2019) 5-12.
[106] M.E. Murphy, Ironing out how p53 regulates ferroptosis, Proc Natl Acad Sci U S A 113(44) (2016) 12350-12352.
[107] A.V. Vaseva, N.D. Marchenko, K. Ji, S.E. Tsirka, S. Holzmann, U.M. Moll, p53 opens the mitochondrial permeability transition pore to trigger necrosis, Cell 149(7) (2012) 1536-48.
[108] Y. Xie, S. Zhu, X. Song, X. Sun, Y. Fan, J. Liu, M. Zhong, H. Yuan, L. Zhang, T.R. Billiar, M.T. Lotze, H.J. Zeh, 3rd, R. Kang, G. Kroemer, D. Tang, The Tumor Suppressor p53 Limits Ferroptosis by Blocking DPP4 Activity, Cell Rep 20(7) (2017) 1692-1704.
[109] A. Linkermann, G. Chen, G. Dong, U. Kunzendorf, S. Krautwald, Z. Dong, Regulated cell death in AKI, J Am Soc Nephrol 25(12) (2014) 2689-701.
[110] M. Jiang, Z. Dong, Regulation and pathological role of p53 in cisplatin nephrotoxicity, J Pharmacol Exp Ther 327(2) (2008) 300-7.
[111] S. Zhu, N. Pabla, C. Tang, L. He, Z. Dong, DNA damage response in cisplatin-induced nephrotoxicity, Arch Toxicol 89(12) (2015) 2197-205.
[112] K. Singaravelu, B.J. Padanilam, p53 target Siva regulates apoptosis in ischemic kidneys, Am J Physiol Renal Physiol 300(5) (2011) F1130-41.
[113] D. Zhang, Y. Liu, Q. Wei, Y. Huo, K. Liu, F. Liu, Z. Dong, Tubular p53 regulates multiple genes to mediate AKI, J Am Soc Nephrol 25(10) (2014) 2278-89.
[114] K.J. Kelly, Z. Plotkin, S.L. Vulgamott, P.C. Dagher, P53 mediates the apoptotic response to GTP depletion after renal ischemia-reperfusion: protective role of a p53 inhibitor, J Am Soc Nephrol 14(1) (2003) 128-38.
[115] A.V. Vaseva, U.M. Moll, The mitochondrial p53 pathway, Biochim Biophys Acta 1787(5) (2009) 414-20.
[116] B.A. Molitoris, P.C. Dagher, R.M. Sandoval, S.B. Campos, H. Ashush, E. Fridman, A. Brafman, A. Faerman, S.J. Atkinson, J.D. Thompson, H. Kalinski, R. Skaliter, S. Erlich,

E. Feinstein, siRNA targeted to p53 attenuates ischemic and cisplatin-induced acute kidney injury, J Am Soc Nephrol 20(8) (2009) 1754-64.
[117] Y. Ying, J. Kim, S.N. Westphal, K.E. Long, B.J. Padanilam, Targeted deletion of p53 in the proximal tubule prevents ischemic renal injury, J Am Soc Nephrol 25(12) (2014) 2707-16.
[118] T.A. Sutton, T. Hato, E. Mai, M. Yoshimoto, S. Kuehl, M. Anderson, H. Mang, Z. Plotkin, R.J. Chan, P.C. Dagher, p53 is renoprotective after ischemic kidney injury by reducing inflammation, J Am Soc Nephrol 24(1) (2013) 113-24.
[119] P.C. Dagher, E.M. Mai, T. Hato, S.Y. Lee, M.D. Anderson, S.C. Karozos, H.E. Mang, N.L. Knipe, Z. Plotkin, T.A. Sutton, The p53 inhibitor pifithrin-α can stimulate fibrosis in a rat model of ischemic acute kidney injury, Am J Physiol Renal Physiol 302(2) (2012) F284-91.
[120] L. Yang, T.Y. Besschetnova, C.R. Brooks, J.V. Shah, J.V. Bonventre, Epithelial cell cycle arrest in G2/M mediates kidney fibrosis after injury, Nat Med 16(5) (2010) 535-43, 1p following 143.
[121] Q. Wei, G. Dong, T. Yang, J. Megyesi, P.M. Price, Z. Dong, Activation and involvement of p53 in cisplatin-induced nephrotoxicity, Am J Physiol Renal Physiol 293(4) (2007) F1282-91.
[122] L. Zhou, P. Fu, X.R. Huang, F. Liu, K.N. Lai, H.Y. Lan, Activation of p53 promotes renal injury in acute aristolochic acid nephropathy, J Am Soc Nephrol 21(1) (2010) 31-41.
[123] E. Homsi, S. Mota da Silva, Jr., S. Machado de Brito, E. Bouçada Inácio Peixoto, J. Butori Lopes de Faria, P. Janino, p53-Mediated oxidative stress and tubular injury in rats with glycerol-induced acute kidney injury, Am J Nephrol 33(1) (2011) 49-59.
[124] J. Chen, J. Wang, H. Li, S. Wang, X. Xiang, D. Zhang, p53 activates miR-192-5p to mediate vancomycin induced AKI, Sci Rep 6 (2016) 38868.
[125] F. Tögel, J. Isaac, Z. Hu, K. Weiss, C. Westenfelder, Renal SDF-1 signals mobilization and homing of CXCR4-positive cells to the kidney after ischemic injury, Kidney Int 67(5) (2005) 1772-84.
[126] C.C. Bleul, M. Farzan, H. Choe, C. Parolin, I. Clark-Lewis, J. Sodroski, T.A. Springer, The lymphocyte chemoattractant SDF-1 is a ligand for LESTR/fusin and blocks HIV-1 entry, Nature 382(6594) (1996) 829-33.
[127] E. Oberlin, A. Amara, F. Bachelerie, C. Bessia, J.L. Virelizier, F. Arenzana-Seisdedos, O. Schwartz, J.M. Heard, I. Clark-Lewis, D.F. Legler, M. Loetscher, M. Baggiolini, B. Moser, The CXC chemokine SDF-1 is the ligand for LESTR/fusin and prevents infection by T-cell-line-adapted HIV-1, Nature 382(6594) (1996) 833-5.
[128] B.A. Teicher, S.P. Fricker, CXCL12 (SDF-1)/CXCR4 pathway in cancer, Clin Cancer Res 16(11) (2010) 2927-31.
[129] J.V. Bonventre, A. Zuk, Ischemic acute renal failure: an inflammatory disease?, Kidney Int 66(2) (2004) 480-5.
[130] G.R. Kinsey, L. Li, M.D. Okusa, Inflammation in acute kidney injury, Nephron Exp Nephrol 109(4) (2008) e102-7.
[131] A. Aiuti, I.J. Webb, C. Bleul, T. Springer, J.C. Gutierrez-Ramos, The chemokine SDF-1 is a chemoattractant for human CD34+ hematopoietic progenitor cells and provides a new mechanism to explain the mobilization of CD34+ progenitors to peripheral blood, J Exp Med 185(1) (1997) 111-20.

[132] T. Nagasawa, K. Tachibana, T. Kishimoto, A novel CXC chemokine PBSF/SDF-1 and its receptor CXCR4: their functions in development, hematopoiesis and HIV infection, Semin Immunol 10(3) (1998) 179-85.
[133] K. Jujo, H. Hamada, A. Iwakura, T. Thorne, H. Sekiguchi, T. Clarke, A. Ito, S. Misener, T. Tanaka, E. Klyachko, K. Kobayashi, J. Tongers, J. Roncalli, Y. Tsurumi, N. Hagiwara, D.W. Losordo, CXCR4 blockade augments bone marrow progenitor cell recruitment to the neovasculature and reduces mortality after myocardial infarction, Proc Natl Acad Sci U S A 107(24) (2010) 11008-13.
[134] T.C. Fang, W.R. Otto, J. Rao, R. Jeffery, T. Hunt, M.R. Alison, H.T. Cook, N.A. Wright, R. Poulsom, Haematopoietic lineage-committed bone marrow cells, but not cloned cultured mesenchymal stem cells, contribute to regeneration of renal tubular epithelium after HgCl 2 -induced acute tubular injury, Cell Prolif 41(4) (2008) 575-91.
[135] C. Lange, F. Tögel, H. Ittrich, F. Clayton, C. Nolte-Ernsting, A.R. Zander, C. Westenfelder, Administered mesenchymal stem cells enhance recovery from ischemia/reperfusion-induced acute renal failure in rats, Kidney Int 68(4) (2005) 1613-7.
[136] B. Li, A. Cohen, T.E. Hudson, D. Motlagh, D.L. Amrani, J.S. Duffield, Mobilized human hematopoietic stem/progenitor cells promote kidney repair after ischemia/reperfusion injury, Circulation 121(20) (2010) 2211-20.
[137] F. Lin, K. Cordes, L. Li, L. Hood, W.G. Couser, S.J. Shankland, P. Igarashi, Hematopoietic stem cells contribute to the regeneration of renal tubules after renal ischemia-reperfusion injury in mice, J Am Soc Nephrol 14(5) (2003) 1188-99.
[138] D. Patschan, K. Krupincza, S. Patschan, Z. Zhang, C. Hamby, M.S. Goligorsky, Dynamics of mobilization and homing of endothelial progenitor cells after acute renal ischemia: modulation by ischemic preconditioning, Am J Physiol Renal Physiol 291(1) (2006) F176-85.
[139] C.H. Wu, J.S. Song, K.H. Chang, J.J. Jan, C.T. Chen, M.C. Chou, K.C. Yeh, Y.C. Wong, C.T. Tseng, S.H. Wu, C.F. Yeh, C.Y. Huang, M.H. Wang, A.A. Sadani, C.P. Chang, C.Y. Cheng, L.K. Tsou, K.S. Shia, Stem cell mobilizers targeting chemokine receptor CXCR4: renoprotective application in acute kidney injury, J Med Chem 58(5) (2015) 2315-25.
[140] A. Zuk, M. Gershenovich, Y. Ivanova, R.T. MacFarland, S.P. Fricker, S. Ledbetter, CXCR4antagonism as a therapeutic approach to prevent acute kidney injury, Am J Physiol Renal Physiol 307(7) (2014) F783-97.
[141] A. Song, A. Jiang, W. Xiong, C. Zhang, The Role of CXCL12 in Kidney Diseases: A Friend or Foe?, Kidney Dis (Basel) 7(3) (2021) 176-185.
[142] G.M. Chertow, E. Burdick, M. Honour, J.V. Bonventre, D.W. Bates, Acute kidney injury, mortality, length of stay, and costs in hospitalized patients, J Am Soc Nephrol 16(11) (2005) 3365-70.
[143] A. Lassnigg, D. Schmidlin, M. Mouhieddine, L.M. Bachmann, W. Druml, P. Bauer, M. Hiesmayr, Minimal changes of serum creatinine predict prognosis in patients after cardiothoracic surgery: a prospective cohort study, J Am Soc Nephrol 15(6) (2004) 1597-605.
[144] J. Vanmassenhove, G. Glorieux, E. Hoste, A. Dhondt, R. Vanholder, W. Van Biesen, Urinary output and fractional excretion of sodium and urea as indicators of transient versus intrinsic acute kidney injury during early sepsis, Crit Care 17(5) (2013) R234.

[145] J.A. Kellum, P. Romagnani, G. Ashuntantang, C. Ronco, A. Zarbock, H.J. Anders, Acute kidney injury, Nat Rev Dis Primers 7(1) (2021) 52.
[146] A. Khwaja, KDIGO clinical practice guidelines for acute kidney injury, Nephron Clin Pract 120(4) (2012) c179-84.
[147] C.Y. Hsu, G.M. Chertow, C.E. McCulloch, D. Fan, J.D. Ordoñez, A.S. Go, Nonrecovery of kidney function and death after acute on chronic renal failure, Clin J Am Soc Nephrol 4(5) (2009) 891-8.
[148] C.Y. Hsu, J.D. Ordoñez, G.M. Chertow, D. Fan, C.E. McCulloch, A.S. Go, The risk of acute renal failure in patients with chronic kidney disease, Kidney Int 74(1) (2008) 101-7.
[149] A. Ishani, J.L. Xue, J. Himmelfarb, P.W. Eggers, P.L. Kimmel, B.A. Molitoris, A.J. Collins, Acute kidney injury increases risk of ESRD among elderly, J Am Soc Nephrol 20(1) (2009) 223-8.
[150] N. Pannu, M. James, B.R. Hemmelgarn, J. Dong, M. Tonelli, S. Klarenbach, Modification of outcomes after acute kidney injury by the presence of CKD, Am J Kidney Dis 58(2) (2011) 206-13.
[151] J.P. Lafrance, O. Djurdjev, A. Levin, Incidence and outcomes of acute kidney injury in a referred chronic kidney disease cohort, Nephrol Dial Transplant 25(7) (2010) 2203-9.
[152] S.S. Waikar, J.V. Bonventre, Creatinine kinetics and the definition of acute kidney injury, J Am Soc Nephrol 20(3) (2009) 672-9.
[153] J.A. Kellum, F.E. Sileanu, R. Murugan, N. Lucko, A.D. Shaw, G. Clermont, Classifying AKI by Urine Output versus Serum Creatinine Level, J Am Soc Nephrol 26(9) (2015) 2231-8.
[154] P. Priyanka, A. Zarbock, J. Izawa, T.G. Gleason, R.W. Renfurm, J.A. Kellum, The impact of acute kidney injury by serum creatinine or urine output criteria on major adverse kidney events in cardiac surgery patients, J Thorac Cardiovasc Surg 162(1) (2021) 143-151.e7.
[155] J.L. Alge, J.M. Arthur, Biomarkers of AKI: a review of mechanistic relevance and potential therapeutic implications, Clin J Am Soc Nephrol 10(1) (2015) 147-55.
[156] S.M. Bagshaw, M. Zappitelli, L.S. Chawla, Novel biomarkers of AKI: the challenges of progress 'Amid the noise and the haste', Nephrol Dial Transplant 28(2) (2013) 235-8.
[157] N.H. Lameire, R.C. Vanholder, W.A. Van Biesen, How to use biomarkers efficiently in acute kidney injury, Kidney Int 79(10) (2011) 1047-50.
[158] J. Vanmassenhove, R. Vanholder, E. Nagler, W. Van Biesen, Urinary and serum biomarkers for the diagnosis of acute kidney injury: an in-depth review of the literature, Nephrol Dial Transplant 28(2) (2013) 254-73.
[159] M. Ostermann, A. Zarbock, S. Goldstein, K. Kashani, E. Macedo, R. Murugan, M. Bell, L. Forni, L. Guzzi, M. Joannidis, S.L. Kane-Gill, M. Legrand, R. Mehta, P.T. Murray, P. Pickkers, M. Plebani, J. Prowle, Z. Ricci, T. Rimmelé, M. Rosner, A.D. Shaw, J.A. Kellum, C. Ronco, Recommendations on Acute Kidney Injury Biomarkers From the Acute Disease Quality Initiative Consensus Conference: A Consensus Statement, JAMA Netw Open 3(10) (2020) e2019209.
[160] L. Cai, J. Rubin, W. Han, P. Venge, S. Xu, The origin of multiple molecular forms in urine of HNL/NGAL, Clin J Am Soc Nephrol 5(12) (2010) 2229-35.
[161] P. Devarajan, Review: neutrophil gelatinase-associated lipocalin: a troponin-like biomarker for human acute kidney injury, Nephrology (Carlton) 15(4) (2010) 419-28.

[162] P.K. Mishra, H. Luckraz, J. Nandi, A. Nevill, R. Giri, A. Panayiotou, J. Nicholas, Long-term quality of life postacute kidney injury in cardiac surgery patients, Ann Card Anaesth 21(1) (2018) 41-45.
[163] Z.H. Endre, J.W. Pickering, R.J. Walker, P. Devarajan, C.L. Edelstein, J.V. Bonventre, C.M. Frampton, M.R. Bennett, Q. Ma, V.S. Sabbisetti, V.S. Vaidya, A.M. Walcher, G.M. Shaw, S.J. Henderson, M. Nejat, J.B. Schollum, P.M. George, Improved performance of urinary biomarkers of acute kidney injury in the critically ill by stratification for injury duration and baseline renal function, Kidney Int 79(10) (2011) 1119-30.
[164] K. Makris, N. Markou, E. Evodia, E. Dimopoulou, I. Drakopoulos, K. Ntetsika, D. Rizos, G. Baltopoulos, A. Haliassos, Urinary neutrophil gelatinase-associated lipocalin (NGAL) as an early marker of acute kidney injury in critically ill multiple trauma patients, Clin Chem Lab Med 47(1) (2009) 79-82.
[165] D.R. McIlroy, G. Wagener, H.T. Lee, Neutrophil gelatinase-associated lipocalin and acute kidney injury after cardiac surgery: the effect of baseline renal function on diagnostic performance, Clin J Am Soc Nephrol 5(2) (2010) 211-9.
[166] A. Perrotti, G. Miltgen, A. Chevet-Noel, C. Durst, D. Vernerey, K. Bardonnet, S. Davani, S. Chocron, Neutrophil gelatinase-associated lipocalin as early predictor of acute kidney injury after cardiac surgery in adults with chronic kidney failure, Ann Thorac Surg 99(3) (2015) 864-9.
[167] T. Ichimura, J.V. Bonventre, V. Bailly, H. Wei, C.A. Hession, R.L. Cate, M. Sanicola, Kidney injury molecule-1 (KIM-1), a putative epithelial cell adhesion molecule containing a novel immunoglobulin domain, is up-regulated in renal cells after injury, J Biol Chem 273(7) (1998) 4135-42.
[168] T. Ichimura, E.J. Asseldonk, B.D. Humphreys, L. Gunaratnam, J.S. Duffield, J.V. Bonventre, Kidney injury molecule-1 is a phosphatidylserine receptor that confers a phagocytic phenotype on epithelial cells, J Clin Invest 118(5) (2008) 1657-68.
[169] J.M. Arthur, E.G. Hill, J.L. Alge, E.C. Lewis, B.A. Neely, M.G. Janech, J.A. Tumlin, L.S. Chawla, A.D. Shaw, Evaluation of 32 urine biomarkers to predict the progression of acute kidney injury after cardiac surgery, Kidney Int 85(2) (2014) 431-8.
[170] Y. Yang, M. Song, Y. Liu, H. Liu, L. Sun, Y. Peng, F. Liu, M.A. Venkatachalam, Z. Dong, Renoprotective approaches and strategies in acute kidney injury, Pharmacol Ther 163 (2016) 58-73.
[171] X. Su, X. Xie, L. Liu, J. Lv, F. Song, V. Perkovic, H. Zhang, Comparative Effectiveness of 12 Treatment Strategies for Preventing Contrast-Induced Acute Kidney Injury: A Systematic Review and Bayesian Network Meta-analysis, Am J Kidney Dis 69(1) (2017) 69-77.
[172] H. Yu, D. Liu, G. Shu, F. Jin, Y. Du, Recent advances in nanotherapeutics for the treatment and prevention of acute kidney injury, Asian Journal of Pharmaceutical Sciences (2020).
[173] R. Duncan, R. Gaspar, Nanomedicine(s) under the microscope, Mol Pharm 8(6) (2011) 2101-41.
[174] R. Singh, J.W. Lillard, Jr., Nanoparticle-based targeted drug delivery, Exp Mol Pathol 86(3) (2009) 215-23.
[175] A.Z. Wang, R. Langer, O.C. Farokhzad, Nanoparticle delivery of cancer drugs, Annu Rev Med 63 (2012) 185-98.

[176] R.M. Williams, E.A. Jaimes, D.A. Heller, Nanomedicines for kidney diseases, Kidney Int 90(4) (2016) 740-5.
[177] M.F. Attia, N. Anton, J. Wallyn, Z. Omran, T.F. Vandamme, An overview of active and passive targeting strategies to improve the nanocarriers efficiency to tumour sites, J Pharm Pharmacol 71(8) (2019) 1185-1198.
[178] V. Torchilin, Tumor delivery of macromolecular drugs based on the EPR effect, Adv Drug Deliv Rev 63(3) (2011) 131-5.
[179] D. Liu, Y. Du, F.Y. Jin, X.L. Xu, Y.Z. Du, Renal Cell-Targeted Drug Delivery Strategy for Acute Kidney Injury and Chronic Kidney Disease: A Mini-Review, Mol Pharm (2021).
[180] Z.X. Yuan, X. Sun, T. Gong, H. Ding, Y. Fu, Z.R. Zhang, Randomly 50% N-acetylated low molecular weight chitosan as a novel renal targeting carrier, J Drug Target 15(4) (2007) 269-78.
[181] Y. Huang, J. Wang, K. Jiang, E.J. Chung, Improving kidney targeting: The influence of nanoparticle physicochemical properties on kidney interactions, J Control Release 334 (2021) 127-137.
[182] H. Pavenstädt, W. Kriz, M. Kretzler, Cell biology of the glomerular podocyte, Physiol Rev 83(1) (2003) 253-307.
[183] C.P. Liu, Y. Hu, J.C. Lin, H.L. Fu, L.Y. Lim, Z.X. Yuan, Targeting strategies for drug delivery to the kidney: From renal glomeruli to tubules, Med Res Rev 39(2) (2019) 561-578.
[184] R.M. Williams, J. Shah, B.D. Ng, D.R. Minton, L.J. Gudas, C.Y. Park, D.A. Heller, Mesoscale nanoparticles selectively target the renal proximal tubule epithelium, Nano Lett 15(4) (2015) 2358-64.
[185] M.E. Dolman, S. Harmsen, G. Storm, W.E. Hennink, R.J. Kok, Drug targeting to the kidney: Advances in the active targeting of therapeutics to proximal tubular cells, Adv Drug Deliv Rev 62(14) (2010) 1344-57.
[186] S.C. Satchell, F. Braet, Glomerular endothelial cell fenestrations: an integral component of the glomerular filtration barrier, Am J Physiol Renal Physiol 296(5) (2009) F947-56.
[187] C. Lemarchand, R. Gref, P. Couvreur, Polysaccharide-decorated nanoparticles, Eur J Pharm Biopharm 58(2) (2004) 327-41.
[188] J.B. Hu, S.J. Li, X.Q. Kang, J. Qi, J.H. Wu, X.J. Wang, X.L. Xu, X.Y. Ying, S.P. Jiang, J. You, Y.Z. Du, CD44-targeted hyaluronic acid-curcumin prodrug protects renal tubular epithelial cell survival from oxidative stress damage, Carbohydr Polym 193 (2018) 268-280.
[189] D. Liu, F. Jin, G. Shu, X. Xu, J. Qi, X. Kang, H. Yu, K. Lu, S. Jiang, F. Han, J. You, Y. Du, J. Ji, Enhanced efficiency of mitochondria-targeted peptide SS-31 for acute kidney injury by pH-responsive and AKI-kidney targeted nanopolyplexes, Biomaterials 211 (2019) 57-67.
[190] A.C. Midgley, Y. Wei, D. Zhu, F. Gao, H. Yan, A. Khalique, W. Luo, H. Jiang, X. Liu, J. Guo, C. Zhang, G. Feng, K. Wang, X. Bai, W. Ning, C. Yang, Q. Zhao, D. Kong, Multifunctional Natural Polymer Nanoparticles as Antifibrotic Gene Carriers for CKD Therapy, J Am Soc Nephrol 31(10) (2020) 2292-2311.

[191] Z.W. Huang, Y. Shi, Y.Y. Zhai, C.C. Du, J. Zhai, R.J. Yu, L. Kou, J. Xiao, Y.Z. Zhao, Q. Yao, Hyaluronic acid coated bilirubin nanoparticles attenuate ischemia reperfusion-induced acute kidney injury, J Control Release 334 (2021) 275-289.
[192] D. Liu, G. Shu, F. Jin, J. Qi, X. Xu, Y. Du, H. Yu, J. Wang, M. Sun, Y. You, M. Zhu, M. Chen, L. Zhu, Q. Shen, X. Ying, X. Lou, S. Jiang, Y. Du, ROS-responsive chitosan-SS31 prodrug for AKI therapy via rapid distribution in the kidney and long-term retention in the renal tubule, Sci Adv 6(41) (2020).
[193] X.Y. Zhai, R. Nielsen, H. Birn, K. Drumm, S. Mildenberger, R. Freudinger, S.K. Moestrup, P.J. Verroust, E.I. Christensen, M. Gekle, Cubilin- and megalin-mediated uptake of albumin in cultured proximal tubule cells of opossum kidney, Kidney Int 58(4) (2000) 1523-33.
[194] Z. Zhang, Q. Zheng, J. Han, G. Gao, J. Liu, T. Gong, Z. Gu, Y. Huang, X. Sun, Q. He, The targeting of 14-succinate triptolide-lysozyme conjugate to proximal renal tubular epithelial cells, Biomaterials 30(7) (2009) 1372-81.
[195] X. Wang, Y. Lin, Y. Zeng, X. Sun, T. Gong, Z. Zhang, Effects of mycophenolic acid-glucosamine conjugates on the base of kidney targeted drug delivery, Int J Pharm 456(1) (2013) 223-34.
[196] Z. Chen, H. Peng, C. Zhang, Advances in kidney-targeted drug delivery systems, Int J Pharm 587 (2020) 119679.
[197] K. Hironaka, H. Makino, Y. Yamasaki, Z. Ota, Pores in the glomerular basement membrane revealed by ultrahigh-resolution scanning electron microscopy, Nephron 64(4) (1993) 647-9.
[198] D. Ni, D. Jiang, H.F. Valdovinos, E.B. Ehlerding, B. Yu, T.E. Barnhart, P. Huang, W. Cai, Bioresponsive Polyoxometalate Cluster for Redox-Activated Photoacoustic Imaging-Guided Photothermal Cancer Therapy, Nano Lett 17(5) (2017) 3282-3289.
[199] T. Liu, B. Xiao, F. Xiang, J. Tan, Z. Chen, X. Zhang, C. Wu, Z. Mao, G. Luo, X. Chen, J. Deng, Ultrasmall copper-based nanoparticles for reactive oxygen species scavenging and alleviation of inflammation related diseases, Nat Commun 11(1) (2020) 2788.
[200] H. Yu, F. Jin, D. Liu, G. Shu, X. Wang, J. Qi, M. Sun, P. Yang, S. Jiang, X. Ying, Y. Du, ROS-responsive nano-drug delivery system combining mitochondria-targeting ceria nanoparticles with atorvastatin for acute kidney injury, Theranostics 10(5) (2020) 2342-2357.
[201] D. Ni, D. Jiang, C.J. Kutyreff, J. Lai, Y. Yan, T.E. Barnhart, B. Yu, H.J. Im, L. Kang, S.Y. Cho, Z. Liu, P. Huang, J.W. Engle, W. Cai, Molybdenum-based nanoclusters act as antioxidants and ameliorate acute kidney injury in mice, Nat Commun 9(1) (2018) 5421.
[202] D.Y. Zhang, M.R. Younis, H. Liu, S. Lei, Y. Wan, J. Qu, J. Lin, P. Huang, Multi-enzyme mimetic ultrasmall iridium nanozymes as reactive oxygen/nitrogen species scavengers for acute kidney injury management, Biomaterials 271 (2021) 120706.
[203] J. Hou, H. Wang, Z. Ge, T. Zuo, Q. Chen, X. Liu, S. Mou, C. Fan, Y. Xie, L. Wang, Treating Acute Kidney Injury with Antioxidative Black Phosphorus Nanosheets, Nano Lett 20(2) (2020) 1447-1454.
[204] D. Jiang, Z. Ge, H.J. Im, C.G. England, D. Ni, J. Hou, L. Zhang, C.J. Kutyreff, Y. Yan, Y. Liu, S.Y. Cho, J.W. Engle, J. Shi, P. Huang, C. Fan, H. Yan, W. Cai, DNA origami nanostructures can exhibit preferential renal uptake and alleviate acute kidney injury, Nat Biomed Eng 2(11) (2018) 865-877.

[205] A. Favron, E. Gaufrès, F. Fossard, A.L. Phaneuf-L'Heureux, N.Y. Tang, P.L. Lévesque, A. Loiseau, R. Leonelli, S. Francoeur, R. Martel, Photooxidation and quantum confinement effects in exfoliated black phosphorus, Nat Mater 14(8) (2015) 826-32.
[206] P. Zhou, X. Sun, Z. Zhang, Kidney-targeted drug delivery systems, Acta Pharm Sin B 4(1) (2014) 37-42.
[207] A. Ruggiero, C.H. Villa, E. Bander, D.A. Rey, M. Bergkvist, C.A. Batt, K. Manova-Todorova, W.M. Deen, D.A. Scheinberg, M.R. McDevitt, Paradoxical glomerular filtration of carbon nanotubes, Proc Natl Acad Sci U S A 107(27) (2010) 12369-74.
[208] S. Alidori, N. Akhavein, D.L.J. Thorek, K. Behling, Y. Romin, D. Queen, B.J. Beattie, K. Manova-Todorova, M. Bergkvist, D.A. Scheinberg, M.R. McDevitt, Targeted fibrillar nanocarbon RNAi treatment of acute kidney injury, Sci Transl Med 8(331) (2016) 331ra39-331ra39.
[209] H.B.D. Thai, K.R. Kim, K.T. Hong, T. Voitsitskyi, J.S. Lee, C. Mao, D.R. Ahn, Kidney-Targeted Cytosolic Delivery of siRNA Using a Small-Sized Mirror DNA Tetrahedron for Enhanced Potency, ACS Cent Sci 6(12) (2020) 2250-2258.
[210] R.L. Mehta, J.A. Kellum, S.V. Shah, B.A. Molitoris, C. Ronco, D.G. Warnock, A. Levin, Acute Kidney Injury Network: report of an initiative to improve outcomes in acute kidney injury, Critical care 11(2) (2007) R31.
[211] N. Srisawat, J.A. Kellum, Acute kidney injury: definition, epidemiology, and outcome, Current opinion in critical care 17(6) (2011) 548-555.
[212] R.L. Mehta, M.T. Pascual, S. Soroko, G.M. Chertow, P.S. Group, Diuretics, mortality, and nonrecovery of renal function in acute renal failure, Jama 288(20) (2002) 2547-2553.
[213] E.A. Hoste, S.M. Bagshaw, R. Bellomo, C.M. Cely, R. Colman, D.N. Cruz, K. Edipidis, L.G. Forni, C.D. Gomersall, D. Govil, Epidemiology of acute kidney injury in critically ill patients: the multinational AKI-EPI study, Intensive care medicine 41(8) (2015) 1411-1423.
[214] C.-y. Hsu, Yes, AKI truly leads to CKD, Am Soc Nephrol, 2012.
[215] R. Bellomo, J.A. Kellum, C. Ronco, R. Wald, J. Martensson, M. Maiden, S.M. Bagshaw, N.J. Glassford, Y. Lankadeva, S.T. Vaara, Acute kidney injury in sepsis, Intensive care medicine 43(6) (2017) 816-828.
[216] A. Khwaja, KDIGO clinical practice guidelines for acute kidney injury, Nephron Clinical Practice 120(4) (2012) c179-c184.
[217] H. Rabb, M.D. Griffin, D.B. McKay, S. Swaminathan, P. Pickkers, M.H. Rosner, J.A. Kellum, C. Ronco, Inflammation in AKI: current understanding, key questions, and knowledge gaps, Journal of the American Society of Nephrology 27(2) (2016) 371-379.
[218] A.D. Luster, Chemokines—chemotactic cytokines that mediate inflammation, New England Journal of Medicine 338(7) (1998) 436-445.
[219] B.H. Rovin, L.T. Phan, Chemotactic factors and renal inflammation, American journal of kidney diseases 31(6) (1998) 1065-1084.
[220] G. Ramesh, W.B. Reeves, Inflammatory cytokines in acute renal failure, Kidney International 66 (2004) S56-S61.
[221] H. Zhao, L. Guo, H. Zhao, J. Zhao, H. Weng, B. Zhao, CXCR4 over-expression and survival in cancer: a system review and meta-analysis, Oncotarget 6(7) (2015) 5022.

[222] R.L. Sleightholm, B.K. Neilsen, J. Li, M.M. Steele, R.K. Singh, M.A. Hollingsworth, D. Oupicky, Emerging roles of the CXCL12/CXCR4 axis in pancreatic cancer progression and therapy, Pharmacology & therapeutics 179 (2017) 158-170.
[223] F. Tögel, J. Isaac, Z. Hu, K. Weiss, C. Westenfelder, Renal SDF-1 signals mobilization and homing of CXCR4-positive cells to the kidney after ischemic injury, Kidney international 67(5) (2005) 1772-1784.
[224] Y. Wang, Y. Xie, D. Oupický, Potential of CXCR4/CXCL12 chemokine axis in cancer drug delivery, Current pharmacology reports 2(1) (2016) 1-10.
[225] A. Zlotnik, A.M. Burkhardt, B. Homey, Homeostatic chemokine receptors and organ-specific metastasis, Nature Reviews Immunology 11(9) (2011) 597-606.
[226] C.C. Bleul, M. Farzan, H. Choe, C. Parolin, I. Clark-Lewis, J. Sodroski, T.A. Springer, The lymphocyte chemoattractant SDF-1 is a ligand for LESTR/fusin and blocks HIV-1 entry, Nature 382(6594) (1996) 829-833.
[227] A. Yuan, Y. Lee, U. Choi, G. Moeckel, A. Karihaloo, Chemokine receptor Cxcr4 contributes to kidney fibrosis via multiple effectors, American Journal of Physiology-Renal Physiology 308(5) (2015) F459-F472.
[228] A. Zuk, M. Gershenovich, Y. Ivanova, R.T. MacFarland, S.P. Fricker, S. Ledbetter, CXCR4 antagonism as a therapeutic approach to prevent acute kidney injury, American Journal of Physiology-Renal Physiology 307(7) (2014) F783-F797.
[229] C. Tang, Z. Ma, J. Zhu, Z. Liu, Y. Liu, Y. Liu, J. Cai, Z. Dong, P53 in kidney injury and repair: mechanism and therapeutic potentials, Pharmacology & therapeutics 195 (2019) 5-12.
[230] H. Horn, K. Vousden, Coping with stress: multiple ways to activate p53, Oncogene 26(9) (2007) 1306-1316.
[231] M.E. Murphy, Ironing out how p53 regulates ferroptosis, Proceedings of the National Academy of Sciences 113(44) (2016) 12350-12352.
[232] A.V. Vaseva, N.D. Marchenko, K. Ji, S.E. Tsirka, S. Holzmann, U.M. Moll, p53 opens the mitochondrial permeability transition pore to trigger necrosis, Cell 149(7) (2012) 1536-1548.
[233] Y. Xie, S. Zhu, X. Song, X. Sun, Y. Fan, J. Liu, M. Zhong, H. Yuan, L. Zhang, T.R. Billiar, The tumor suppressor p53 limits ferroptosis by blocking DPP4 activity, Cell reports 20(7) (2017) 1692-1704.
[234] A. Linkermann, G. Chen, G. Dong, U. Kunzendorf, S. Krautwald, Z. Dong, Regulated cell death in AKI, Journal of the American Society of Nephrology 25(12) (2014) 2689-2701.
[235] Y. Ying, B.J. Padanilam, Regulation of necrotic cell death: p53, PARP1 and cyclophilin D-overlapping pathways of regulated necrosis?, Cellular and Molecular Life Sciences 73(11) (2016) 2309-2324.
[236] M. Jiang, X. Yi, S. Hsu, C.-Y. Wang, Z. Dong, Role of p53 in cisplatin-induced tubular cell apoptosis: dependence on p53 transcriptional activity, American Journal of Physiology-Renal Physiology 287(6) (2004) F1140-F1147.
[237] Q. Wei, G. Dong, T. Yang, J. Megyesi, P.M. Price, Z. Dong, Activation and involvement of p53 in cisplatin-induced nephrotoxicity, American Journal of Physiology-Renal Physiology 293(4) (2007) F1282-F1291.
[238] B.A. Molitoris, P.C. Dagher, R.M. Sandoval, S.B. Campos, H. Ashush, E. Fridman, A. Brafman, A. Faerman, S.J. Atkinson, J.D. Thompson, siRNA targeted to p53 attenuates

ischemic and cisplatin-induced acute kidney injury, Journal of the American Society of Nephrology 20(8) (2009) 1754-1764.
[239] Y. Ying, J. Kim, S.N. Westphal, K.E. Long, B.J. Padanilam, Targeted deletion of p53 in the proximal tubule prevents ischemic renal injury, Journal of the American Society of Nephrology 25(12) (2014) 2707-2716.
[240] D. Zhang, Y. Liu, Q. Wei, Y. Huo, K. Liu, F. Liu, Z. Dong, Tubular p53 regulates multiple genes to mediate AKI, Journal of the American Society of Nephrology 25(10) (2014) 2278-2289.
[241] T.A. Sutton, T. Hato, E. Mai, M. Yoshimoto, S. Kuehl, M. Anderson, H. Mang, Z. Plotkin, R.J. Chan, P.C. Dagher, p53 is renoprotective after ischemic kidney injury by reducing inflammation, Journal of the American Society of Nephrology 24(1) (2013) 113-124.
[242] J. Chen, J. Wang, H. Li, S. Wang, X. Xiang, D. Zhang, p53 activates miR-192-5p to mediate vancomycin induced AKI, Scientific reports 6 (2016) 38868.
[243] K. Kelly, Z. Plotkin, S.L. Vulgamott, P.C. Dagher, P53 mediates the apoptotic response to GTP depletion after renal ischemia-reperfusion: protective role of a p53 inhibitor, Journal of the American Society of Nephrology 14(1) (2003) 128-138.
[244] J. Kim, K. Devalaraja-Narashimha, B.J. Padanilam, TIGAR regulates glycolysis in ischemic kidney proximal tubules, American Journal of Physiology-Renal Physiology 308(4) (2015) F298-F308.
[245] S. Inaba, S. Nagahara, N. Makita, Y. Tarumi, T. Ishimoto, S. Matsuo, K. Kadomatsu, Y. Takei, Atelocollagen-mediated systemic delivery prevents immunostimulatory adverse effects of siRNA in mammals, Molecular Therapy 20(2) (2012) 356-366.
[246] J. Conde, N. Oliva, M. Atilano, H.S. Song, N. Artzi, Self-assembled RNA-triple-helix hydrogel scaffold for microRNA modulation in the tumour microenvironment, Nature materials 15(3) (2016) 353-363.
[247] H. Wang, Y. Jiang, H. Peng, Y. Chen, P. Zhu, Y. Huang, Recent progress in microRNA delivery for cancer therapy by non-viral synthetic vectors, Advanced drug delivery reviews 81 (2015) 142-160.
[248] Y. Chen, W. Tang, F. Yu, Y. Xie, L. Jaramillo, H.-S. Jang, J. Li, B.J. Padanilam, D. Oupický, Determinants of preferential renal accumulation of synthetic polymers in acute kidney injury, International journal of pharmaceutics 568 (2019) 118555.
[249] Z.-x. Yuan, Z.-r. Zhang, D. Zhu, X. Sun, T. Gong, J. Liu, C.-t. Luan, Specific renal uptake of randomly 50% N-acetylated low molecular weight chitosan, Molecular pharmaceutics 6(1) (2009) 305-314.
[250] Z.-X. Yuan, X. Sun, T. Gong, H. Ding, Y. Fu, Z.-R. Zhang, Randomly 50% N-acetylated low molecular weight chitosan as a novel renal targeting carrier, Journal of drug targeting 15(4) (2007) 269-278.
[251] C. Yang, L. Nilsson, M.U. Cheema, Y. Wang, J. Frøkiær, S. Gao, J. Kjems, R. Nørregaard, Chitosan/siRNA nanoparticles targeting cyclooxygenase type 2 attenuate unilateral ureteral obstruction-induced kidney injury in mice, Theranostics 5(2) (2015) 110.
[252] H. Yu, T. Lin, W. Chen, W. Cao, C. Zhang, T. Wang, M. Ding, S. Zhao, H. Wei, H. Guo, Size and temporal-dependent efficacy of oltipraz-loaded PLGA nanoparticles for treatment of acute kidney injury and fibrosis, Biomaterials 219 (2019) 119368.

[253] R.M. Williams, J. Shah, B.D. Ng, D.R. Minton, L.J. Gudas, C.Y. Park, D.A. Heller, Mesoscale nanoparticles selectively target the renal proximal tubule epithelium, Nano letters 15(4) (2015) 2358-2364.
[254] R.M. Williams, J. Shah, H.S. Tian, X. Chen, F. Geissmann, E.A. Jaimes, D.A. Heller, Selective nanoparticle targeting of the renal tubules, Hypertension 71(1) (2018) 87-94.
[255] S.J. Han, R.M. Williams, V. D'Agati, E.A. Jaimes, D.A. Heller, H.T. Lee, Selective nanoparticle-mediated targeting of renal tubular Toll-like receptor 9 attenuates ischemic acute kidney injury, Kidney international 98(1) (2020) 76-87.
[256] S. Alidori, N. Akhavein, D.L. Thorek, K. Behling, Y. Romin, D. Queen, B.J. Beattie, K. Manova-Todorova, M. Bergkvist, D.A. Scheinberg, Targeted fibrillar nanocarbon RNAi treatment of acute kidney injury, Science translational medicine 8(331) (2016) 331ra39-331ra39.
[257] H.B.D. Thai, K.-R. Kim, K.T. Hong, T. Voitsitskyi, J.-S. Lee, C. Mao, D.-R. Ahn, Kidney-Targeted Cytosolic Delivery of siRNA Using a Small-Sized Mirror DNA Tetrahedron for Enhanced Potency, ACS central science 6(12) (2020) 2250-2258.
[258] Y. Wang, S.T. Hazeldine, J. Li, D. Oupický, Development of functional poly (amido amine) CXCR4 antagonists with the ability to mobilize leukocytes and deliver nucleic acids, Advanced healthcare materials 4(5) (2015) 729-738.
[259] Y. Xie, Y. Hang, Y. Wang, R. Sleightholm, D.R. Prajapati, J. Bader, A. Yu, W. Tang, L. Jaramillo, J. Li, R.K. Singh, D. Oupický, Stromal Modulation and Treatment of Metastatic Pancreatic Cancer with Local Intraperitoneal Triple miRNA/siRNA Nanotherapy, ACS nano 14(1) (2020) 255-271.
[260] P. Wu, X. Luo, H. Wu, F. Yu, K. Wang, M. Sun, D. Oupicky, Cholesterol Modification Enhances Antimetastatic Activity and siRNA Delivery Efficacy of Poly(ethylenimine)-Based CXCR4 Antagonists, Macromol Biosci 18(11) (2018) e1800234.
[261] Y. Wang, S. Kumar, S. Rachagani, B.R. Sajja, Y. Xie, Y. Hang, M. Jain, J. Li, M.D. Boska, S.K. Batra, D. Oupický, Polyplex-mediated inhibition of chemokine receptor CXCR4 and chromatin-remodeling enzyme NCOA3 impedes pancreatic cancer progression and metastasis, Biomaterials 101 (2016) 108-120.
[262] Y. Xie, C.J. Wehrkamp, J. Li, Y. Wang, Y. Wang, J.L. Mott, D. Oupický, Delivery of miR-200c Mimic with Poly(amido amine) CXCR4 Antagonists for Combined Inhibition of Cholangiocarcinoma Cell Invasiveness, Mol Pharm 13(3) (2016) 1073-80.
[263] Y. Wang, J. Li, Y. Chen, D. Oupický, Balancing polymer hydrophobicity for ligand presentation and siRNA delivery in dual function CXCR4 inhibiting polyplexes, Biomater Sci 3(7) (2015) 1114-23.
[264] Y. Wang, S.T. Hazeldine, J. Li, D. Oupický, Development of functional poly(amido amine) CXCR4 antagonists with the ability to mobilize leukocytes and deliver nucleic acids, Adv Healthc Mater 4(5) (2015) 729-38.
[265] J. Li, Y. Zhu, S.T. Hazeldine, C. Li, D. Oupický, Dual-function CXCR4 antagonist polyplexes to deliver gene therapy and inhibit cancer cell invasion, Angew Chem Int Ed Engl 51(35) (2012) 8740-3.
[266] J.E. Zuckerman, C.H. Choi, H. Han, M.E. Davis, Polycation-siRNA nanoparticles can disassemble at the kidney glomerular basement membrane, Proc Natl Acad Sci U S A 109(8) (2012) 3137-42.

[267] B. Naeye, H. Deschout, V. Caveliers, B. Descamps, K. Braeckmans, C. Vanhove, J. Demeester, T. Lahoutte, S.C. De Smedt, K. Raemdonck, In vivo disassembly of IV administered siRNA matrix nanoparticles at the renal filtration barrier, Biomaterials 34(9) (2013) 2350-8.
[268] C.E. Nelson, J.R. Kintzing, A. Hanna, J.M. Shannon, M.K. Gupta, C.L. Duvall, Balancing cationic and hydrophobic content of PEGylated siRNA polyplexes enhances endosome escape, stability, blood circulation time, and bioactivity in vivo, ACS Nano 7(10) (2013) 8870-80.
[269] H. Engelberg, Plasma heparin levels in normal man, Circulation 23 (1961) 578-81.
[270] Y. Chen, Development of Polymeric Carriers for the Treatment of Acute Kidney Injury, 2018.
[271] Y. Yuan, H. Wang, Y. Wu, B. Zhang, N. Wang, H. Mao, C. Xing, P53 Contributes to Cisplatin Induced Renal Oxidative Damage via Regulating P66shc and MnSOD, Cell Physiol Biochem 37(4) (2015) 1240-56.
[272] W. Van Biesen, R. Vanholder, N. Lameire, Defining acute renal failure: RIFLE and beyond, Clin J Am Soc Nephrol 1(6) (2006) 1314-9.
[273] R. Bellomo, J.A. Kellum, C. Ronco, Defining and classifying acute renal failure: from advocacy to consensus and validation of the RIFLE criteria, Intensive Care Med 33(3) (2007) 409-13.
[274] H.E. Wang, P. Muntner, G.M. Chertow, D.G. Warnock, Acute kidney injury and mortality in hospitalized patients, Am J Nephrol 35(4) (2012) 349-55.
[275] M. Andersson, U. Nilsson, C. Hjalmarsson, B. Haraldsson, J.S. Nyström, Mild renal ischemia-reperfusion reduces charge and size selectivity of the glomerular barrier, Am J Physiol Renal Physiol 292(6) (2007) F1802-9.
[276] C. Rippe, A. Rippe, A. Larsson, D. Asgeirsson, B. Rippe, Nature of glomerular capillary permeability changes following acute renal ischemia-reperfusion injury in rats, Am J Physiol Renal Physiol 291(6) (2006) F1362-8.
[277] S.A. Lee, S. Noel, M. Sadasivam, A.R.A. Hamad, H. Rabb, Role of Immune Cells in Acute Kidney Injury and Repair, Nephron 137(4) (2017) 282-286.
[278] K. De Filippo, S.M. Rankin, CXCR4, the master regulator of neutrophil trafficking in homeostasis and disease, Eur J Clin Invest 48 Suppl 2(Suppl Suppl 2) (2018) e12949.
[279] K.H. Susek, M. Karvouni, E. Alici, A. Lundqvist, The Role of CXC Chemokine Receptors 1-4 on Immune Cells in the Tumor Microenvironment, Front Immunol 9 (2018) 2159.
[280] L.H. Chen, S.L. Advani, K. Thai, M.G. Kabir, M.M. Sood, I.W. Gibson, D.A. Yuen, K.A. Connelly, P.A. Marsden, D.J. Kelly, R.E. Gilbert, A. Advani, SDF-1/CXCR4 signaling preserves microvascular integrity and renal function in chronic kidney disease, PLoS One 9(3) (2014) e92227.
[281] M. Rahman, F. Shad, M.C. Smith, Acute kidney injury: a guide to diagnosis and management, American family physician 86(7) (2012) 631-639.
[282] F. Kork, F. Balzer, C.D. Spies, K.-D. Wernecke, A.A. Ginde, J. Jankowski, H.K. Eltzschig, Minor postoperative increases of creatinine are associated with higher mortality and longer hospital length of stay in surgical patients, Anesthesiology 123(6) (2015) 1301-1311.
[283] I. Hilmi, D. Damian, A. Al-Khafaji, R. Planinsic, C. Boucek, T. Sakai, C.-C. Chang, J. Kellum, Acute kidney injury following orthotopic liver transplantation: incidence, risk

factors, and effects on patient and graft outcomes, BJA: British Journal of Anaesthesia 114(6) (2015) 919-926.
[284] D.R. Jones, H.T. Lee, Perioperative renal protection, Best Practice & Research Clinical Anaesthesiology 22(1) (2008) 193-208.
[285] S. Aronson, R. Blumenthal, Perioperative renal dysfunction and cardiovascular anesthesia: concerns and controversies, Journal of cardiothoracic and vascular anesthesia 12(5) (1998) 567-586.
[286] M. Malek, M. Nematbakhsh, Renal ischemia/reperfusion injury; from pathophysiology to treatment, Journal of renal injury prevention 4(2) (2015) 20.
[287] B.J. Padanilam, Cell death induced by acute renal injury: a perspective on the contributions of apoptosis and necrosis, American Journal of Physiology-Renal Physiology 284(4) (2003) F608-F627.
[288] J.V. Bonventre, L. Yang, Cellular pathophysiology of ischemic acute kidney injury, The Journal of clinical investigation 121(11) (2011) 4210-4221.
[289] S.J. Han, H.T. Lee, Mechanisms and therapeutic targets of ischemic acute kidney injury, Kidney Res Clin Pract 38(4) (2019) 427-440.
[290] Q. Chen, A.K. Camara, D.F. Stowe, C.L. Hoppel, E.J. Lesnefsky, Modulation of electron transport protects cardiac mitochondria and decreases myocardial injury during ischemia and reperfusion, Am J Physiol Cell Physiol 292(1) (2007) C137-47.
[291] F. Kruiswijk, C.F. Labuschagne, K.H. Vousden, p53 in survival, death and metabolic health: a lifeguard with a licence to kill, Nature reviews Molecular cell biology 16(7) (2015) 393-405.
[292] J.Y. Cao, B. Wang, T.T. Tang, Y. Wen, Z.L. Li, S.T. Feng, M. Wu, D. Liu, D. Yin, K.L. Ma, R.N. Tang, Q.L. Wu, H.Y. Lan, L.L. Lv, B.C. Liu, Exosomal miR-125b-5p deriving from mesenchymal stem cells promotes tubular repair by suppression of p53 in ischemic acute kidney injury, Theranostics 11(11) (2021) 5248-5266.
[293] J.V. Bonventre, A. Zuk, Ischemic acute renal failure: an inflammatory disease?, Kidney international 66(2) (2004) 480-485.
[294] G.R. Kinsey, L. Li, M.D. Okusa, Inflammation in acute kidney injury, Nephron Experimental Nephrology 109(4) (2008) e102-e107.
[295] E. Oberlin, A. Amara, C. Bessia, J.-L. Virelizier, F. Arenzana-Seisdedos, O. Schwartz, J.-M. Heard, I. Clark-Lewis, D.F. Legler, M. Loetscher, The CXC chemokine SDF-1 is the ligand for LESTR/fusin and prevents infection by T-cell-line-adapted HIV-1, Nature 382(6594) (1996) 833-835.
[296] C. Lange, F. Tögel, H. Ittrich, F. Clayton, C. Nolte-Ernsting, A.R. Zander, C. Westenfelder, Administered mesenchymal stem cells enhance recovery from ischemia/reperfusion-induced acute renal failure in rats, Kidney international 68(4) (2005) 1613-1617.
[297] B. Li, A. Cohen, T.E. Hudson, D. Motlagh, D.L. Amrani, J.S. Duffield, Mobilized human hematopoietic stem/progenitor cells promote kidney repair following ischemia reperfusion injury, Circulation 121(20) (2010) 2211.
[298] F. Lin, K. Cordes, L. Li, L. Hood, W.G. Couser, S.J. Shankland, P. Igarashi, Hematopoietic stem cells contribute to the regeneration of renal tubules after renal ischemia-reperfusion injury in mice, Journal of the American Society of Nephrology 14(5) (2003) 1188-1199.

[299] J.F. DiPersio, I.N. Micallef, P.J. Stiff, B.J. Bolwell, R.T. Maziarz, E. Jacobsen, A. Nademanee, J. McCarty, G. Bridger, G. Calandra, Phase III prospective randomized double-blind placebo-controlled trial of plerixafor plus granulocyte colony-stimulating factor compared with placebo plus granulocyte colony-stimulating factor for autologous stem-cell mobilization and transplantation for patients with non-Hodgkin's lymphoma, Journal of Clinical Oncology 27(28) (2009) 4767-4773.
[300] S. Gao, S. Hein, F. Dagnæs-Hansen, K. Weyer, C. Yang, R. Nielsen, E.I. Christensen, R.A. Fenton, J. Kjems, Megalin-mediated specific uptake of chitosan/siRNA nanoparticles in mouse kidney proximal tubule epithelial cells enables AQP1 gene silencing, Theranostics 4(10) (2014) 1039.
[301] D. Liu, G. Shu, F. Jin, J. Qi, X. Xu, Y. Du, H. Yu, J. Wang, M. Sun, Y. You, ROS-responsive chitosan-SS31 prodrug for AKI therapy via rapid distribution in the kidney and long-term retention in the renal tubule, Science advances 6(41) (2020) eabb7422.
[302] J. Li, Y. Zhu, S.T. Hazeldine, C. Li, D. Oupický, Dual-function CXCR4 antagonist polyplexes to deliver gene therapy and inhibit cancer cell invasion, Angewandte Chemie 124(35) (2012) 8870-8873.
[303] Y. Xie, Y. Wang, J. Li, Y. Hang, D. Oupický, Promise of chemokine network-targeted nanoparticles in combination nucleic acid therapies of metastatic cancer, Wiley Interdisciplinary Reviews: Nanomedicine and Nanobiotechnology 11(2) (2019) e1528.
[304] M. Alameh, M. Lavertu, N. Tran-Khanh, C.Y. Chang, F. Lesage, M. Bail, V. Darras, A. Chevrier, M.D. Buschmann, siRNA Delivery with Chitosan: Influence of Chitosan Molecular Weight, Degree of Deacetylation, and Amine to Phosphate Ratio on in Vitro Silencing Efficiency, Hemocompatibility, Biodistribution, and in Vivo Efficacy, Biomacromolecules 19(1) (2018) 112-131.
[305] K.T. Hwang, S.T. Jung, G.D. Lee, M.S. Chinnan, Y.S. Park, H.J. Park, Controlling molecular weight and degree of deacetylation of chitosan by response surface methodology, J Agric Food Chem 50(7) (2002) 1876-82.
[306] F. Togel, J. Isaac, Z. Hu, K. Weiss, C. Westenfelder, Renal SDF-1 signals mobilization and homing of CXCR4-positive cells to the kidney after ischemic injury, Kidney Int. 67(5) (2005) 1772-84.
[307] A. Zuk, M. Gershenovich, Y. Ivanova, R.T. MacFarland, S.P. Fricker, S. Ledbetter, CXCR(4)antagonism as a therapeutic approach to prevent acute kidney injury, Am J Physiol Renal Physiol 307(7) (2014) F783-97.
[308] X.R. Shao, X.Q. Wei, X. Song, L.Y. Hao, X.X. Cai, Z.R. Zhang, Q. Peng, Y.F. Lin, Independent effect of polymeric nanoparticle zeta potential/surface charge, on their cytotoxicity and affinity to cells, Cell Prolif 48(4) (2015) 465-74.
[309] Y. Xie, Y. Wang, J. Li, Y. Hang, D. Oupický, Promise of chemokine network-targeted nanoparticles in combination nucleic acid therapies of metastatic cancer, Wiley Interdiscip Rev Nanomed Nanobiotechnol 11(2) (2019) e1528.
[310] Y. Zhou, F. Yu, F. Zhang, G. Chen, K. Wang, M. Sun, J. Li, D. Oupický, Cyclam-Modified PEI for Combined VEGF siRNA Silencing and CXCR4 Inhibition To Treat Metastatic Breast Cancer, Biomacromolecules 19(2) (2018) 392-401.
[311] S.-B. Peng, X. Zhang, D. Paul, L.M. Kays, M. Ye, P. Vaillancourt, M. Dowless, L.F. Stancato, J. Stewart, M.T. Uhlik, H. Long, S. Chu, V.H. Obungu, Inhibition of CXCR4 by LY2624587, a Fully Humanized Anti-CXCR4 Antibody Induces Apoptosis of Hematologic Malignancies, PLoS One 11(3) (2016) e0150585-e0150585.

[312] A.C. Misra, K.E. Luker, H. Durmaz, G.D. Luker, J. Lahann, CXCR4-Targeted Nanocarriers for Triple Negative Breast Cancers, Biomacromolecules 16(8) (2015) 2412-7.
[313] D.Y. Gao, T. Lin Ts, Y.C. Sung, Y.C. Liu, W.H. Chiang, C.C. Chang, J.Y. Liu, Y. Chen, CXCR4-targeted lipid-coated PLGA nanoparticles deliver sorafenib and overcome acquired drug resistance in liver cancer, Biomaterials 67 (2015) 194-203.
[314] B. Le Bon, N. Van Craynest, J.M. Daoudi, C. Di Giorgio, A.J. Domb, P. Vierling, AMD3100 conjugates as components of targeted nonviral gene delivery systems: synthesis and in vitro transfection efficiency of CXCR4-expressing cells, Bioconjug Chem 15(2) (2004) 413-23.
[315] M. Uehara, T. Kusaba, T. Ida, K. Nakai, T. Nakata, A. Tomita, N. Watanabe-Uehara, K. Ikeda, T. Kitani, N. Yamashita, Pharmacological inhibition of ataxia-telangiectasia mutated exacerbates acute kidney injury by activating p53 signaling in mice, Scientific reports 10(1) (2020) 1-13.
[316] Y. Yuan, H. Wang, Y. Wu, B. Zhang, N. Wang, H. Mao, C. Xing, P53 contributes to cisplatin induced renal oxidative damage via regulating P66shc and MnSOD, Cellular Physiology and Biochemistry 37(4) (2015) 1240-1256.
[317] D. Moon, J. Kim, Cyclosporin A aggravates hydrogen peroxide-induced cell death in kidney proximal tubule epithelial cells, Anatomy & cell biology 52(3) (2019) 312-323.
[318] M. Jiang, X. Yi, S. Hsu, C.Y. Wang, Z. Dong, Role of p53 in cisplatin-induced tubular cell apoptosis: dependence on p53 transcriptional activity, Am J Physiol Renal Physiol 287(6) (2004) F1140-7.
[319] S.W. Jones, R.A. Roberts, G.R. Robbins, J.L. Perry, M.P. Kai, K. Chen, T. Bo, M.E. Napier, J.P. Ting, J.M. DeSimone, Nanoparticle clearance is governed by Th1/Th2 immunity and strain background, The Journal of clinical investigation 123(7) (2013) 3061-3073.
[320] H.J. Kim, T. Ishii, M. Zheng, S. Watanabe, K. Toh, Y. Matsumoto, N. Nishiyama, K. Miyata, K. Kataoka, Multifunctional polyion complex micelle featuring enhanced stability, targetability, and endosome escapability for systemic siRNA delivery to subcutaneous model of lung cancer, Drug delivery and translational research 4(1) (2014) 50-60.
[321] Y. Oe, R.J. Christie, M. Naito, S.A. Low, S. Fukushima, K. Toh, Y. Miura, Y. Matsumoto, N. Nishiyama, K. Miyata, Actively-targeted polyion complex micelles stabilized by cholesterol and disulfide cross-linking for systemic delivery of siRNA to solid tumors, Biomaterials 35(27) (2014) 7887-7895.
[322] M.A. Jackson, T.A. Werfel, E.J. Curvino, F. Yu, T.E. Kavanaugh, S.M. Sarett, M.D. Dockery, K.V. Kilchrist, A.N. Jackson, T.D. Giorgio, Zwitterionic nanocarrier surface chemistry improves siRNA tumor delivery and silencing activity relative to polyethylene glycol, ACS nano 11(6) (2017) 5680-5696.
[323] T. Nomoto, Y. Matsumoto, K. Miyata, M. Oba, S. Fukushima, N. Nishiyama, T. Yamasoba, K. Kataoka, In situ quantitative monitoring of polyplexes and polyplex micelles in the blood circulation using intravital real-time confocal laser scanning microscopy, Journal of controlled release 151(2) (2011) 104-109.
[324] M. Andersson, U. Nilsson, C. Hjalmarsson, B. Haraldsson, J.S.r. Nyström, Mild renal ischemia-reperfusion reduces charge and size selectivity of the glomerular barrier, American Journal of Physiology-Renal Physiology 292(6) (2007) F1802-F1809.

[325] S.I. Tyritzis, M. Zachariades, K. Evangelou, V.G. Gorgoulis, A. Kyroudi-Voulgari, K. Pavlakis, T.G. Troupis, C.A. Constantinides, Effects of prolonged warm and cold ischemia in a solitary kidney animal model after partial nephrectomy: an ultrastructural investigation, Ultrastructural pathology 35(2) (2011) 60-65.
[326] C. Rippe, A. Rippe, A. Larsson, D. Asgeirsson, B. Rippe, Nature of glomerular capillary permeability changes following acute renal ischemia-reperfusion injury in rats, American Journal of Physiology-Renal Physiology 291(6) (2006) F1362-F1368.
[327] W. Van Biesen, R. Vanholder, N. Lameire, Defining acute renal failure: RIFLE and beyond, Clinical journal of the American Society of Nephrology 1(6) (2006) 1314-1319.
[328] R. Bellomo, J.A. Kellum, C. Ronco, Defining and classifying acute renal failure: from advocacy to consensus and validation of the RIFLE criteria, Intensive care medicine 33(3) (2007) 409-413.
[329] D.K. Ysebaert, K.E. De Greef, S.R. Vercauteren, M. Ghielli, G.A. Verpooten, E.J. Eyskens, M.E. De Broe, Identification and kinetics of leukocytes after severe ischaemia/reperfusion renal injury, Nephrology Dialysis Transplantation 15(10) (2000) 1562-1574.
[330] H.R. Jang, H. Rabb, Immune cells in experimental acute kidney injury, Nature Reviews Nephrology 11(2) (2015) 88-101.
[331] M.S.a.T.A. Kaden, One-Step Synthesis of Mono-N-subdtituted Azamacrocycles with a Carboxylic Group in the Side-Chain and theri Complexes with Cu^{2+} and Ni^{2+}, Helvetica Chimica Acta 69 (1986) 2081-2086.
[332] S.T.J. Kwon T. Hwang, Gee D. Lee, Manjeet S. Chinnan, You S. Park and Hyun J. Park, Controlling Molecular Weight and Degree of Deacetylation of Chitosan by Response Surface Methodology, Agricultural and Food Chemistry 50 (2002) 1876-1882.
[333] E. Yoo, A.C.D. Salyer, M.J.H. Brush, Y. Li, K.L. Trautman, N.M. Shukla, A. De Beuckelaer, S. Lienenklaus, K. Deswarte, B.N. Lambrecht, B.G. De Geest, S.A. David, Hyaluronic Acid Conjugates of TLR7/8 Agonists for Targeted Delivery to Secondary Lymphoid Tissue, Bioconjug Chem 29(8) (2018) 2741-2754.
[334] Y. Hang, S. Tang, W. Tang, D. Vetvicka, C. Zhang, Y. Xie, F. Yu, A. Yu, D. Sil, J. Li, R.K. Singh, D. Oupicky, Polycation fluorination improves intraperitoneal siRNA delivery in metastatic pancreatic cancer, J Control Release 333 (2021) 139-150.
[335] C. Castaldo, T. Benicchi, M. Otrocka, E. Mori, E. Pilli, P. Ferruzzi, S. Valensin, D. Diamanti, W. Fecke, M. Varrone, V. Porcari, CXCR4 Antagonists: A Screening Strategy for Identification of Functionally Selective Ligands, J Biomol Screen 19(6) (2014) 859-69.
[336] J. Li, D. Oupický, Effect of biodegradability on CXCR4 antagonism, transfection efficacy and antimetastatic activity of polymeric Plerixafor, Biomaterials 35(21) (2014) 5572-5579.
[337] L.S. Chawla, P.W. Eggers, R.A. Star, P.L. Kimmel, Acute kidney injury and chronic kidney disease as interconnected syndromes, N Engl J Med 371(1) (2014) 58-66.
[338] R.L. Mehta, J. Cerdá, E.A. Burdmann, M. Tonelli, G. García-García, V. Jha, P. Susantitaphong, M. Rocco, R. Vanholder, M.S. Sever, D. Cruz, B. Jaber, N.H. Lameire, R. Lombardi, A. Lewington, J. Feehally, F. Finkelstein, N. Levin, N. Pannu, B. Thomas, E. Aronoff-Spencer, G. Remuzzi, International Society of Nephrology's 0by25 initiative for acute kidney injury (zero preventable deaths by 2025): a human rights case for nephrology, Lancet 385(9987) (2015) 2616-43.

[339] A.J. Lewington, J. Cerdá, R.L. Mehta, Raising awareness of acute kidney injury: a global perspective of a silent killer, Kidney Int 84(3) (2013) 457-67.
[340] A. Zuk, J.V. Bonventre, Acute Kidney Injury, Annu Rev Med 67 (2016) 293-307.
[341] R. Alobaidi, R.K. Basu, S.L. Goldstein, S.M. Bagshaw, Sepsis-associated acute kidney injury, Semin Nephrol 35(1) (2015) 2-11.
[342] R. Bellomo, J.A. Kellum, S.M. Bagshaw, Normotensive ischemic acute renal failure, N Engl J Med 357(21) (2007) 2205; author reply 2205-6.
[343] C. Ortega-Loubon, M. Fernández-Molina, Y. Carrascal-Hinojal, E. Fulquet-Carreras, Cardiac surgery-associated acute kidney injury, Ann Card Anaesth 19(4) (2016) 687-698.
[344] M. Legrand, S. Bell, L. Forni, M. Joannidis, J.L. Koyner, K. Liu, V. Cantaluppi, Pathophysiology of COVID-19-associated acute kidney injury, Nat Rev Nephrol (2021) 1-14.
[345] S.G. Coca, S. Singanamala, C.R. Parikh, Chronic kidney disease after acute kidney injury: a systematic review and meta-analysis, Kidney Int 81(5) (2012) 442-8.
[346] H. Rabb, M.D. Griffin, D.B. McKay, S. Swaminathan, P. Pickkers, M.H. Rosner, J.A. Kellum, C. Ronco, X.W.G. Acute Dialysis Quality Initiative Consensus, Inflammation in AKI: Current Understanding, Key Questions, and Knowledge Gaps, Journal of the American Society of Nephrology : JASN 27(2) (2016) 371-379.
[347] A.M. Tomsa, A.L. Alexa, M.L. Junie, A.L. Rachisan, L. Ciumarnean, Oxidative stress as a potential target in acute kidney injury, PeerJ 7 (2019) e8046-e8046.
[348] M. Murashima, M. Nishimoto, M. Kokubu, T. Hamano, M. Matsui, M. Eriguchi, K.-i. Samejima, Y. Akai, K. Tsuruya, Inflammation as a predictor of acute kidney injury and mediator of higher mortality after acute kidney injury in non-cardiac surgery, Scientific Reports 9(1) (2019) 20260.
[349] A. Akcay, Q. Nguyen, C.L. Edelstein, Mediators of inflammation in acute kidney injury, Mediators Inflamm 2009 (2009) 137072.
[350] B. De Klerck, L. Geboes, S. Hatse, H. Kelchtermans, Y. Meyvis, K. Vermeire, G. Bridger, A. Billiau, D. Schols, P. Matthys, Pro-inflammatory properties of stromal cell-derived factor-1 (CXCL12) in collagen-induced arthritis, Arthritis Res Ther 7(6) (2005) R1208-20.
[351] P. Matthys, S. Hatse, K. Vermeire, A. Wuyts, G. Bridger, G.W. Henson, E. De Clercq, A. Billiau, D. Schols, AMD3100, a potent and specific antagonist of the stromal cell-derived factor-1 chemokine receptor CXCR4, inhibits autoimmune joint inflammation in IFN-gamma receptor-deficient mice, J Immunol 167(8) (2001) 4686-92.
[352] M.R. Lattanzio, N.P. Kopyt, Acute kidney injury: new concepts in definition, diagnosis, pathophysiology, and treatment, J Am Osteopath Assoc 109(1) (2009) 13-9.
[353] E. De Clercq, The AMD3100 story: the path to the discovery of a stem cell mobilizer (Mozobil), Biochem Pharmacol 77(11) (2009) 1655-64.
[354] W.C. Liles, H.E. Broxmeyer, E. Rodger, B. Wood, K. Hübel, S. Cooper, G. Hangoc, G.J. Bridger, G.W. Henson, G. Calandra, D.C. Dale, Mobilization of hematopoietic progenitor cells in healthy volunteers by AMD3100, a CXCR4 antagonist, Blood 102(8) (2003) 2728-30.
[355] R.L. Chevalier, The proximal tubule is the primary target of injury and progression of kidney disease: role of the glomerulotubular junction, American journal of physiology. Renal physiology 311(1) (2016) F145-F161.

[356] L.M.S. Gerhardt, J. Liu, K. Koppitch, P.E. Cippà, A.P. McMahon, Single-nuclear transcriptomics reveals diversity of proximal tubule cell states in a dynamic response to acute kidney injury, Proceedings of the National Academy of Sciences of the United States of America 118(27) (2021) e2026684118.
[357] A.H. van Asbeck, J. Dieker, M. Boswinkel, J. van der Vlag, R. Brock, Kidney-targeted therapies: A quantitative perspective, J Control Release 328 (2020) 762-775.
[358] S. Gao, S. Hein, F. Dagnæs-Hansen, K. Weyer, C. Yang, R. Nielsen, E.I. Christensen, R.A. Fenton, J. Kjems, Megalin-mediated specific uptake of chitosan/siRNA nanoparticles in mouse kidney proximal tubule epithelial cells enables AQP1 gene silencing, Theranostics 4(10) (2014) 1039-1051.
[359] X. Huang, Y. Ma, Y. Li, F. Han, W. Lin, Targeted Drug Delivery Systems for Kidney Diseases, Front Bioeng Biotechnol 9 (2021) 683247.
[360] R.C. Cheung, T.B. Ng, J.H. Wong, W.Y. Chan, Chitosan: An Update on Potential Biomedical and Pharmaceutical Applications, Mar Drugs 13(8) (2015) 5156-86.
[361] A.J. Lewington, B.J. Padanilam, D.R. Martin, M.R. Hammerman, Expression of CD44 in kidney after acute ischemic injury in rats, Am J Physiol Regul Integr Comp Physiol 278(1) (2000) R247-54.
[362] H. Kamada, Y. Tsutsumi, K. Sato-Kamada, Y. Yamamoto, Y. Yoshioka, T. Okamoto, S. Nakagawa, S. Nagata, T. Mayumi, Synthesis of a poly(vinylpyrrolidone-co-dimethyl maleic anhydride) co-polymer and its application for renal drug targeting, Nat Biotechnol 21(4) (2003) 399-404.
[363] A. Mitra, A. Nan, H. Ghandehari, E. McNeill, J. Mulholland, B.R. Line, Technetium-99m-Labeled N-(2-hydroxypropyl) methacrylamide copolymers: synthesis, characterization, and in vivo biodistribution, Pharm Res 21(7) (2004) 1153-9.
[364] Y. Chen, W. Tang, F. Yu, Y. Xie, L. Jaramillo, H.S. Jang, J. Li, B.J. Padanilam, D. Oupický, Determinants of preferential renal accumulation of synthetic polymers in acute kidney injury, Int J Pharm 568 (2019) 118555.
[365] H. Priya James, R. John, A. Alex, K.R. Anoop, Smart polymers for the controlled delivery of drugs - a concise overview, Acta Pharm Sin B 4(2) (2014) 120-7.
[366] J.K. Oh, Polymers in Drug Delivery: Chemistry and Applications, Mol Pharm 14(8) (2017) 2459.
[367] F. Alexis, E. Pridgen, L.K. Molnar, O.C. Farokhzad, Factors affecting the clearance and biodistribution of polymeric nanoparticles, Mol Pharm 5(4) (2008) 505-15.
[368] Y.K. Sung, S.W. Kim, Recent advances in polymeric drug delivery systems, Biomater Res 24 (2020) 12.
[369] W.B. Liechty, D.R. Kryscio, B.V. Slaughter, N.A. Peppas, Polymers for drug delivery systems, Annu Rev Chem Biomol Eng 1 (2010) 149-173.
[370] G. Córdoba-David, A. Duro-Castano, R.C. Castelo-Branco, C. González-Guerrero, P. Cannata, A.B. Sanz, M.J. Vicent, A. Ortiz, A.M. Ramos, Effective Nephroprotection Against Acute Kidney Injury with a Star-Shaped Polyglutamate-Curcuminoid Conjugate, Sci Rep 10(1) (2020) 2056.
[371] Y. Zhao, M. Pu, Y. Wang, L. Yu, X. Song, Z. He, Application of nanotechnology in acute kidney injury: From diagnosis to therapeutic implications, J Control Release 336 (2021) 233-251.
[372] Y. Hang, S. Tang, W. Tang, D. Větvička, C. Zhang, Y. Xie, F. Yu, A. Yu, D. Sil, J. Li, R.K. Singh, D. Oupický, Polycation fluorination improves intraperitoneal siRNA

delivery in metastatic pancreatic cancer, Journal of Controlled Release 333 (2021) 139-150.
[373] J. Li, D. Oupický, Effect of biodegradability on CXCR4 antagonism, transfection efficacy and antimetastatic activity of polymeric Plerixafor, Biomaterials 35(21) (2014) 5572-9.
[374] B.K.D. Ngo, M.A. Grunlan, Protein Resistant Polymeric Biomaterials, ACS Macro Letters 6(9) (2017) 992-1000.
[375] K. Tryggvason, J. Wartiovaara, How does the kidney filter plasma?, Physiology (Bethesda) 20 (2005) 96-101.
[376] E. Blanco, H. Shen, M. Ferrari, Principles of nanoparticle design for overcoming biological barriers to drug delivery, Nat Biotechnol 33(9) (2015) 941-51.
[377] Y. Yoshida, J.I. Furukawa, S. Naito, K. Higashino, Y. Numata, Y. Shinohara, Identification of unique glycoisoforms of vitamin D-binding protein and haptoglobin as biomarker candidates in hepatocarcinogenesis of STAM mice, Glycoconj J 35(5) (2018) 467-476.
[378] Q. Yu, L. Zhao, C. Guo, B. Yan, G. Su, Regulating Protein Corona Formation and Dynamic Protein Exchange by Controlling Nanoparticle Hydrophobicity, Frontiers in bioengineering and biotechnology 8 (2020) 210-210.